ETH Institute for Particle Physics

ETHZ-IPP Internal Report 2008-12
August 2008

Determination of Muon Reconstruction and Identification Efficiencies in the CMS Experiment

Diploma Thesis

presented by

Marco Eli Reinhard

Prof. Dr. U. Langenegger, Supervisor

Abstract

The present Diploma Thesis treats the implementation of the Tag and Probe method which provides an analysis tool to determine muon reconstruction and identification efficiencies on real data. Its application is shown on simulated data. After an overview of the muon trigger system, reconstruction and identification mechanisms, the principles of the method are introduced. The crucial part in its implementation was to obtain a stable fit procedure for a relatively large number of distinct mass histograms. This was achieved and efficiencies for muons of prompt and nonprompt J/ψ decays could be expressed in dependence of their transverse momentum and pseudorapidity. Corresponding plots were widely confirmed by efficiencies relying on MC truth information. Nevertheless there remain some dark spots in the analysis which could not be enlighted. Discrepancies between MC truth efficiencies alone, but evaluated on different sets of muons occur on certain CSA07 samples. In addition, the impact of the background level on efficiency values could be roughly estimated but on the other hand the background level itself was not considered in a realistic way.

A comprehensive study of the systematic errors was performed.

Contents

List of Figures

List of Tables

1 Introduction

Despite of its success the Standard Model of particle physics is clearly limited. Confirmed by various probes but yet not able to describe phenomena at GUT scale nor to include gravity, extensions or alternatives have become popular.
The Large Hadron Collider (LHC) located at CERN in Geneva (Switzerland) will be able to glimpse beyond the borders of the Standard Model and thus set the direction in which to go deeper into fundamental particle physics.

1.1 Experimental Means

The LHC will let protons collide at the not yet reached center of mass energy of 14 TeV. Crossings of proton bunches will take place every 25 ns and there shall be on average about 20 proton-proton interactions per crossing.
The LHC is designed to reach an integrated luminosity of up to 100 fb^{-1} per year while setting new centre of mass energy frontiers. Thus, the LHC will be able to probe the Standard Model (SM) beyond the TeV scale and therefore be sensitive to potential new physics phenomena such as the existence of supersymmetric particles or extra spatial dimensions.
Its center of mass energy will be sufficient to cover the fully allowed mass range of a possible Standard Model Higgs Boson such that this will either be detected or ruled out. A "gold plated" signal to discover the SM Higgs boson is given by its decay into ZZ or $\text{Z}Z^*$ and their subsequent decays into four charged leptons. The four-particle mass resolution will be best if these leptons are muons.

This is one example among others which shows the relevance of high quality muon detection for studies of interesting processes at the LHC. For this reason one of the two general purpose experiments at LHC, the Compact Muon Solenoid (CMS), has been designed to identify and reconstruct muons with high efficiency and accuracy. A schematic view of the detector can be seen in figure 1.1.

CMS has an overall length of 21,60 m, an overall diameter of 15 m and a total weight of 12,500 t, hence its density exceeds the density of water.
The coordinate system of CMS is defined such that the origin is the collision point. The x-axis is horizontal pointing to the LHC center, the y-axis points vertically upwards and the z-axis horizontally to the west. The small tilt of the LHC plane is neglected.
A useful variable to describe the direction of emerging tracks is the pseudorapidity η. It may later also be used to distinct certain detector regions. Pseudorapidity is defined as

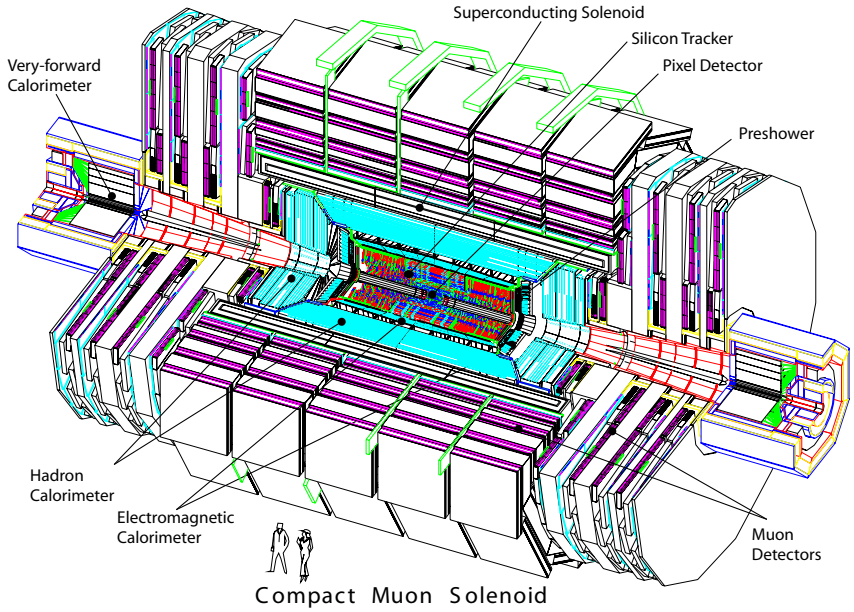

Figure 1.1: Schematic view of the CMS detector

$$\eta = -\ln\tan(\frac{\theta}{2}) \tag{1.1}$$

such that its sign is equal to the sign of the z-axis: θ is the polar angle defined between the flying path of the particle and the z-direction along the beam axis. Thus, $\theta = 0$ corresponds to the positive z-axis. Equation (1.1) shows that $|\eta| \to \infty$ if the particle heading becomes parallel with the beam axis. Since particles may escape through the beam pipe, the geometrical acceptance of the detector is restricted to $|\eta| \lesssim 2.4$.
As can be seen from figure 1.1 the CMS detector is divided into a barrel region which is passed by particles with $|\eta| \lesssim 1.2$ and two endcap regions ($|\eta| \gtrsim 1.2$). Leaving a hit in the muon system which is the outermost part of the detector a particle will have emerged from the interaction point and have passed the pixel detector followed by the silicon tracker, the electromagnetic calorimeter (ECAL), the hadronic calorimeter (HCAL) and the 4 T superconducting coil before it finally arrived in the outermost wheel where three layers of the iron return yoke of the coil alternate with layers of muon chambers. The buildup of the muon system differs in the barrel and the endcap regions which will be explained more detailed in chapter 2.

1.2 What to look for?

Besides the previous example a particular second one is chosen:
Supersymmetry is an extension of the Standard Model predicting the existence of many

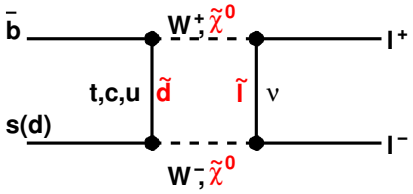

Figure 1.2: Box diagram for $B_s^0 \rightarrow \mu^+\mu^-$.

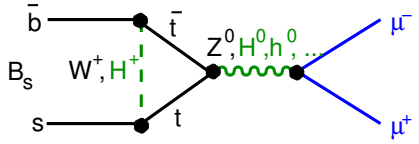

Figure 1.3: Triangle graph for $B_s^0 \rightarrow \mu^+\mu^-$

yet unseen particles. It provides not only a solution to the hierarchy problem[1] but it also offers the possibility to include gravity.
If they exist, supersymmetric particles could contribute to loop-corrections of tree-level SM processes.

Since no such contributions to amplitudes of measured processes could be detected so far, they must be small, if they even exist at all. Small contributions again are best detected in processes which are strongly suppressed or even forbidden in the Standard Model. LHC will be able to set new upper limits on or even determine corresponding branching fractions. Such measurements can lead to restrictions of the supersymmetric parameter space.
As an example the decay $B_s^0 \rightarrow \mu^+\mu^-$ is considered. Its SM branching fraction of $\mathcal{B} = (3.42 \pm 0.54) \cdot 10^{-9}$ can be significantly enhanced in possible extensions. Figures 1.2 and 1.3 show the Feynman graphs of the B_s^0 decay into two oppositely charged leptons according to a box diagram and a triangle graph where neutralinos ($\tilde{\chi}^0$), squarks ($\tilde{q}$) and sleptons ($\tilde{l}$) may occur as internal lines. In the Minimal Supersymmetric Standard Model (MSSM) the relation $\mathcal{B}(B_s^0 \rightarrow \mu^+\mu^-) \propto (\tan\beta)^6$ provides access to $\tan\beta$, the ratio of the vacuum expectation values of the up-type and the down-type Higgs doublets [Lan06].

Normalizing with respect to the decay $B^+ \rightarrow J/\psi\ K^+ \rightarrow \mu^+\mu^- K^+$ the branching ratio $\mathcal{B}(B_s^0 \rightarrow \mu^+\mu^-)$ can be expressed as

$$\mathcal{B}(B_s^0 \rightarrow \mu^+\mu^-) = \frac{n_{B_s^0}}{n_{B^+}} \cdot \frac{\epsilon_{B^+}}{\epsilon_{B_s^0}} \cdot \frac{f(\bar{b} \rightarrow B^+)}{f(\bar{b} \rightarrow B_s^0)} \cdot \mathcal{B}(B^+ \rightarrow J/\psi K^+) \cdot \mathcal{B}(J/\psi \rightarrow \mu^+\mu^-) \quad (1.2)$$

where $n_{B_s^0}$ (n_{B^+}) is the number of reconstructed B_s^0 (B^+)-candidates and $f(\bar{b} \rightarrow B_s^0)$ is the B_s^0 production fraction. The efficiencies $\epsilon_{B_s^0}$ / ϵ_{B^+} are the fraction of generated $B_s^0 \rightarrow \mu^+\mu^-$ / $B^+ \rightarrow J/\psi K^+ \rightarrow \mu^+\mu^- K^+$ which are observed in the data. These efficiencies in turn each contain the single muon efficiency ϵ_μ as a multiplicative factor whose determination is the aim of this diploma thesis.

This is one particular example where high muon reconstruction and identification efficiencies, as provided by CMS, are relevant. The next chapter will introduce the design

[1] The question why the ratio of the Planck mass and the 300 GeV energy scale of electroweak symmetry breaking is so large.

of the CMS muon system with focus rather on muon reconstruction and identification mechanisms than on the technical aspects of the hardware.

Subsequently, the "Tag and Probe" method is introduced and single muon efficiencies are determined from $J/\psi \rightarrow \mu^+\mu^-$ samples.

2 The Muon System of CMS

The muon system was designed to identify muons, to act as a muon trigger and to determine their momenta and charge even at highest LHC luminosities.
Centrally produced muons are first measured in the inner tracker and subsequently in the muon system. If their momentum is determined using the muon system only, it is essentially given by the muon bending angle at their exit of the 4 T coil with the interaction point taken as their origin. Up to 200 GeV the resolution is restricted by multiple scattering in the material before the first muon station is reached. For higher p_T-values the spatial resolution of the muon chambers becomes dominant.
For high momentum muons a combination of the inner tracker and the muon detector measurements will improve the momentum resolution of the two individual detectors. For low momentum muons the combination will not lead to an improvement with respect to the resolution obtained from the inner tracker information alone [Del06].

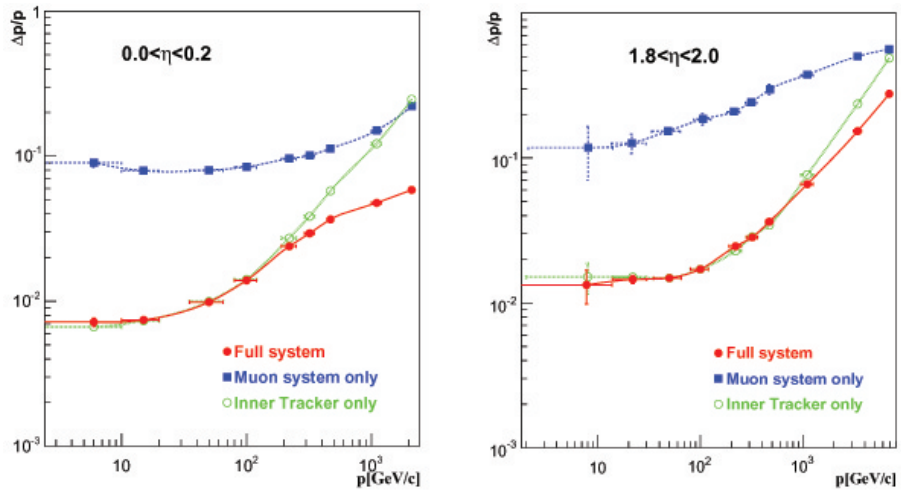

Figure 2.1: Momentum resolution of the muon system, the tracker and their combination.

Figure 2.1 illustrates this issue for a barrel region ($0.0 < \eta < 0.2$) and an endcap region ($1.8 < \eta < 2.0$).

2.1 Technical Design

Figure 2.2 shows a transverse slice of the CMS detector including the barrel part of the muon system.

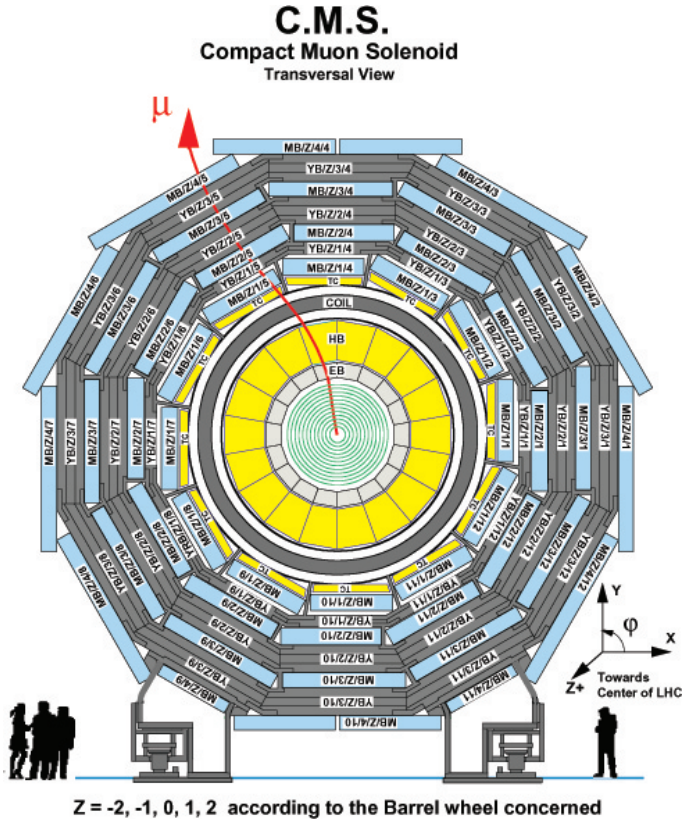

Figure 2.2: Transverse view of the muon system of CMS.

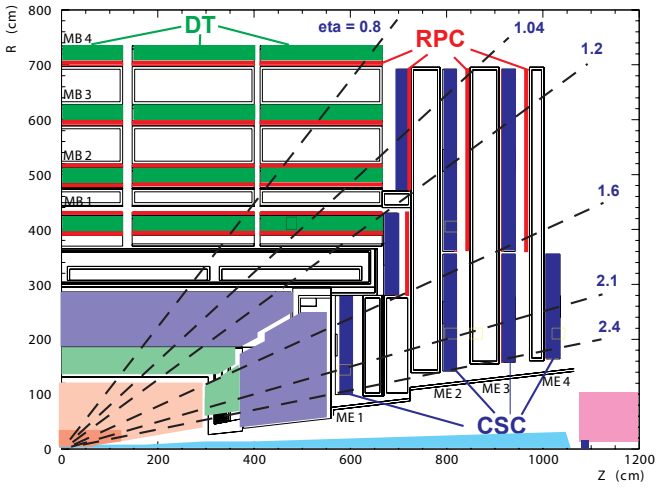

Figure 2.3: Longitudinal slice of the CMS detector.

The muon system consists of four stations of muon chambers (MB/Z/1 - MB/Z/4) covering the full ϕ-range. YB/Z/1 - YB/Z/3 denote the three stations of the return yoke which contains most of the return flux of the magnetic field such that the muon chambers are not affected too much thereby. The chambers of every station are arranged such that each muon would pass at least three out of the four stations provided its energy is high enough.

Event selection happens in two stages in CMS. First, a hardware based fast decision made by the Level-1 trigger reduces the rate of data for further processing by the software oriented HLT trigger.
The hardware of the Level-1 muon trigger system consists of three different detector types which all support their own trigger systems. Drift Tubes (DT) were chosen in the barrel region ($|\eta| \lesssim 1.2$) where the residual magnetic field in the muon chambers, muon rates and the neutron induced background are low. Cathode Strip Chambers (CSC) were chosen in the endcap regions where the magnetic field, muon and neutron induced background rates are all high. CSC cover the region $0.9 < |\eta| < 2.4$. Complementary the range $|\eta| < 2.1$ ($|\eta| < 1.6$ for the CMS start-up phase) is also covered by Resistive Plate Chambers (RPC) which have coarser position resolution but good time resolution in order to determine the bunch-crossing from which a particle emerged.

In stations which are denoted as MB1 and MB2 every drift tube chamber is located between two resistive plate chambers while for the layers MB3 and MB4 only one resistive plate chamber is attached to the inner side of a drift tube chamber.

In order to understand the mechanisms of muon reconstruction and muon identification the basic concepts of the muon system with its subsystems will be briefly discussed. The following sections will first summarize the functionality of the three detector subsystems (DT, CSC, RPC), then illuminate their connection to the global muon trigger, further draft how Level-1 muon trigger decisions are made and finally give a coarse description of the HLT trigger system which is seeded by L1 candidates. This will lead to the definition of global muons. More detailed descriptions of these issues can be found in [Del06].

Drift Tube Chambers

Muon chambers in the barrel part are made of DT which have a transversal dimension of 42 x 3 mm^2. Their length can vary between two and three meters. Every chamber consists of independent, gastight subunits called superlayers (SL) which are each made out of four layers of Drift Tubes. Generally a DT chamber consists of three SLs which are glued together. The external SLs (ΦSL) have wires parallel to the beam direction and orthogonal to the wires of the medium SL (ΘSL). Three-dimensional track segments are formed within a SL.
The chamber electronics contains the local trigger system: For every SL the bunch and track identifier (BTI) identifies the position, angle and time of passage of a particle. On the chamber level the Track Correlator (TRACO) combines the BTI information of the

two tracks belonging to the ΦSL of the DT chamber in order to reduce noise and to improve the angular resolution. For each chamber, information of the two best segments is forwarded to the drift tube track finder (DTTF) which matches all of these segments belonging to chambers of the maximally four stations into a full track and assigns p_T, ϕ, η and quality. Finally the Wedge and Barrel Sorters select the four highest-p_T muon candidates in the barrel and forwards them to the Global Muon Trigger (GMT).

Cathode Strip Chambers

In each endcap region there are four stations of Cathode Strip Chambers (CSC) differentiated in the z-direction, separated by disks of the return yoke. Each trapezoidal shaped CSC contains six planes of cathode strips alternating with planes of anode wires. Thus, a muon can leave up to 6 x 4 = 24 hits in successive CSCs. Muon acceptance is guaranteed by overlap of the CSCs in Φ.

The design of cathode and anode electronics algorithms differs such that each of them can measure some of the coordinates with higher accuracy. Thus, cathode electronics is optimized to measure ϕ and the direction of a track while anode electronics is optimized to assign the correct muon bunch-crossing to a track and further to determine its η-value.

Each of the six layers of a CSC measures the cylindric coordinates (r, ϕ, z) which leads to a track segment. Muon candidate reconstruction is then performed in angular segments and finally the four best candidates of the entire CSC system are forwarded to the GMT.

Resistive Plate Chambers RPC

The RPC Pattern Comparator Trigger checks spatial and time coincidence of hits in the RPC muon stations. Its electronics has two functions: First, it assignes a p_T-value to a candidate track formed by a pattern of hits which was matched with one of many predefined patterns obtained from simulations. It adopts the p_T value of the adequate pattern.
Second, it requires time coincidence of hits in patterns which allows the bunch-crossing assignment to the candidate.
Finally, up to eight muon candidates (4 barrel, 4 endcaps) are forwarded to the GMT.

Global Muon Trigger (GMT)

Figure 2.4 summarizes the previous subsections and shows the hierarchical structure of local reconstruction followed by regional and global reconstruction. The track finders act as regional triggers.

The GMT accepts the four best muons from the DT trigger system, the four best muons from the CSC trigger system as well as the 4 + 4 best muons from the RPC trigger system trying to match muons from the two complementary systems in ϕ and η. After successful matching of two muons the parameters of the resulting muon are optimized in precision. Finally, up to four muon candidates are forwarded to the High Level Trigger (HLT) for

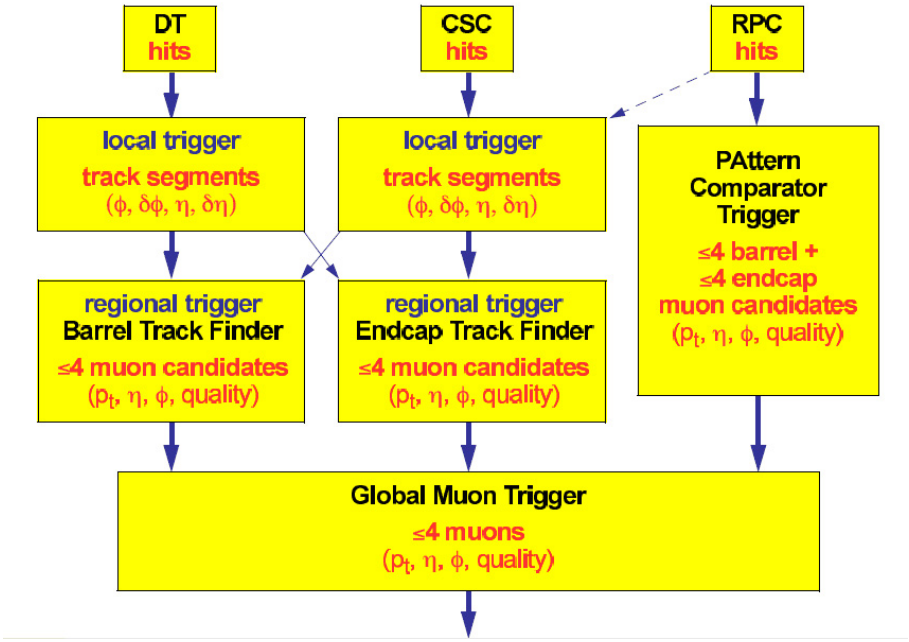

Figure 2.4: Input to the global muon trigger.

further processing. The GMT has also the possibility to forward muon candidates which are confirmed only by one of the two complementary systems if a certain qualitity value was assigned.

The Level-1 Muon Trigger of CMS

A Level-1 (L1) trigger decision is based on data from the global muon trigger which in turn relies on the trigger systems of the three detector types DT, CSC and RPC as described above.
The purpose of the L1 muon trigger of CMS is to identify muons, assign them to a particular beam crossing and to determine their transverse momenta and passed locations. It decides whether the data from a particular beam crossing is kept for further processing or not.

The L1 muon trigger analyzes each 25-ns bunch crossing withing a latency of 3 μs and thus provides a fast estimate of the transverse momentum of muons. Events which are accepted by the L1 muon trigger must satisfy one of the L1 muon trigger paths based on the output of the GMT. The two main L1 muon sub-triggers are single-muon and double-muon triggers each with one of several possible p_T threshold conditions.
The HLT muon trigger may then operate with a longer latency period than the L1 trigger.

2.2 Identification and Reconstruction of Muons

There are some differences between muon reconstruction and muon identification. These shall be illuminated in the following.

Muon reconstruction works from the outside-in starting in the muon system reconstructing muon candidates step by step. On the other side muon identification works from the inside-out starting with a track which has a priori nothing to do with a muon and attempts to assign a 'muon compatibility' by using the muon system.

Muon reconstruction happens in three stages. It begins with local reconstruction, followed by stand-alone reconstruction and global reconstruction.
Local reconstruction starts with hits from the DT/CSC to reconstruct track segments. These local track stubs are then used as input to the stand-alone reconstruction (using the global muon trigger) which produces a reconstructed track not containing any silicon tracker information.

High Level Trigger

The online selection of muons based on decisions of the High Level Trigger (HLT) happens in two stages.
First, the Level-2 muon reconstruction which is seeded by Level-1 candidates is performed. It shall confirm the decision of the Level-1 trigger and reduce the rate of candidates which is relevant in the following sense: The output of the Level-2 trigger is the seed for the Level-3 trigger which uses information from the silicon tracker. Level-3 only considers tracks from the silicon tracker if they are compatible with hits in the muon system. Thus, the HLT reconstruction algorithm depends on the precision of the Level-1 seed which defines the region of interest in the silicon tracker.
Level-2 and Level-3 reconstruction are refered to as HLT standalone and HLT global reconstruction.

2.2.1 Stand-alone Muon Reconstruction

Standalone / Level-2 muon reconstruction does not include data from the silicon tracker. It uses information from the DT or CSC system in each case combined with data from the RPC system. Reconstruction starts with track segments from the muon chambers which result from local reconstruction (see section 2.1). State vectors containing the track position, their momentum and direction are used to seed the muon trajectories upon which the track reconstruction based on Kalman-filter technique relies. These tracks in the muon system are finally extrapolated to the nominal interaction point such that a vertex-constrained fit to the track parameters can be performed. But yet the fit is restricted to the muon system. To generate a positive Level-2 muon trigger decision stand-alone tracks must exceed a p_T-threshold depending on the specific Level-2 muon trigger path.

2.2.2 Global Muon Reconstruction

Global / Level-3 muon reconstruction extends muon trajectories to include hits in the silicon tracker. Therefore it starts with a stand-alone reconstructed muon and extrapolates its trajectory from the innermost muon station through the coil and both calorimeters to the outer tracker surface. The result of this extrapolation determines the region of interest in the silicon tracker in which regional track reconstruction is performed.
Track reconstruction in the silicon tracker is also done using Kalman-filter technique.

Since a significant energy fraction of pions and kaons can be carried away by neutrinos corresponding muons will have clearly lower energies such that their trajectories will recognizably differ from those of pions and kaons. Thus, requiring a good matching between stand-alone muons and tracks from the silicon tracker reduces pion and kaon fake rates [Oli07].

2.2.3 Muon Identification

As described in the previous subsections muon reconstruction starts with stand-alone muon tracks reconstructed in the muon system and attempts to combine them with tracks from the silicon tracker. Identifying muon tracks from the inside-out provides another analysis tool. Information from the ECAL is used to verify the compatibility of a track with the muon hypothesis (minimal ionizing particle). Further, the algorithm considers hits of muon segments even if these are not associated with a standalone muon track. This can be of advantage for low-p_T muons which do not reach the outer muon detector layers. They will potentially be identified offline with the muon identification algorithm but not reconstructed as global muons.

Muons emerging of such a muon identification algorithm are referred to as tracker muons. Tracker muon reconstruction may as well be used as a synonym for muon identification.

3 Efficiencies

The previous chapter gave a short overview of the muon system of CMS showing how muon candidates emerge from positive trigger decisions. As motivated in chapter 1 it is crucial to know the probabilities that a muon generated in the detector leads to such a candidate. These probabilities are given by the trigger efficiencies of the respective trigger systems. In this chapter Level-1 muon reconstruction efficiencies as well as tracker muon identification and global muon reconstruction efficiencies are considered.

In general muon trigger efficiencies can be written as

$$\epsilon = \frac{N_{\mathbf{trig}}}{N_{\mathbf{prod}}} \tag{3.1}$$

where $N_{\mathbf{prod}}$ is the number of produced muons and $N_{\mathbf{trig}}$ the number of elements of the subset of $N_{\mathbf{prod}}$ which passed the trigger path under study.

For a particular trigger path the efficiency may be decomposed, e.g. for a single muon trigger path with isolation criterion as

$$\epsilon_\mu := \epsilon_{rec} \cdot \epsilon_{isol} \cdot \epsilon_{trig} \tag{3.2}$$

where ϵ_{rec} is the reconstruction efficiency, ϵ_{isol} the probability that a reconstructed muon is isolated and ϵ_{trig} the probability that a reconstructed and isolated muon is triggered according to a given p_T-threshold. In the applied analysis no isolation criterion has been used and in the following only reconstruction efficiencies ϵ_{rec} are considered.

Since the detector is not homogeneous, efficiencies depend on where the muons pass through the detector. Thus, efficiencies may depend on the variables p_T, η, and ϕ. However, due to the approximate azimuthal symmetry of the detector with respect to the beam axis it is expected that efficiencies do not significantly depend on the azimuthal angle ϕ. Further, efficiency drops are expected for the following η-values: $|\eta| \sim 0.3$ which corresponds to the gap between two wheels in the barrel where cables and other services pass, around $|\eta| = 1.2$ where the DT and CSC systems overlap and also around $\eta = 1.7 \sim 1.8$.
The penetration depth of a muon into the muon system depends on its energy and hence on its momentum $|\vec{p}|$. If low-p_T muons travel such that they would in principle be measured in the barrel region this implies that also their transverse momentum component parallel to the beam axis (p_z) and thus $|\vec{p}|$ are low. They will probably not lead to a

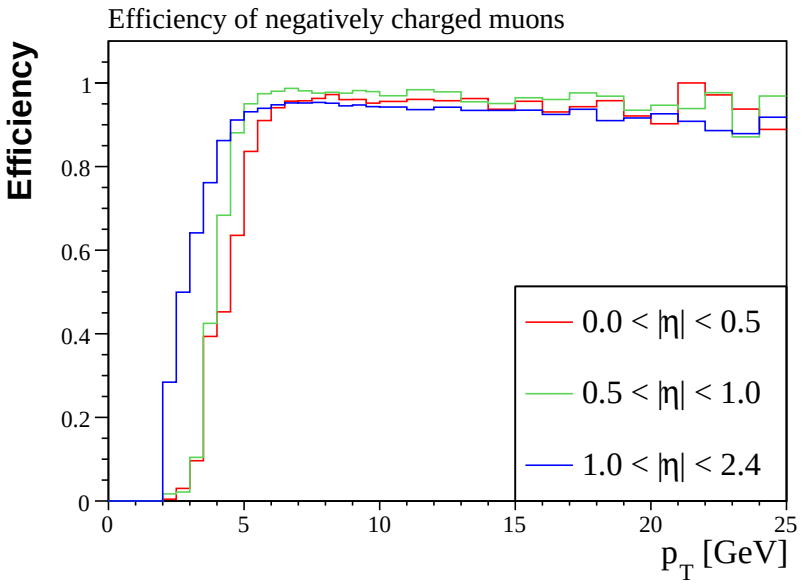

Figure 3.1: Global muon reconstruction efficiency vs. p_T of the muons in different $|\eta|$-bins. Based on MC truth information.

stand-alone muon where more than one station of the muon system needs to be hit. That is why reconstruction efficiencies are low in the low-p_T range. However, in the endcap regions low-p_T does not necessarily imply low p_z and low $|\vec{p}|$. Therefore the effect of low efficiencies in the low-p_T region is weakened if only muons with higher $|\eta|$-values are considered.
The same effect can be seen considering efficiency vs. η plots which will have a dip in the central (barrel) region whose shape will be weakend by considering only high-p_T muons.

These are some general attributes of efficiencies. Aspects which are more specific to the particular efficiencies are described in the following sections. They show MC truth based plots of global muon reconstruction and tracker muon identification efficiencies which were all produced by the division of two p_T- or η- distribution histograms where the denominator histograms contained the corresponding distribution of all generator level muons and the nominator histograms its subset of muons passing the global muon or tracker muon criteria, respectively.

3.1 Global Muon Reconstruction Efficiency

Global muon reconstruction efficiencies correspond to the probability that a produced muon is reconstructed as global / Level-3 muon. The generator level plots are shown in figures 3.1 and 3.2.

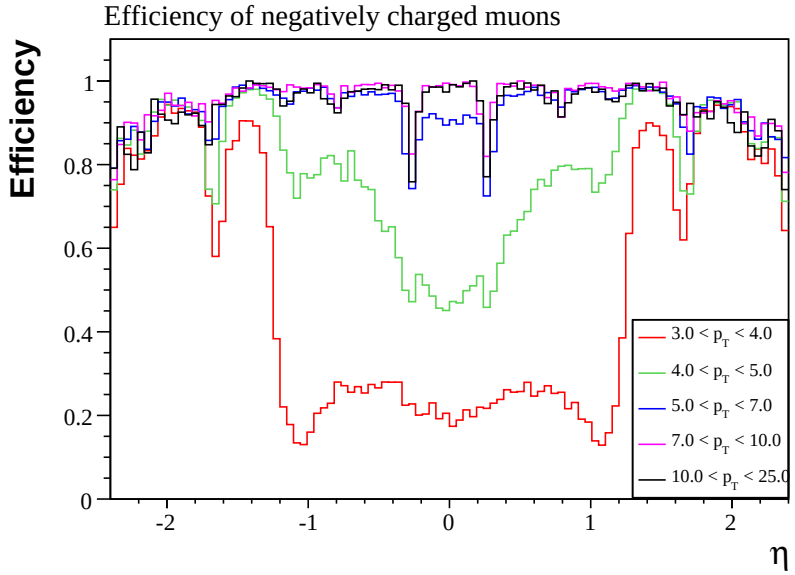

Figure 3.2: Global muon reconstruction efficiency vs. η of the muons in different p_T-bins. Based on MC truth information.

3.2 Tracker Muon Identification Efficiency

Tracker muon identification efficiencies correspond to the probability that a produced muon is identified as tracker muon. As argued in section 2.2.3 low-p_T muons are better identified as tracker muons than reconstructed as global muons which can be seen by comparing figures 3.3 and 3.4 with 3.1 and 3.2. Further, comparing 3.2 with 3.4 shows that the efficiency drops originating from the build-up of the muon system in the endcap regions are not present for tracker efficiencies. This may be ascribed to the fact that, unlike global muons, tracker muons do not require a positive Level-1 muon trigger decision.

3.3 (p_T, η)-Distributions and Average Efficiencies

To obtain average efficiencies out of the p_T- and η-dependent forms distribution functions have to be considered. The expression looks as:

$$\langle \epsilon \rangle = \int \epsilon(p_T, \eta) \cdot f(p_T, \eta) dp_T d\eta \tag{3.3}$$

where $\langle \epsilon \rangle$ is the average efficiency and f is a normalized distribution function for muons. A particular f for muons from the prompt decay[1] $J/\psi \rightarrow \mu^+\mu^-$ is visualized with the aid of MC truth information in figures 3.5 and 3.6.

[1]The J/ψ was either produced directly or indirectly from excited charmonium states, but not in a B decay (nonprompt).

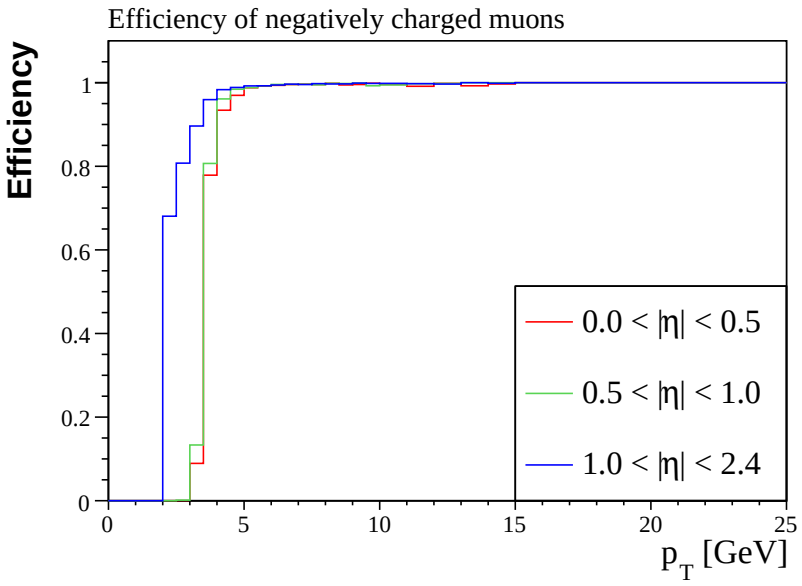

Figure 3.3: Tracker muon identification efficiency vs. p_T of the muons in different $|\eta|$-bins. Based on MC truth information.

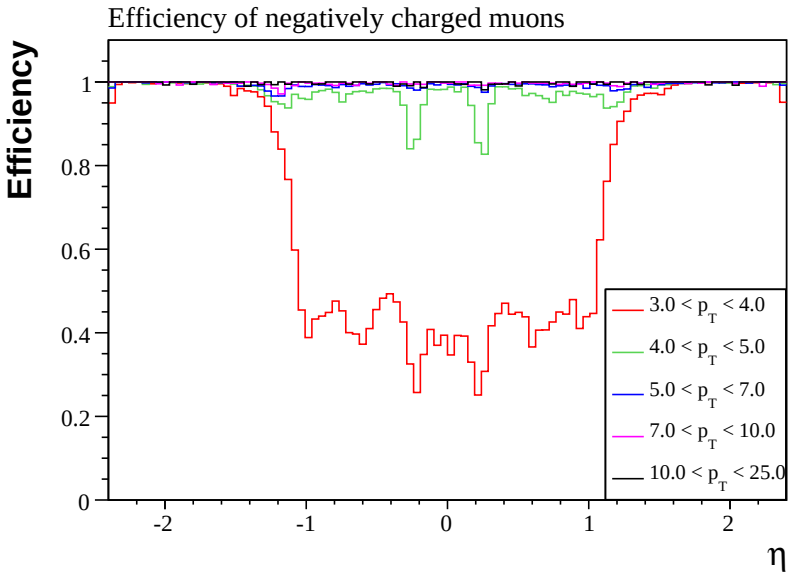

Figure 3.4: Muon identification efficiency vs. η of the muons in different p_T-bins. Based on MC truth information.

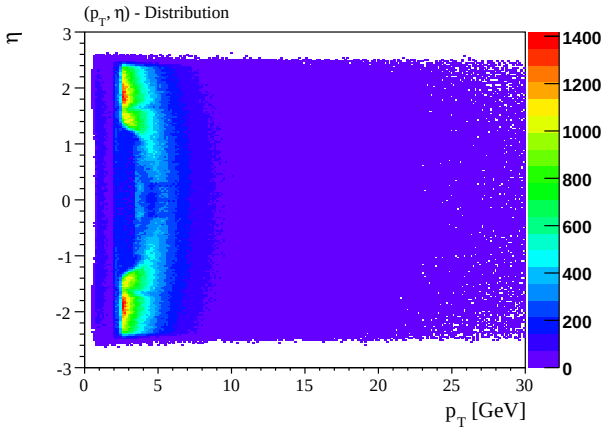

Figure 3.5: (p_T, η)-distribution of truth matched muon tracks.

It can be seen that the muon entries are concentrated around a low-p_T peak value in both endcap regions where the more radiation resistent and faster CSC (compared to the DT chambers) were used. The projections on the axes are shown in figure 3.6.

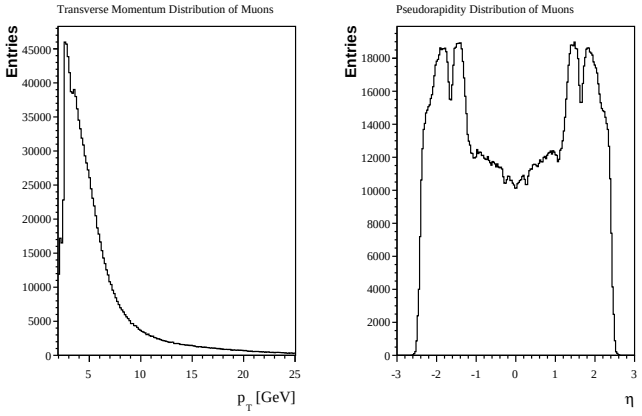

Figure 3.6: Transverse momentum and pseudorapidity distributions of negatively charged truth matched muon tracks. The drop for $|\eta| \sim 1.7$ may be ascribed to an inefficiency in the truth matching of the tracks.

4 Tag and Probe Method

The previous chapter summarized the main properties of efficiencies including particular MC truth-based efficiency plots. However, when determining efficiencies from real data, MC truth information about the real nature of a particle is no longer accessible and must therefore be substituted. The Tag and Probe method allows for the determination of efficiencies from real data providing this substitution. Its general idea as well as its specific implementation for the efficiencies discussed in chapter 3 are described in the following.

4.1 Method Description

So far muon efficiencies were expressed as $\epsilon = N_1/N_2$ where N_2 is the number of produced muons and N_1 is some subset of muons which is chosen according to the trigger system under study. N_2 was determined using MC truth information. Out of real data N_2 can be obtained considering a specific particle decay into two muons. If one of the muons is well reconstructed (tag muon) then the set of all reconstructed silicon tracks in the event can be searched for a suitable track trying to reconstruct the decayed particle out of the assumed muon and this track. A successful reconstruction is presumably obtained if the invariant mass of the combination of the assumed muon and the chosen silicon track lies on the mass peak of the decayed particle and it either exposes the chosen silicon track to belong to a muon before its matching with a stand-alone muon[1] or with hits in the muon system[2] is actually checked, or the event belongs to the combinatoric underground which will subsequently be subtracted in the procedure. Events with such a tag muon + track combination, not belonging to the combinatoric underground, count for N_2. N_1 is then obtained as subset of events of N_2 which was really matched.

If $p_{\mathbf{tag}}$ and $p_{\mathbf{probe}}$ are the four-momenta of the tag muon and track respectively then the invariant mass m of the particle is given by:

$$m = \sqrt{(p_{\mathbf{tag}} + p_{probe})^2} \tag{4.1}$$

For reasons which were motivated in chapter 1 efficiencies were determined from a $J/\psi \to \mu^+\mu^-$ sample. The technical chain runs as follows: All events of the J/ψ samples are passed through. An event is kept if there is found a tag muon + probe track combination satisfying the predefined criteria. In this case the invariant mass of the combination enters a muon-track mass histogram. The criteria for the choice of both, tag and probe,

[1] In case of global muon reconstruction efficiency
[2] In case of tracker muon identification efficiency

should be defined such that background is reduced and the J/ψ mass peak is clearly visible.

If the track is subsequently identified as a global / tracker muon the invariant mass of the tag and probe combination enters another muon-muon mass histogram. The latter should contain almost exclusively $J/\psi \to \mu^+\mu^-$ events. The presence of background excludes the possibility of simple counting the number of histogram entries in order to obtain N_1 and N_2. Instead, a fit was applied to the histograms. The fit function was additively composed of a linear background and a gaussian peak function. Integration of the whole function, subsequent background subtraction and division by the chosen histogram bin width reproduces the number of histogram entries N_1 and N_2, respectively.

4.1.1 Combinatorics

The two muons of a $J/\psi \to \mu^+\mu^-$ event can in principle pass both tag and probe criteria. There are three possible combinations TT, TP and TF, where T stands for passing the tag criteria, P for passing the probe criteria and the criteria of the efficiency under study, if this is not equal to the tag criteria and F for passing the probe criteria but failing the criteria of the efficiency under study. Taking equation (3.1) and decomposing its nominator and denominator according to all possibilities gives:

$$N_1 = 2N_{\mathrm{TT}} + N_{\mathrm{TP}} \tag{4.2}$$

$$N_2 = 2N_{\mathrm{TT}} + N_{TP} + N_{TF} \tag{4.3}$$

Such that equation (3.1) reads:

$$\epsilon = \frac{2N_{\mathrm{TT}} + N_{\mathrm{TP}}}{2N_{\mathrm{TT}} + N_{TP} + N_{TF}} \tag{4.4}$$

As described in section 4.2 the tag criteria are chosen to be unique such that N_{TT} vanishes.

The probe selection, however, may be ambiguous such that there can be several tracks satisfying the probe criteria. Which one among these will be chosen is accidental.

4.2 Selection of the Tag Muon

It is relevant to choose a track from the silicon tracker which belongs with high probability to a muon. If it is no muon then the combined invariant mass of tag and probe might as well lie in the region of pure background outside the range of the J/ψ mass peak and would therefore be lost for both N_1 and N_2 events. Thus, a bad choice of the tag may reduce statistics in particular for muon-muon mass histograms which in turn can lead to fitting problems as discussed in section 4.4.2.

Thus, the tag muon was always chosen to be a global muon. However, this choice is not unique and in particular in the relevant case where the event contains a $J/\psi \to \mu^+\mu^-$ decay it is likely that each of these two muons is a global muon. Considering the p_T-distribution (see figure 3.5) it turned out that the choice of the leading muon[3] leads to the

[3]Muon with the highest transverse momentum

same unwanted effect as depicted above, namely a reduction of statistics in the high-p_T region where the number of events is already small.

Finally, the following criteria were applied in the given order for the tag selection in an event:

1. Minimal p_T requirement: To assure the quality of the tag muon, its transverse momentum is required to be above 3 GeV.

2. Fixing the charge of the tag muon: Thus, muon efficiencies are determined for a specific charge.

3. Choice of the leading muon of the predefined charge: Among all muons with given charge and which satisfy the minimal p_T requirement the one with maximal transverse momentum is chosen. The opposite charge requirement prevents from the danger of reducing statistics in the high-p_T region.

If there exist muons satisfying the above rules and if there are no two muons with exactly the same transverse momentum in the same event the tag muon is uniquely determined through this procedure.

4.3 Selection of the Probe Track

The probe track is searched for in all tracks of the event provided a tag has been found. The track associated to the tag is excluded. In order to restrict the number of candidate probe tracks several cuts are applied.
From a technical / implementation viewpoint one could make use of the fact that if all cuts act on variables which form a connected space the remaining subset of candidate probe tracks will be independent of the order of application of the cuts. In this case it is sensible to choose the cuts in an order which optimizes the speed of the implementation. However, this attitude was not pursued very forceful.

The selection procedure looks as follows:

1. Skip events in which no tag muon has been found.

2. Skip tracks with the same charge as the tag muon.

3. Skip tracks with $p_T < 2$ GeV

4. Skip tracks with $|\eta| > 2.4$.

5. Skip tracks which lead together with the tag muon to a combined invariant mass (see equation (4.1)) which lies outside the mass window [2.5 GeV, 3.5 GeV] around the J/ψ-mass peak at 3096.916 $\pm$ 0.011 MeV [W.-06].

This procedure does not determine the probe track uniquely. The search is finished as soon as a track is found which satisfies all criteria. Further optimization could eventually affect statistics but this was not examined. Figure 4.1 shows the number of events containing N probe tracks for the 'Stew_AllEvents_100pb' sample (see section 4.4.1). It shows that in most cases where a tag muon was found no probe track was selected. But usually there are approximately up to three probe tracks among which in most cases only one truth matched muon track could be found. This shows that breaking the search after the first muon was found, does only induce a small error which is thus neglected in the present analysis.

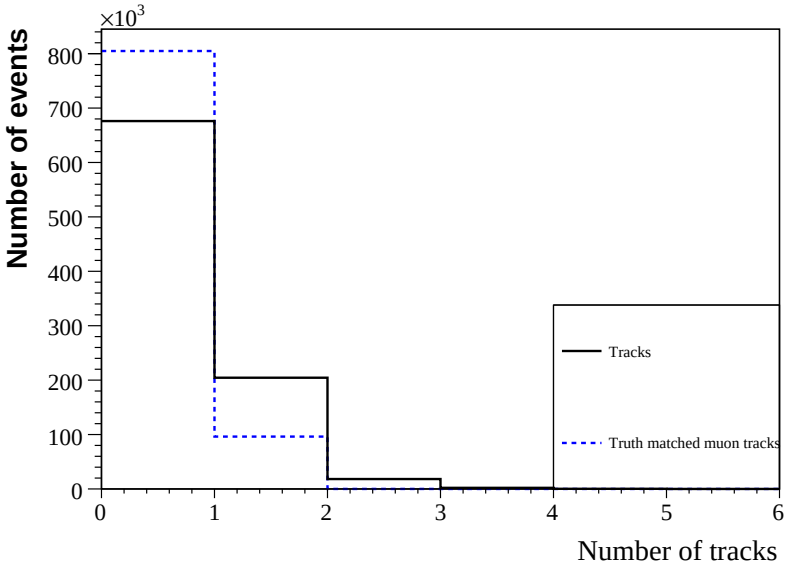

Figure 4.1: Number of probe tracks / truth matched muon tracks per event in which a tag muon was found (Stew_AllEvents_100pb, see table 4.1).

All events in which such a probe track was selected enter an invariant mass histogram called "mt(i, j)" according to equation (4.1) where the indices i and j stand for the (p_T, η)-bin to which the probe track corresponds. If the probe track is subsequently identified as a global / tracker muon the invariant mass enters a second histogram called "mm(i, j)".

To get efficiencies in p_T (η)-dependence a fine (coarse) p_T- and a coarse (fine) η-binning were chosen. This leads to n different efficiency vs. p_T (η) plots, where n is the number of coarse η (p_T)-bins. Details about the chosen bin widths can be found in chapter 5.

4.4 Mass Histogram Fits

To obtain a stable fit procedure two main hurdles had to be taken. On one hand considering figures 3.5 and 3.6 makes clear that the number of mt(i, j) and mm(i, j) histogram entries can vary extensively for varying (i, j) ((p_T, η)-bin). On the other hand the fit procedure should work independently of the background-level which varies with (i, j) within a particular sample but obviously also for different samples. The following section gives a short description of the used samples.

4.4.1 Sample Description

Samples were used from the Spring 07 (SPR07) as well as from the Computing, Software and Analysis 07 (CSA07) production. They were mixed together according to a certain luminosity value in order to get various signal with background samples. Since CSA07 samples were produced with a different CMSSW version they were not mixed with the SPR07 production. The samples are listed in table 4.1 with reference values for N_{evt} and $\mathcal{L}_{gen}$.

Table 4.1: Sample overview. N/A: Not applicable

Sample name	Production	N_{evt}	$\mathcal{L}_{gen}$ [pb^{-1}]
BtoJpsi_152	CSA07	1 M	13.5
BbartoJpsi_152	CSA07	1 M	13.5
Charmonium_0_20_152	CSA07	1 M	3.1
BB2MuMu_noMassCut	CSA07	2.8 M	8.6
Stew_AllEvents_100pb	CSA07	1.8 M	N/A
NonPromptJpsi	SPR07	600 K	4.6
BB2MuMu[4]	SPR07	1 M	7.4

The CSA07 data consists of more than 150M events of various SM processes, roughly representing the first 100 pb^{-1} of LHC data. It consists of three soups each in turn containing various Primary Datasets (PD). Table 4.2 shows the PD contained in the Stew. Since all these PD have different integrated luminosities event weighting has to be applied in order to obtain consistent samples out of the Stew. The event weight is calculated as cross section times luminosity divided by the number of events. However, for the Stew_AllEvents_100pb[5] sample which was used to produce most of the plots in the results chapter[6] no event weighting was considered and thus no luminosity can be given in table 4.1. The sample is therefore not suited for realistic background estimations.

Table 4.2: Primary Datasets contained in the Stew. They were all produced with PHYTIA and filtered.

Datasets	Events	Cross Section x BR	Int. Lum.
BbartoJpsi	509'527	55 mb	9.26 / μb
BtoJpsi	556'324	55 mb	10.12 / μb
QCD_Pt_0_15	733'104	55 mb	0.195 / fb
Bottomonium_Pt_0_20	972'597	9.09 μb	0.1 / pb
Bottomonium_Pt_20_inf	1'107'068	37.9 nb	0.03 / fb
Charmonium_Pt_0_20	1'021'134	0.354 mb	2.9 / nb
Charmonium_Pt_20_inf	1'012'650	0.101 μb	10.0262 / pb
bbe_Pt_5_50	2'907'738	55 mb	52.868 / μb
bbe_Pt_50_170	2'910'966	24.3 μb	0.119793 / pb
bbe_Pt_170_up	2'599'997	0.13 μb	20 / pb
Electron_ppEleX	8'682'737	55 mb	157.868 / μb
Muon_ppMuX	20'697'806	55 mb	376.324 / μb

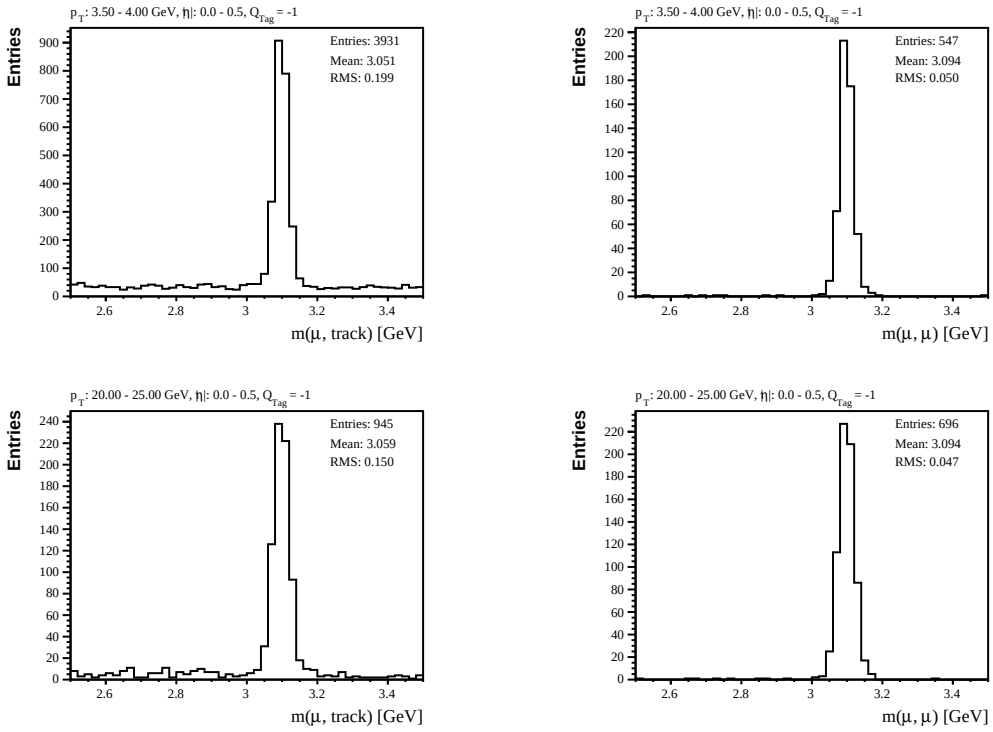

Figure 4.2: muon-track and muon-muon histograms for two different p_T-bins in the central (barrel) region (Stew_AllEvents_100pb). Entries in muon-muon histograms were selected as global muons.

4.4.2 Fitting

Figure 4.2 shows examples of mass histograms. The comparison of muon-track with muon-muon histograms shows that requiring the track to be a global muon reduces background and thus leads to an improvement of the mean (compared with $m_{J/\psi} = 3096.916 \pm 0.011$ MeV [W.-06] and a smaller RMS error[7]. As can be seen the number of entries is large and the efficiency is low in the $3.5 < p_T < 4.0$ GeV bin and on the other side there are less entries in the $20.0 < p_T < 25.0$ GeV bin where the efficiency is high. The number of entries is governed by the (p_T, η)-distribution (see figures 3.5 and 3.6).

The fits were performed using the C++ framework "root" developped at CERN [BR$^+$01]. It offers the choice between χ^2-minimizing and binned log-likelihood fits. The latter option was chosen because it is advantageous for low-entry histograms with low signal to background ratio.
Fitting a histogram in root requires the prior choice of a fit function as well as the specification of initial values for its parameters. Hence, there are basically two possibilities to affect fitting results:

1. Adroitly chosen initial values will augment the probability for the fit to converge towards the global extremum.
2. Restricting allowed parameter ranges will prevent the fit procedure to converge towards possible local extrema which are not the global extremum. On the other hand too tight constraints could exclude the global extremum from the allowed parameter space and lead to wrong errors if the fit procedure ends in regions close to the parameter range borders.

For the above reasons the focus was on the determination of the initial values with adequate precision such that restrictions could be avoided, if possible. These issues are discussed extensively in the following.

Figure 4.2 suggests the choice of a Gaussian fit function for the signal and a linear function $\tilde{g}$ for the background:

$$\begin{aligned} \tilde{f}(m) &:= \tilde{g}(m) + a_2 \cdot exp(-\frac{(m-a_3)^2}{a_4^2}) \\ \tilde{g}(m) &:= a_0 + a_1 \cdot m \end{aligned} \tag{4.5}$$

The tilde denotes the function before fitting, the variable m is the invariant mass of the tag muon + track combination and the a_j (j = 0, 1, 2, 3, 4) are the estimated initial values of the fit parameters.

[5]The calibration / alignment constants are based on a 100 pb^{-1} sample.
[6]If not, it will be explicitely mentioned.
[7]Denoted as RMS, since for historical reasons this is the name of the *root* function giving the RMS error.

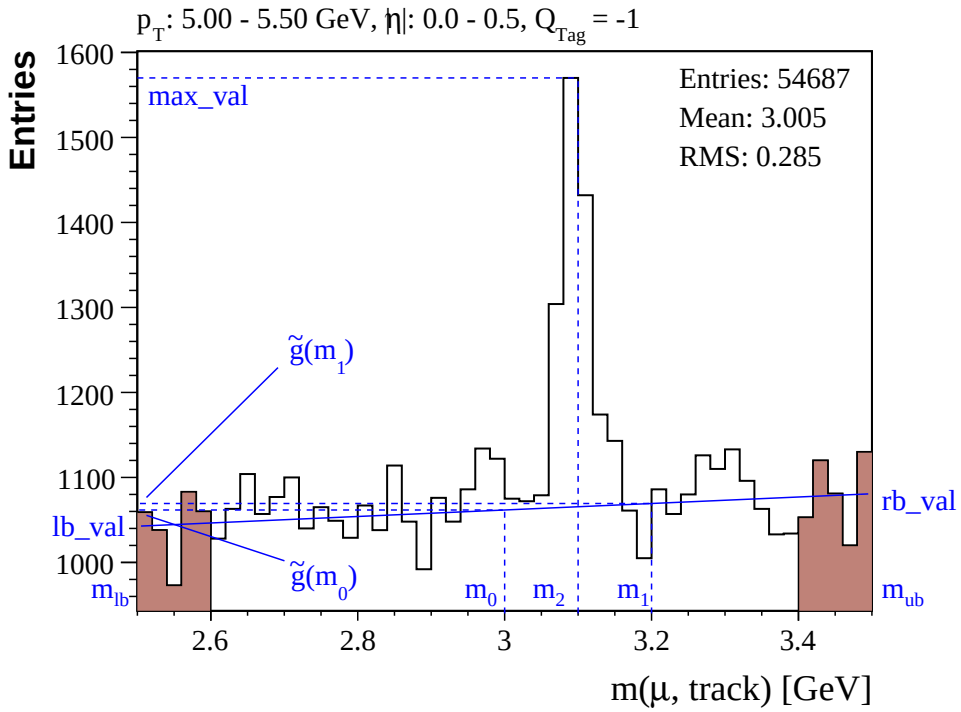

Figure 4.3: A low-p_T muon-track mass histogram is shown. For demonstrative reasons its signal to background ratio was tuned to be around 0.5 and the slope of the linear background function $\tilde{g}$ was multiplied with 50. Therefore 52'937 artificial background events have been added. (see section 4.4.3).

Slope of background fit function: a_1

The initial slope value is calculated from:

$$a_1 = \frac{\text{rb\_val} - \text{lb\_val}}{m_{ub} - m_{lb}} \tag{4.6}$$

m_{lb} and m_{ub} are chosen to be the lower and upper edge of the histogram invariant mass range and lb_val / ub_val are calculated as arithmetic means of the first / last 10 % of bins as shown in figure 4.3.

Figure 4.3 shows a low-p_T muon-track mass histogram. There was added artificial background in order to illustrate the determination of the parameter more clearly. The absolute level of the slope was augmented by a factor of 50. The linear function $\tilde{g}$ is directly given by the calculated initial values a_0 and a_1. Therefore, figure 4.3 is an example demonstrating that $\tilde{g}$ already fits well the background distribution even before χ^2- / log-likelihood optimization is applied.

Constant of Background Fit Function: a_0

a_0 is obtained from a_1, and e.g. m_0 with $\tilde{g}(m_0)$:

$$a_0 = \tilde{g}(m_0) - a_1 \cdot m_0 \tag{4.7}$$

Constant of Gauss Fit Function: a_2

a_2 was calculated by first determining the bin with maximal bin content. It could then be assigned to the mass value m_2 shown in figure 4.3. Considering that the J/ψ-peak might only be a local maximum the search is restricted to the range 3.0 - 3.2 GeV around the J/ψ-peak. If max_val is known a_2 is given by:

$$a_2 = \text{max\_val} - \tilde{g}(m_2) \tag{4.8}$$

Expectation Value of Gauss Function: a_3

The expectation value of the Gauss function corresponds to the measured J/ψ-mass which can be compared with 3096.916 $\pm$ 0.011 MeV [W.-06]. As in chapter 5 is shown the reconstructed J/ψ-mass varies in (p_T, η). The initial value for a_3 was chosen to be constantly 3.1 GeV.

Standard Deviation of Gauss Function: a_4

Fitting various muon-track / muon-muon mass histograms using several samples it turned out that the fit stability is not very sensitive on the initial value of a_4. Motivated by the mass resolution distribution (σ) of the J/ψ which will be shown in figures 5.3 and 5.7 a constant initial value of $a_4 = 0.03$ GeV was chosen.

Parameter Restrictions

Table 4.3 shows the applied restrictions. Their choice corresponds to a coarse estimation of the occuring maximal / minimal values considering mean- / σ-plots of the samples described in table 4.1.

Table 4.3: Parameter restrictions applied to the linear + Gaussian fit function.

a_0	a_1	a_2	a_3	a_4
none	none	none	3.05 - 3.15 GeV	0.012 - 0.05 GeV

4.4.3 Artificial Background

In the previous section a_0 - a_4 denoted the initial values of the fit parameters before fitting. In order to add artificial background, which was implemented as an option, first a fit of the original histogram is performed. The resulting fit parameters are then denoted

as p_0, p_1, A, μ and σ. The addition of artificial background was implemented such that the resulting signal to background ratio S'/B' and slope of the linear function p_1' can both be varied in order to validate the fit procedure. In chapter 5 it will be shown how Tag and Probe efficiency values vary with S'/B'. Artificial background was generated under the already previously made assumption that real background is well approximated by a linear fit function. S'/B' and p_1' are then the inputs governing the background addition to a given histogram. According to equation (4.5) S' and B' can approximately be calculated as

$$S' \approx f_{BG}(\mu) - g_{BG}(\mu) = A \cdot exp(-(\frac{m-\mu}{\sigma})^2) \mid_{m=\mu} = A \tag{4.9}$$

$$B' \approx g_{BG}(\mu) = p_0' + p_1' \cdot \mu \tag{4.10}$$

where the parameters of the Gaussian are left unchanged by the background addition. Thus, S'/B' is nearly given by

$$S'/B' \approx \frac{A}{p_0' + p_1' \cdot \mu} \tag{4.11}$$

which can be solved for the background constant p_0' after the addition of artificial background:

$$p_0' = \frac{A}{S'/B'} - p_1' \cdot \mu \tag{4.12}$$

The number of added background entries was calculated with

$$N_{BG} = \left\lfloor \frac{1}{\Delta m} \cdot \int_{m_{lb}}^{m_{ub}} g_{BG}(m) dm \right\rfloor \tag{4.13}$$

with the constant histogram bin width Δm.

4.5 Systematics

Efficiencies represent the geometrical and conceptual design of the detector and depend on the kinematic properties of the muons. However, using the Tag and Probe method particular decisions which restrict the procedure in its generality had to be made. These decisions give rise to systematic errors and are therefore discussed in the following. Estimations of the systematic errors may be found in chapter 5.

4.5.1 Choice of the Fit Function

Using a Gaussian to fit the signal part of the mass histograms was justified rather pragmatically. Indeed, as in chapter 5 is shown the invariant mass of a J/ψ is a function of its (p_T, η) such that it increases with both. Since all mass histograms contain entries corresponding to different (p_T, η), the effective distribution is an overlap of Gaussians generally leading to an asymmetric total distribution. If the binning is fine enough the deviation from the Gaussian shape should be small and the next simplest approach is to

consider a double Gaussian (sum of two Gaussians) fit function. Since the linear background function was kept, this gives rise to three more parameters whose initial values and allowed ranges have to be determined such that the stability of the fitting procedure is maintained. The fit function then looks as follows:

$$f_{DG}(m) := a_0 \cdot m + a_1 + a_2 \cdot exp(-\frac{(m-a_3)^2}{a_4^2}) + a_5 \cdot exp(-\frac{(m-a_6)^2}{a_7^2}) \tag{4.14}$$

Since the second Gaussian should only introduce a small correction accounting for the asymmetry somewhere in the range m > $m_{J/\psi}$[8] its influence on the shape of the 'main' function is neglected and the parameter calculation scheme for a_0, a_1 and a_2 was simply adopted from the single Gaussian fit. Since the parameter space of a double Gaussian is expected to offer more local extrema for minimization / maximization fit procedures it is restricted more stringently compared to the fit function including the single Gaussian. All initial values and restrictions can be seen from table 4.4.

Table 4.4: Fit parameters for linear background function with double Gaussian. p_0, p_1 and GaussMax are determined for every histogram in the same way as for a single Gaussian (section 4.4.2). The average (Av) is calculated as arithmetic mean of the values from the first 50 and the last 20 bins of the histogram (total 100 bins) which is an approximate choice to exclude the peak region.

Parameter	a_0	a_1	a_2	a_3
Initial Value	p_0	p_1	GaussMax	3.1
Lower Limit	-0.04·GaussMax	0.8· Av	0.6·GaussMax	3.05
Upper Limit	0.6·GaussMax	1.2· Av	1.5·GaussMax	3.15
Parameter	a_4	a_5	a_6	a_7
Initial Value	0.03	0.2·GaussMax	3.15	0.01
Lower Limit	0.01	0.05·GaussMax	3.1	0.04
Upper Limit	0.05	0.25·GaussMax	3.2	0.09

4.5.2 Tag Charge Difference

As described in section 4.2, tag muons are accepted only if they have the required charge and efficiencies are evaluated only on muons from the opposite charge. It is not expected that efficiencies are different on positively and negatively charged muons. Therefore, a possible difference will contribute to the systematic error.

4.5.3 Pass - fail vs. Normalization method

According to the normalization method [Mar01] efficiencies may be expressed as

$$\epsilon(\text{test, control}) = \frac{\text{N(test, control)}}{\text{N(none, control)}} \tag{4.15}$$

[8]This condition is derived from experimental evidence.

with 'test' and 'control' appropriately defined. This was the method as used so far. But since N(test, control) and N(none, control) are obtained from a fit, efficiencies can exceed the value of one. The Pass-fail method [Mar01] defines efficiencies as

$$\epsilon(\text{test, control}) = \frac{\text{N(test, control)}}{\text{N(test, control)} + \text{N}(\overline{\text{test}}, \text{control})} \tag{4.16}$$

and thus efficiencies can not exceed one, provided the fit results are not negative. On the other hand the Pass-fail method requires fitting of histograms belonging to N($\overline{\text{test}}$, control). These histograms contain background and not reconstructed / identified muons such that, given the case that efficiencies are high, they will show a poor signal to background ratio. Fitting such histograms is analyzed in section 5.4 of chapter 5.

In order to obtain muon reconstruction / identification efficiencies the control and test sets have to be defined such that the control set contains all events in which a tag muon and a track satisfying all selection criteria (see section 4.2) were found and "test" selects the subset of elements of the control set in which the track was matched to a global / tracker muon.

If the yields were known exactly, there would not be any difference between the application of the Normalization / Pass-fail method, however, since they are not, both terms in (4.16) are statistically independent and simple error propagation from the calculated numbers of histogram entries to the efficiencies as in (4.17) can be applied.

$$\langle \Delta\epsilon_{tc} \rangle = \sqrt{(\frac{\partial\epsilon}{\partial N_{tc}} \langle \Delta N_{tc} \rangle)^2 + (\frac{\partial\epsilon}{\partial N_{\bar{t}c}} \langle \Delta N_{\bar{t}c} \rangle)^2} \tag{4.17}$$

Where N_{tc} and $N_{\bar{t}c}$ were used as shortcuts for N(test, control) and N($\overline{\text{test}}$, control).

In 4.15, N(test, control) and N(none, control) depend on each other and binomial errors are calculated for efficiencies.

$$\langle \Delta\epsilon_{tc} \rangle = \frac{1}{N_{nc}} \sqrt{\left| (1 - 2\frac{N_{tc}}{N_{nc}}) \Delta N_{tc}^2 + (\frac{N_{tc}}{N_{nc}})^2 \Delta N_{nc}^2 \right|} \tag{4.18}$$

Where N_{tc} and N_{nc} stand for N(test, control) and N(none, control).

4.5.4 χ^2- vs. Binned Maximum Likelihood Fit

Fitting in *root* uses the minimization packet 'Minuit' originating from FORTRAN and can either be performed with a χ^2- or binned maximum likelihood method (ML). Minuit contains the program part 'Migrad' which minimizes the corresponding function and assigns parabolic errors to the bin values, as well as 'Minos' which can be used additionally as an option for better error estimations. The default procedure is χ^2-minimization with parabolic errors, however, binned likelihood was chosen because this is more reliable for

histograms with a low number of entries. Improved error estimation using Minos was applied.
Both methods are shortly described in the following. For details see [COW98].

χ^2-Method

For a bin with N entries the χ^2 - method assigns an error of $\sqrt{N}$. As a measure for the quality of the fit the ratio χ^2/dof is considered where χ^2 for a fit function f is defined as

$$\chi^2 = \sum_{i=0}^{n} (N_i - f(m_i; a_0, ..., a_k))^2, \tag{4.19}$$

with m_i the mass value corresponding to the i-th bin, N_i the number of entries in the i-th bin and the a_i are the parameters of the fit function. They are determined by the fitting procedure such that χ^2 is minimized. The number of degrees of freedom (dof) is equal to the number of bins of the mass histogram minus the number of parameters of the fit function. A fit is considered to be good if $\chi^2/\text{dof} \sim 1$.

Binned Maximum Likelihood Method (ML)

Each mass histogram with N bins containing entries $\vec{n} = (n_1, \ldots, n_N)$ can be considered as a single measurement of an N-dimensional random vector for which the joint probability distribution function (p.d.f.) is given by

$$f_{joint}(\vec{n}, \vec{\nu}) = \frac{n_{tot}!}{n_1! \ldots n_N!} (\frac{\nu_1}{n_{tot}})^{n_1} \ldots (\frac{\nu_N}{n_{tot}})^{n_N} \tag{4.20}$$

ν_i is the expectation value for the i-th bin given by

$$\nu_i(\vec{a}) = n_{tot} \int_{m_i^{min}}^{m_i^{max}} f(m, \vec{a}) dm \tag{4.21}$$

n_{tot} is the total number of histogram entries and m_i^{min} / m_i^{max} are the bin edges of the i-th bin. The log-likelihood function is then given by the logarithm of the joint p.d.f.:

$$\log L(\vec{a}) = \sum_{i=1}^{N} n_i \log \nu_i(\vec{a}) + \text{Terms independent from } \vec{a} \tag{4.22}$$

where $\vec{a} = (a_1, \ldots, a_n)$ denotes the parameter vector of the fit function f. Maximizing this expression[9] gives the set of parameters $\vec{a}$. In the limit of large N or small bin widths the likelihood function becomes the same as that of the maximum likelihood method without bins [COW98]. Thus, the binned ML technique is safe if some of the bins have few or no entries.
As goodness-of-fit criterion simply χ^2/dof defined as for χ^2-minimization may be considered.

[9] For practical reasons its negative value is minimized.

5 Results

Following the logic of the Tag and Probe method, first mass histogram fit results and corresponding integral values are discussed. Then, efficiency plots for global and tracker muons are shown and compared with the MC plots followed by the analysis of the behaviour of Tag and Probe efficiency results under addition of artificial background and finally the systematic error is estimated. Up to then, error indications will only contain the statistical contribution.

5.1 Mass Histogram Fits

5.1.1 Binnings

Motivated by the transverse momentum distribution shown in figure 3.6 the p_T-bin edges were chosen as shown in table 5.1. Since the η-distribution of muons is more homogeneous there was no stringent reason to choose the binning adequately.

Table 5.1: Used p_T- and η-bin edges for the mass histograms.

Binning	Number of Bins									
Fine p_T	24	0.0	0.5	1.0	1.5	2.0	2.5	3.0	3.5	4.0
		4.5	5.0	5.5	6.0	6.5	7.0	7.5	8.0	8.5
		9.0	9.5	10.0	12.5	15.0	20.0	25.0		
Coarse p_T	5	3.0	4.0	5.0	7.0	10.0	25.0			
Fine η	10	-2.5	-2.0	-1.5	-1.0	-0.5	0.0	0.5	1.0	1.5
		2.0	2.5							
Coarse $\lvert\eta\rvert$	3	0	0.5	1.0	2.5					

As already mentioned in chapter 4, efficiencies in p_T- / η-dependence are obtained combining the fine p_T- / η-binning with the coarse η- / p_T-binning.

5.1.2 Global and Tracker Muon Mass Histogram Fits

All mass histogram fits which were produced to obtain the efficiency vs. p_T plots 5.9 and 5.14 from section 5.2 can be found in the appendixes B and C. They contain the total number of entries governed by the (p_T, η)-distribution (3.5), the mean of all histogram entries, their standard deviation, followed by the fit specific values: χ^2/dof as a measure of goodness-of-fit, the fit probability Prob(χ^2, dof) which is $\gtrsim 0.05$ for a good fit as well as all fit parameters, the integral values with errors (section 5.3.1) and finally the signal

to background ratio S/B.

As can be seen from the histograms, the mean (σ) of the reconstructed J/ψ depend on (p_T, η). This is confirmed by the histograms 5.1 - 5.4. Generally χ^2/dof is increasing with $|\eta|$ (binned) and the fit probability is usually accordingly low in the range $1.0 < |\eta| < 2.5$ which may hint at a lower fit quality in this range. Further, S/B values tend to increase with p_T and decrease with $|\eta|$.
The mass histogram fits belonging to the range 2 GeV $< p_T <$ 3 GeV illustrate that muons are not reconstructed / identified below 3 GeV unless they are in the η-range $1.0 < |\eta| <$ 2.4 (endcap regions). This may again be explain with the fact that low-p_T in the barrel region implies low energy but does practically not restrict muon energies in the endcap regions.

How close the background level of the considered mass histograms comes to reality is unknown. Event weights were not considered in the Stew_AllEvents_100pb sample. How this affects the background level is not known. Further, Stew_AllEvents_100pb only contains ∼1.8M of the total ∼40M events of the Stew which questions the significance of the observed average background level. To estimate how efficiency values behave if background is added, see section 5.4.

5.1.3 Reconstructed J/ψ-Mass and its Resolution σ

Figures 5.1, 5.2, 5.5 and 5.6 show that the reconstructed J/ψ-mass drops in the barrel region but is rather independent of $p_T^{J/\psi}$. Comparing the reconstructed J/ψ-mass values with 3096.916 ± 0.011 MeV [W.-06] shows that this value is closer approached in the central region. Since each mass histogram includes entries in a finite (p_T, η)-range the Gaussian mass peak will in general be asymmetric. This was the original motivation for the alternative choice of a double Gaussian as a fit function and is now confirmed by the fit results.

5.2 Global and Tracker Muon Efficiencies

Figures 5.9 and 5.10 both show global muon reconstruction efficiencies. 5.9 shows the dotted Tag and Probe efficiency as well as the efficiency evaluated on all truth matched muon tracks in the Stew_AllEvents_100pb sample and the efficiency evaluated only on the subset of truth matched muon tracks which passed all selection criteria from section 4.3. There is no physical reason why the two MC histograms should differ as they do in the figures.

The difference on the plateau is strongly reduced for the efficiency on all truth matched muon tracks if only those are considered which originate from a J/ψ decay (see figure 5.11). This leads to the conclusion that the difference may rather be ascribed to a peculiarity of the sample than a bug in the code. Efficiency determinations on other samples,

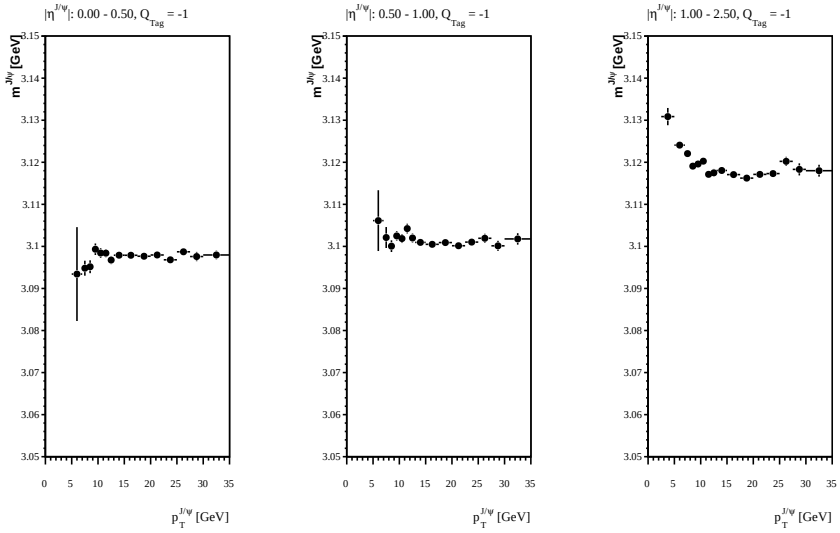

Figure 5.1: Reconstructed J/ψ-mass vs. $p_T^{J/\psi}$ for global muons.

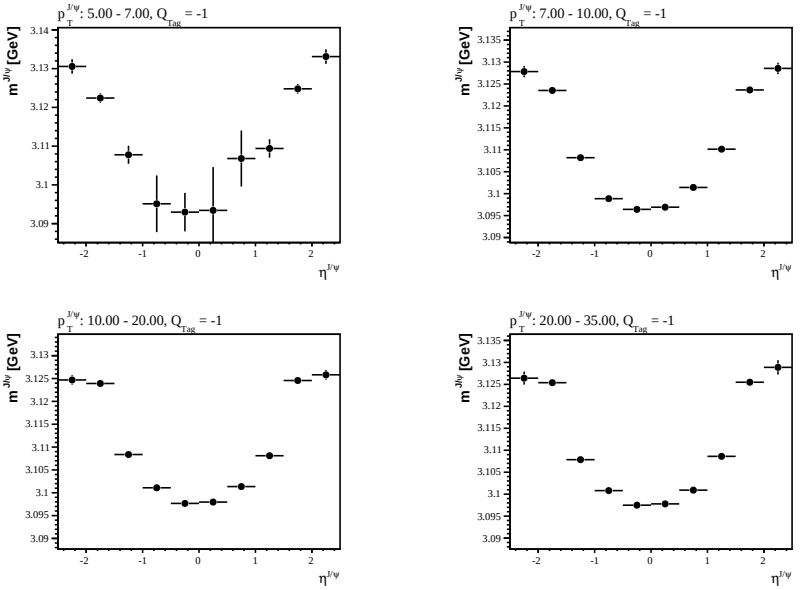

Figure 5.2: Reconstructed J/ψ-mass vs. $\eta^{J/\psi}$ for global muons. $p_T^{J/\psi}$ is above 5 GeV because of the required p_T-thresholds for the tag muon (3 GeV) and the probe track (2 GeV).

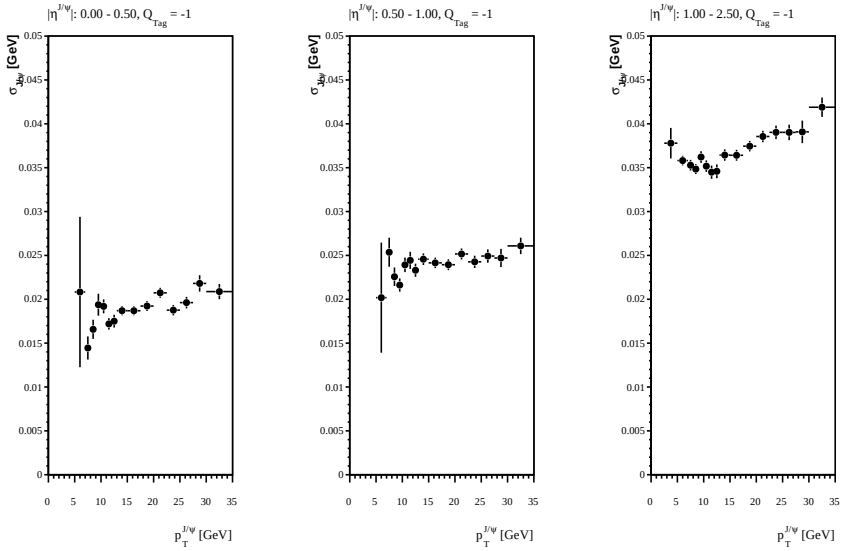

Figure 5.3: J/ψ-mass resolution σ vs. $p_T^{J/\psi}$ for global muons.

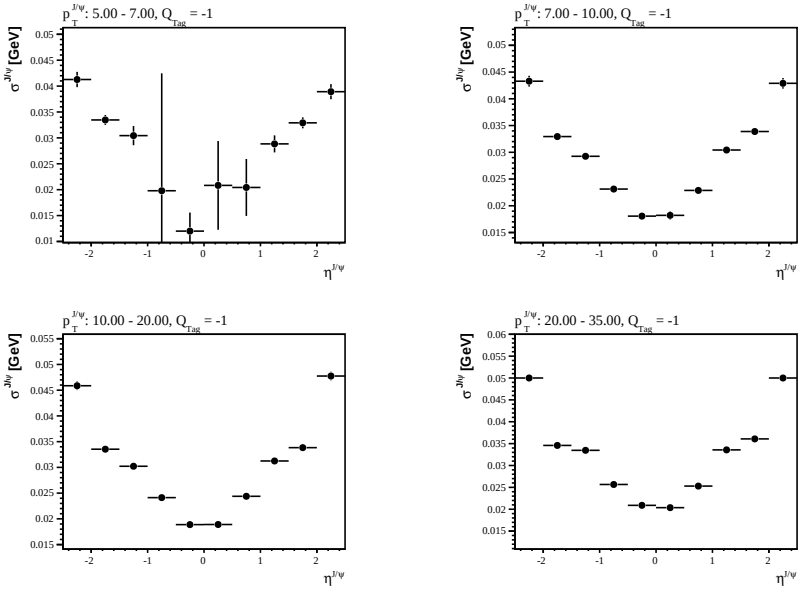

Figure 5.4: J/ψ-mass resolution σ vs. $\eta^{J/\psi}$ for global muons. $p_T^{J/\psi}$ is above 5 GeV because of the required p_T-thresholds for the tag muon (3 GeV) and the probe track (2 GeV).

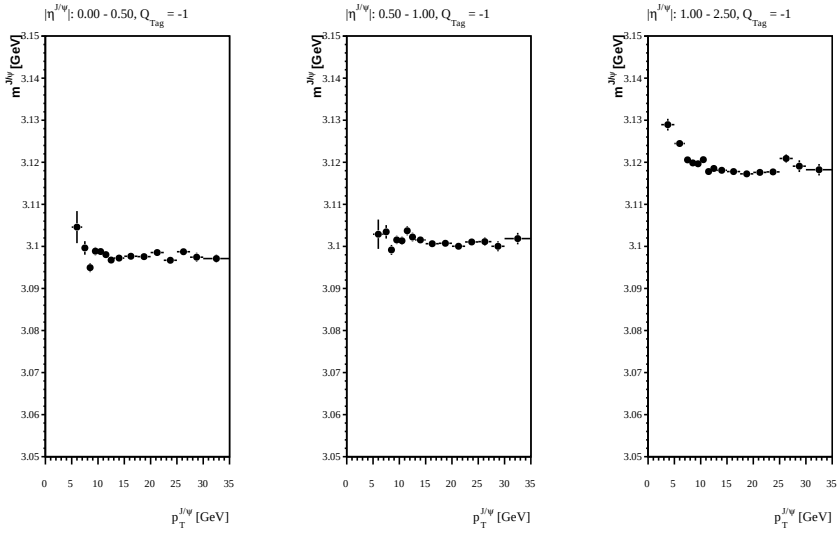

Figure 5.5: Reconstructed J/ψ-mass vs. $p_T^{J/\psi}$ for tracker muons.

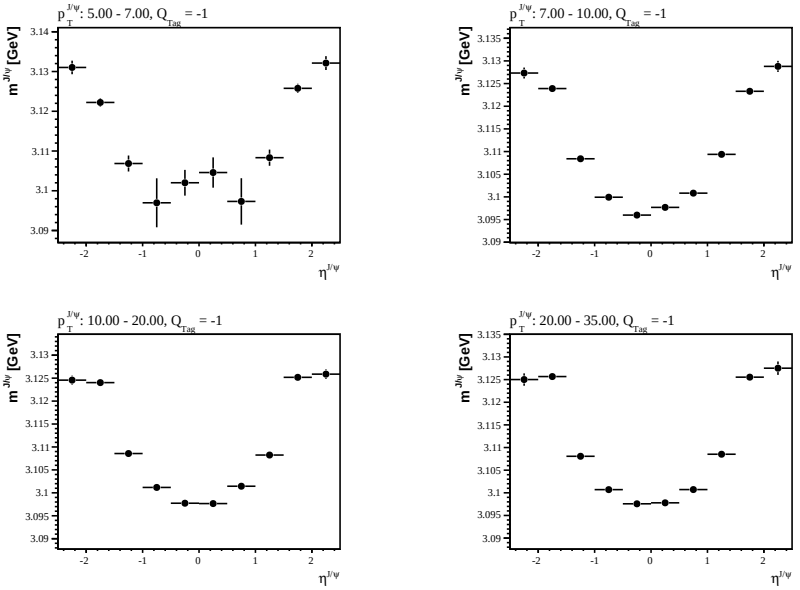

Figure 5.6: Reconstructed J/ψ-mass vs. $\eta^{J/\psi}$ for tracker muons. $p_T^{J/\psi}$ is above 5 GeV because of the required p_T-thresholds for the tag muon (3 GeV) and the probe track (2 GeV).

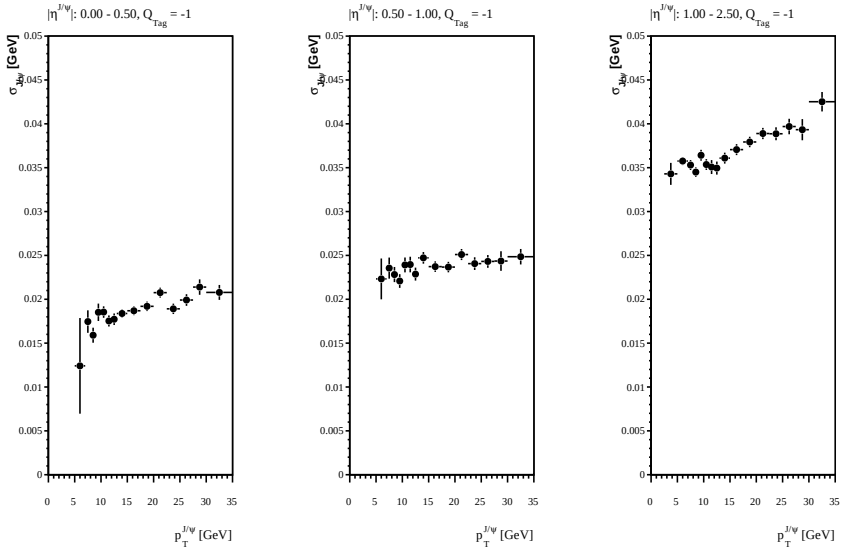

Figure 5.7: J/ψ-mass resolution σ vs. $p_T^{J/\psi}$ for tracker muons.

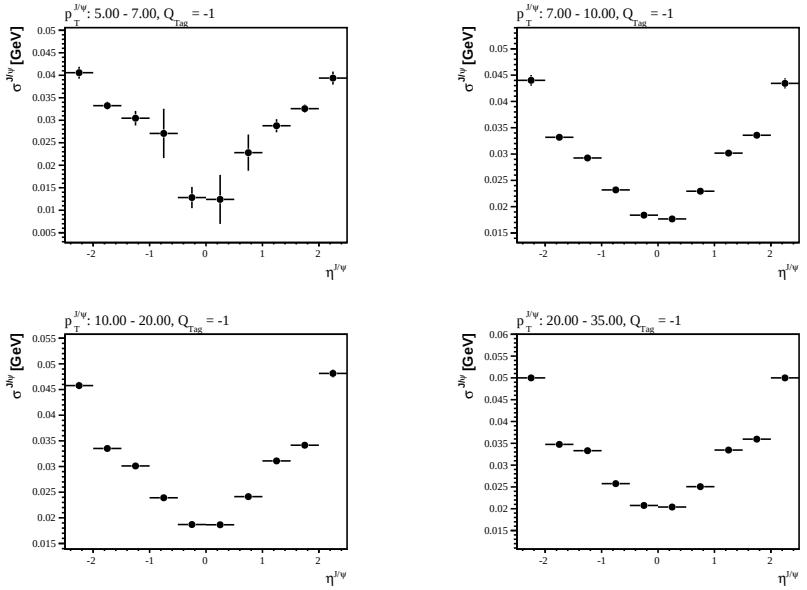

Figure 5.8: J/ψ-mass resolution σ vs. $\eta^{J/\psi}$ for tracker muons. $p_T^{J/\psi}$ is above 5 GeV because of the required p_T-thresholds for the tag muon (3 GeV) and the probe track (2 GeV).

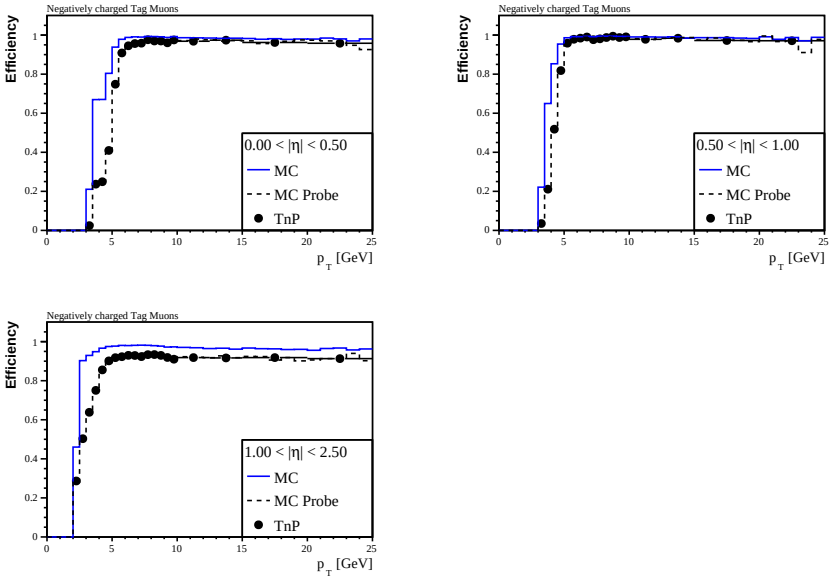

Figure 5.9: Global muon reconstruction efficiency vs. p_T for positively charged muons in different $|\eta|$-bins (Stew_AllEvents_100pb).

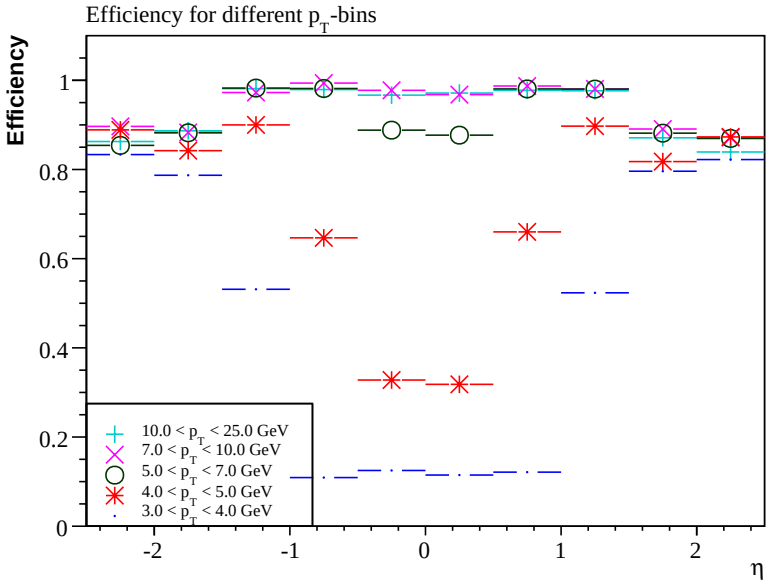

Figure 5.10: Global muon reconstruction efficiency vs. η for positively charged muons in different p_T-bins (Stew_AllEvents_100pb).

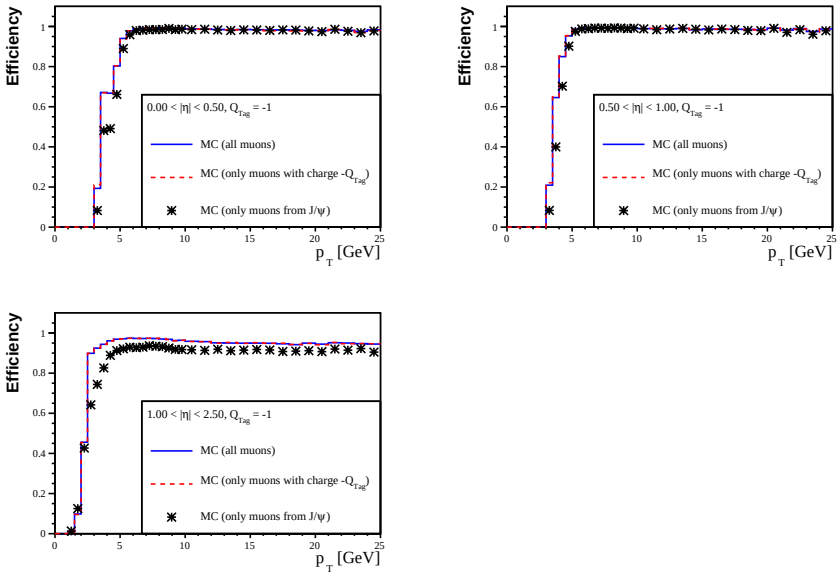

Figure 5.11: Comparison between global muon MC efficiencies. The curve of all muons clearly coicides with the one of only positively charged muons. The restriction to muons only from MC J/ψ leads to a deviation similar to the one observed in figure 5.9 (Stew_AllEvents_100pb).

where the two histograms coincide support this assumption. Further, the MC probe is clearly consistent with the TnP efficiency. Figure 5.12 shows the completely analogous efficiency plots for global muons based on a combined SPR07 sample with BB2MuMu and NonPromptJpsi mixed at $\mathcal{L} \approx 3.1$ pb^{-1} (426'514 + 409'574 = 836'088 events). The corresponding plots for a mixed CSA07 sample containing BB2MuMu_noMassCut and BbartoJpsi_152 at $\mathcal{L} \approx 5.9\ pb^{-1}$ (1'915'192 + 435'124 = 2'350'316 events) are shown in figure 5.13. The MC and MC Probe efficiencies agree well on the SPR07 samples but not on the CSA07 samples.

Comparing the plots for global muons with those for tracker muons the expected difference in the low-p_T region is visible. Figures 5.10 and 5.15 show the η-dependence of efficiencies which agree with the generator level plots 3.2 and 3.4 in their principle behaviour, however their resolution is too coarse such that the mentioned efficiency drops for particular η-values could not be reproduced. In order to improve the η-resolution without increasing the statistical error a larger sample would be necessary.

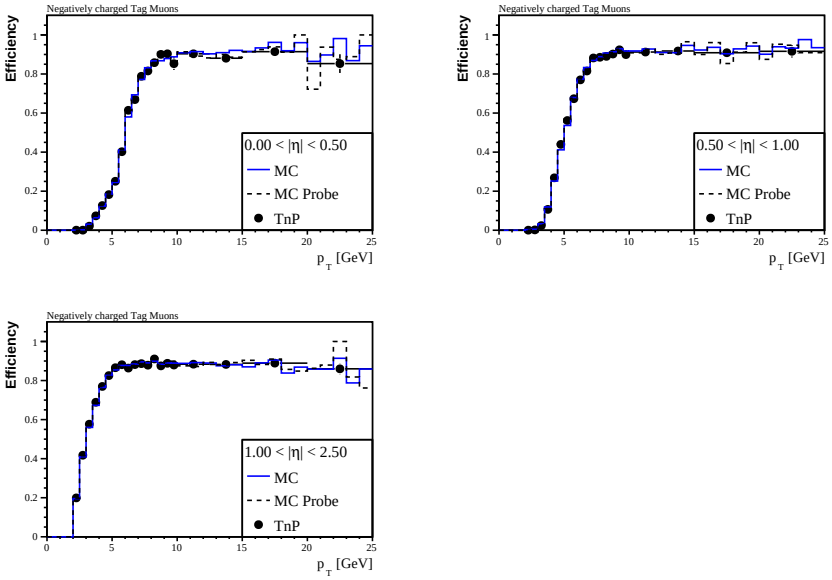

Figure 5.12: Global muon reconstruction efficiency vs. p_T for positively charged muons in different $|\eta|$-bins produced with a combined SPR07 sample containing 426'514 NonPromptJpsi and 409'574 BB2MuMu events corresponding to an integrated luminosity of $\mathcal{L} \approx 3.1$ pb^{-1}.

5.3 Error Estimation

5.3.1 Statistical Errors

As already mentioned the error bars drawn in the previously shown plots only account for the statistical uncertainty. The corresponding errors on efficiencies were propagated from the integral errors printed on the mass histogram fits (appendixes B and C) according to the equations given in section 4.5.3. The errors on the integral values were calculated using *root*. They were determined according to the errors assigned to the estimated parameter values after the fit considering the covariance matrix resulting from the fit. The parameter errors in turn are estimated with 'Minos'. The integral errors are comparable with the uncorrelated error values given by the square root of the integral values.

5.3.2 Systematic Errors

Origins of systematic uncertainties were discussed in section 4.5. Figures 5.16 and 5.17 show four 1D histograms (Stew_AllEvents_100pb) each containing one of the efficiency differences either for positively / negatively charged tag muons, mass histogram fits with single / double Gaussian, integrals calculated with χ^2- / binned log-likelihood minimization and efficiencies calculated with Normalization / Pass-fail method. Since a possible forward / backward asymmetry might as well reflect some real detector anisotropy and

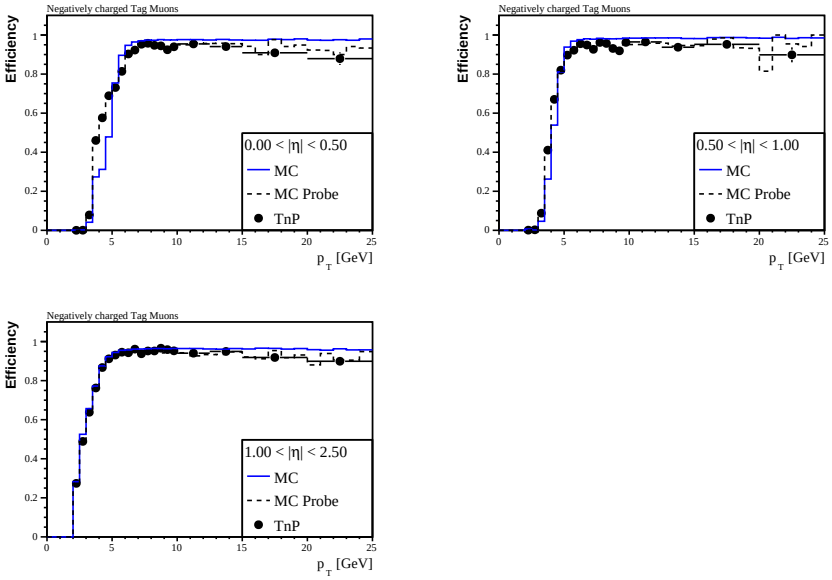

Figure 5.13: Global muon reconstruction efficiency vs. p_T for positively charged muons in different $|\eta|$-bins produced with a combined CSA07 sample containing 1'915'192 BB2MuMu_noMassCut and 435'124 BbartoJpsi_152 events corresponding to an integrated luminosity of $\mathcal{L} \approx 5.9$ pb^{-1}.

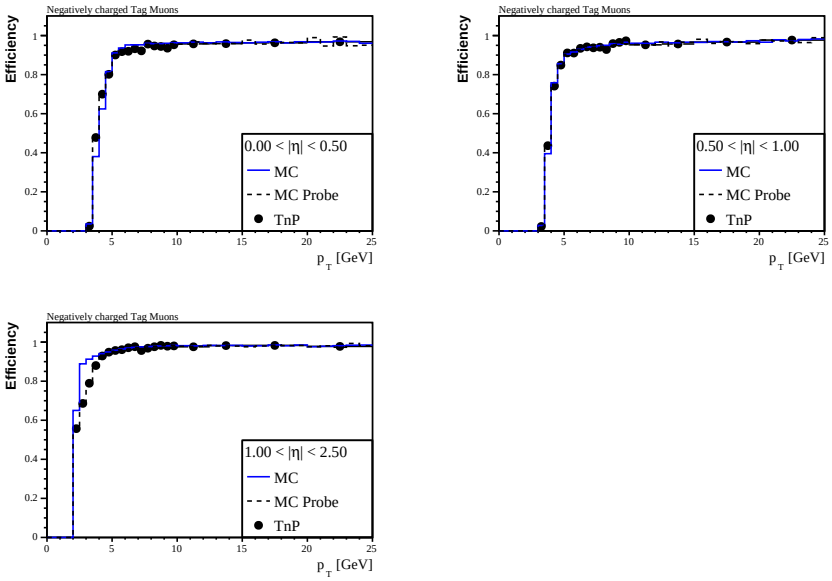

Figure 5.14: Tracker muon identification efficiency vs. p_T for positively charged muons in different $|\eta|$-bins (Stew_AllEvents_100pb).

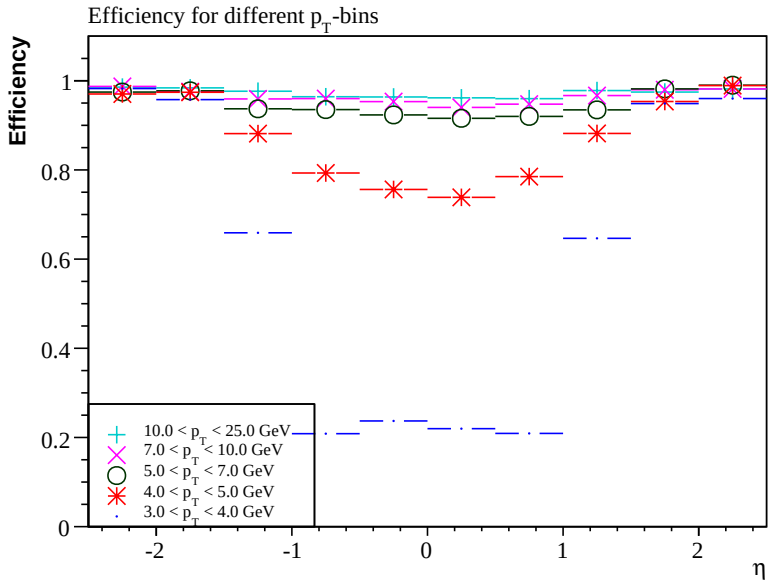

Figure 5.15: Tracker muon identification efficiency vs. η for positively charged muons in different p_T-bins (Stew_AllEvents_100pb).

further, since the efficiency plots 5.9 and 5.14 are based on a $|\eta|$-binning the forward / backward asymmetry contribution was not included in the calculation of the systematic error. The shape of the fit method difference histogram clearly deviates from a Gaussian thus showing that efficiencies calculated with the binned log-likelihood method are systematically higher. The means of the other histograms are compatible with zero, except for the normalization / Pass-fail method difference histogram for tracker muons.

The total systematic error is estimated as

$$\sigma_{sys} = \sqrt{\sigma^2_{+/-} + \sigma^2_{SG/DG} + \sigma^2_{\chi^2/LL} + \sigma^2_{Norm/P-f}} \tag{5.1}$$

where the corresponding standard deviations for global / tracker muon efficiencies are shown in 5.16 / 5.17. They are calculated by *root* using

$$\sigma = \sqrt{\frac{1}{N}\sum_{i=1}^{N}(x_i - \overline{x})^2} \tag{5.2}$$

where $\overline{x}$ is the mean of all histogram entries and x_i stands for the x-axis value of a histogram entry.

Using the values from table 5.2 finally gives

$$\sigma_{sys} \approx 0.017$$

Table 5.2: Standard deviations for global and tracker muon efficiencies

Efficiency	+/-	SG / DG	χ^2 / LL	Norm. / P-f
Global muons	0.01036	0.01285	0.00454	0.00356
Tracker muons	0.01650	0.00983	0.00431	0.00296

for global muons and

$$\sigma_{sys} \approx 0.020$$

for tracker muons. Thus, systematic errors for global and tracker muons are comparable.

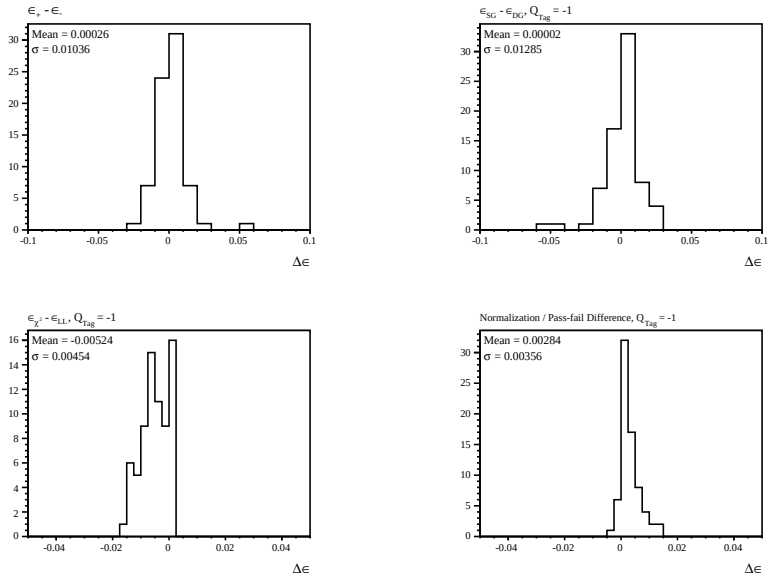

Figure 5.16: Global muon 1D histograms showing differences for positive / negative tag muon charge, SG / DG fits, χ^2 / binned log-likelihood fits and Normalization / Pass-fail method efficiencies.

5.4 Background Estimation

The mass histogram fits from section 5.1 generally exhibit a large S/B. As described in section 4.4.1 this needs not to be realistic and therefore it was examined how lower S/B values affect efficiencies. Figures 5.18 and 5.19 show the difference between the Tag and Probe efficiency and the efficiency of probe tracks which were truth matched to muons in p_T-dependency. Starting with S/B ~ 10, the fluctuations tend to increase with decreasing S/B and $|\eta|$. The differences for global and tracker muon reconstruction efficiencies are comparable.

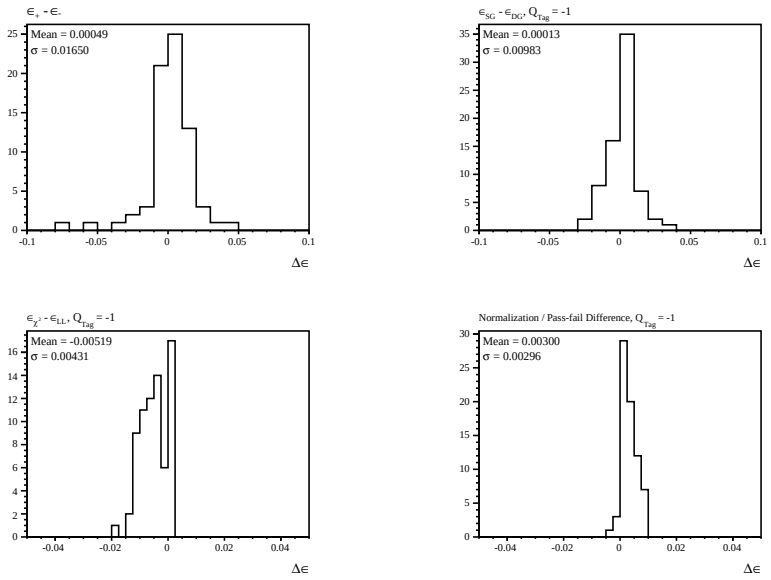

Figure 5.17: Tracker muon 1D histograms showing differences for positive / negative tag muon charge, SG / DG fits, χ^2 / binned log-likelihood fits and Normalization / Pass-fail method efficiencies.

The background slope was left unchanged by the background addition and the influence of its variation on the efficiency difference was not examined.

The plots show that the difference approximately remains below $\sim$0.05 if S/B $\gtrsim$ 5.

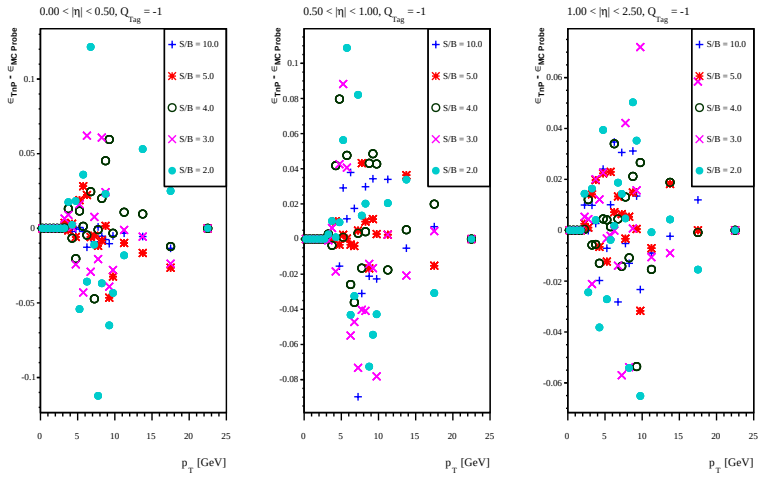

Figure 5.18: Difference between ϵ_{TnP} and $\epsilon_{MCProbe}$ for global muons.

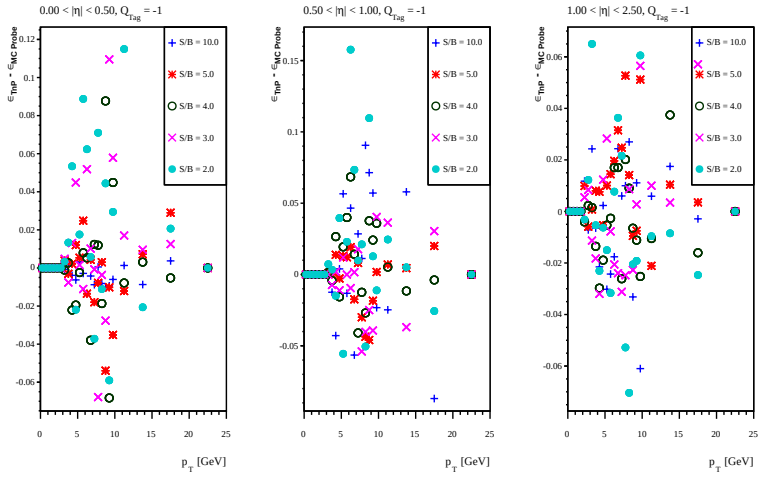

Figure 5.19: Difference between ϵ_{TnP} and $\epsilon_{MCProbe}$ for tracker muons.

6 Conclusions

The aim of this Diploma Thesis was to determine muon reconstruction and identification efficiencies in the CMS experiment using the Tag and Probe method. This was in prinicple established reproducing the MC efficiency plots on probe tracks which were truth matched to muons. However, there remain open questions. MC efficiencies on one hand evaluated on all tracks in the sample which were truth matched to a muon and on the other hand evaluated only on truth matched probe tracks significantly differ for particular samples which has not been understood.

Another relevant uncertainty remaining is the background level, but its effect on efficiencies was estimated.

An additional task could be the determination of L1 muon reconstruction efficiencies which means simply to skip the HLT trigger in order to match already L1 muons with tracks from the inner tracker. This was approached, however, due to the poor p_T-resolution of L1 muons the L1 muon-track matching could only be performed in (η, ϕ)-space, neglecting the effect of the magnetic field on particle trajectories. Such L1 muon reconstruction efficiencies were found to be significantly lower than global / tracker muon efficiencies.

As was exposed in chapter 1 the knowledge of muon reconstruction / identification efficiencies is crucial to determine $\mathcal{B}(B_s^0 \to \mu^+\mu^-)$. It was shown that the Tag and Probe method provides an appropriate tool for this.

Appendix A: Units

In high energy particle physics one usually chooses c = 1 and $\hbar = 1$. Therefore energies, masses, momenta, inverse length and inverse time can all be expressed in the same unit. Typical values for energies, masses and momenta in this work are of the order of GeV. Corresponding length and time scales can be derived from setting the left hand side of the relation

$$\hbar \cdot c \approx 0.2 \text{ GeV} \cdot fm \tag{6.1}$$

to one.

For the sake of simplicity electric charges Q are expressed in units of e which in turn may be defined according to the Gauss system as well as the Heavyside-Lorentz-System.

Appendix B: Global Muon Mass Histogram Fits

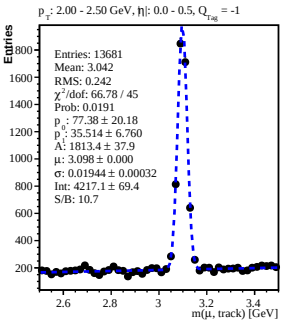

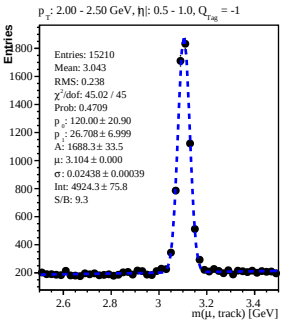

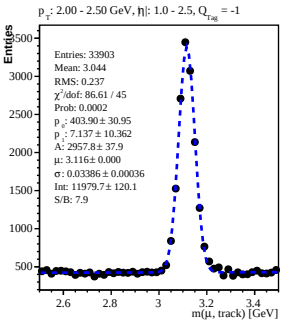

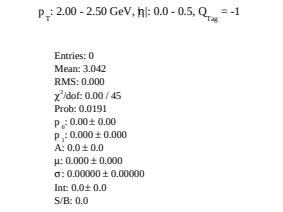

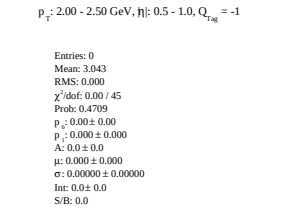

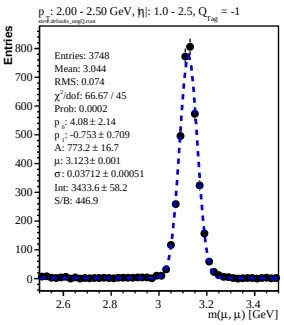

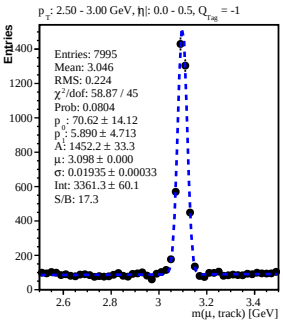

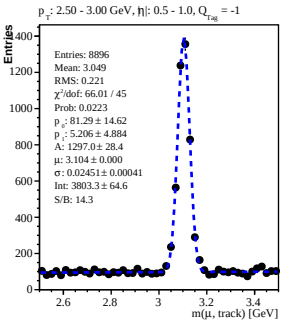

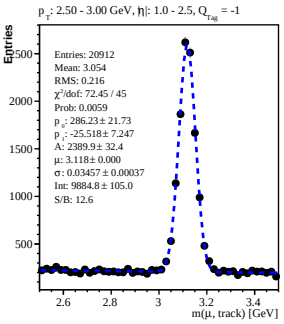

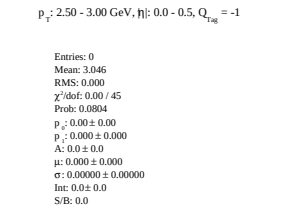

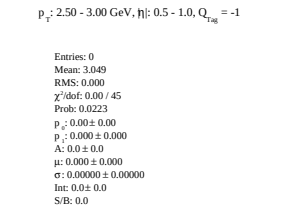

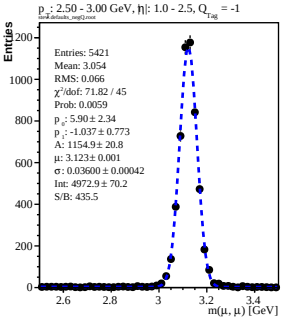

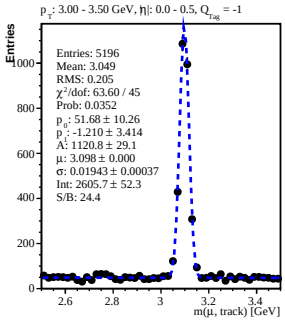
p_T: 3.00 - 3.50 GeV, |η|: 0.0 - 0.5, Q_Tag = -1
Entries: 5196
Mean: 3.049
RMS: 0.205
χ²/dof: 63.60 / 45
Prob: 0.0352
p_0: 51.68 ± 10.26
p_1: -1.210 ± 3.414
A: 1120.8 ± 29.1
μ: 3.098 ± 0.000
σ: 0.01943 ± 0.00037
Int: 2605.7 ± 52.3
S/B: 24.4
Entries
m(μ, track) [GeV]

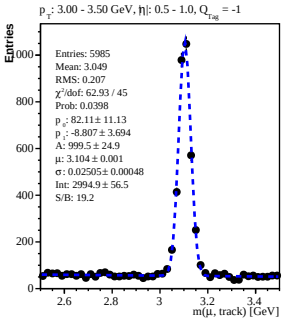
p_T: 3.00 - 3.50 GeV, |η|: 0.5 - 1.0, Q_Tag = -1
Entries: 5985
Mean: 3.049
RMS: 0.207
χ²/dof: 62.93 / 45
Prob: 0.0398
p_0: 82.11 ± 11.13
p_1: -8.807 ± 3.694
A: 999.5 ± 24.9
μ: 3.104 ± 0.001
σ: 0.02505 ± 0.00048
Int: 2994.9 ± 56.5
S/B: 19.2
Entries
m(μ, track) [GeV]

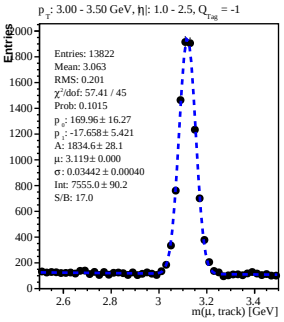
p_T: 3.00 - 3.50 GeV, |η|: 1.0 - 2.5, Q_Tag = -1
Entries: 13822
Mean: 3.063
RMS: 0.201
χ²/dof: 57.41 / 45
Prob: 0.1015
p_0: 169.96 ± 16.27
p_1: -17.658 ± 5.421
A: 1834.6 ± 28.1
μ: 3.119 ± 0.000
σ: 0.03442 ± 0.00040
Int: 7555.0 ± 90.2
S/B: 17.0
Entries
m(μ, track) [GeV]

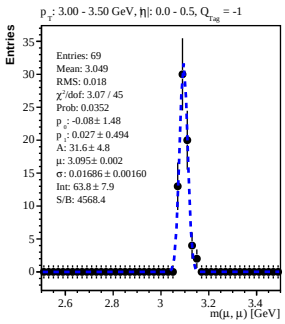
p_T: 3.00 - 3.50 GeV, |η|: 0.0 - 0.5, Q_Tag = -1
Entries: 69
Mean: 3.049
RMS: 0.018
χ²/dof: 3.07 / 45
Prob: 0.0352
p_0: -0.08 ± 1.48
p_1: 0.027 ± 0.494
A: 31.6 ± 4.8
μ: 3.095 ± 0.002
σ: 0.01686 ± 0.00160
Int: 63.8 ± 7.9
S/B: 4568.4
Entries
m(μ, μ) [GeV]

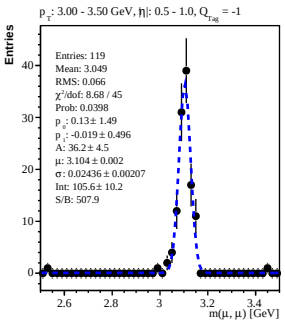
p_T: 3.00 - 3.50 GeV, |η|: 0.5 - 1.0, Q_Tag = -1
Entries: 119
Mean: 3.049
RMS: 0.066
χ²/dof: 8.68 / 45
Prob: 0.0398
p_0: 0.13 ± 1.49
p_1: -0.019 ± 0.496
A: 36.2 ± 4.5
μ: 3.104 ± 0.002
σ: 0.02436 ± 0.00207
Int: 105.6 ± 10.2
S/B: 507.9
Entries
m(μ, μ) [GeV]

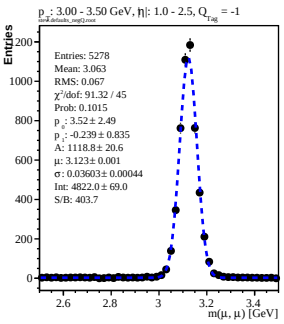
p_T: 3.00 - 3.50 GeV, |η|: 1.0 - 2.5, Q_Tag = -1
Entries: 5278
Mean: 3.063
RMS: 0.067
χ²/dof: 91.32 / 45
Prob: 0.1015
p_0: 3.52 ± 2.49
p_1: -0.239 ± 0.835
A: 1118.8 ± 20.6
μ: 3.123 ± 0.001
σ: 0.03603 ± 0.00044
Int: 4822.0 ± 69.0
S/B: 403.7
Entries
m(μ, μ) [GeV]

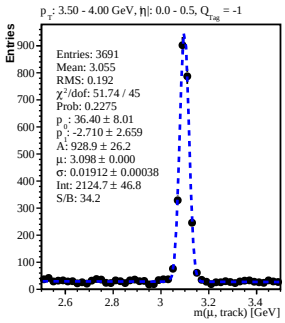
p_T: 3.50 - 4.00 GeV, |η|: 0.0 - 0.5, Q_Tag = -1
Entries: 3691
Mean: 3.055
RMS: 0.192
χ²/dof: 51.74 / 45
Prob: 0.2275
p_0: 36.40 ± 8.01
p_1: -2.710 ± 2.659
A: 928.9 ± 26.2
μ: 3.098 ± 0.000
σ: 0.01912 ± 0.00038
Int: 2124.7 ± 46.8
S/B: 34.2
Entries
m(μ, track) [GeV]

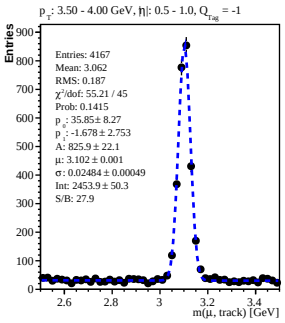
p_T: 3.50 - 4.00 GeV, |η|: 0.5 - 1.0, Q_Tag = -1
Entries: 4167
Mean: 3.062
RMS: 0.187
χ²/dof: 55.21 / 45
Prob: 0.1415
p_0: 35.85 ± 8.27
p_1: -1.678 ± 2.753
A: 825.9 ± 22.1
μ: 3.102 ± 0.001
σ: 0.02484 ± 0.00049
Int: 2453.9 ± 50.3
S/B: 27.9
Entries
m(μ, track) [GeV]

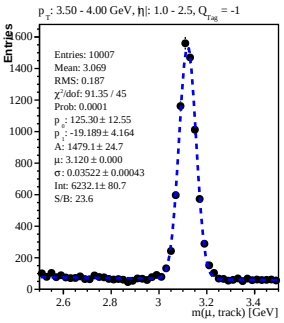
p_T: 3.50 - 4.00 GeV, |η|: 1.0 - 2.5, Q_Tag = -1
Entries: 10007
Mean: 3.069
RMS: 0.187
χ²/dof: 91.35 / 45
Prob: 0.0001
p_0: 125.30 ± 12.55
p_1: -19.189 ± 4.164
A: 1479.1 ± 24.7
μ: 3.120 ± 0.000
σ: 0.03522 ± 0.00043
Int: 6232.1 ± 80.7
S/B: 23.6
Entries
m(μ, track) [GeV]

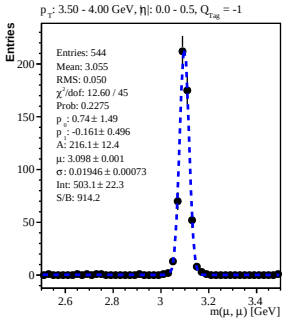
p_T: 3.50 - 4.00 GeV, |η|: 0.0 - 0.5, Q_Tag = -1
Entries: 544
Mean: 3.055
RMS: 0.050
χ²/dof: 12.60 / 45
Prob: 0.2275
p_0: 0.74 ± 1.49
p_1: -0.161 ± 0.496
A: 216.1 ± 12.4
μ: 3.098 ± 0.001
σ: 0.01946 ± 0.00073
Int: 503.1 ± 22.3
S/B: 914.2
Entries
m(μ, μ) [GeV]

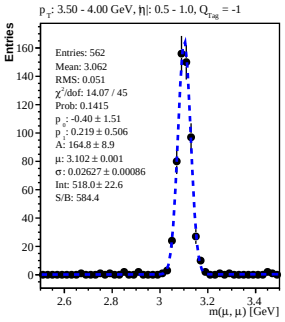
p_T: 3.50 - 4.00 GeV, |η|: 0.5 - 1.0, Q_Tag = -1
Entries: 562
Mean: 3.062
RMS: 0.051
χ²/dof: 14.07 / 45
Prob: 0.1415
p_0: -0.40 ± 1.51
p_1: 0.219 ± 0.506
A: 164.8 ± 8.9
μ: 3.102 ± 0.001
σ: 0.02627 ± 0.00086
Int: 518.0 ± 22.6
S/B: 584.4
Entries
m(μ, μ) [GeV]

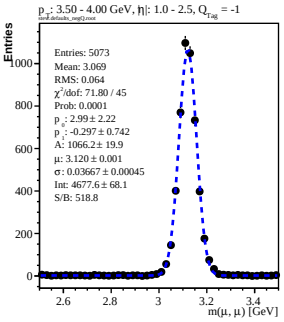
p_T: 3.50 - 4.00 GeV, |η|: 1.0 - 2.5, Q_Tag = -1
Entries: 5073
Mean: 3.069
RMS: 0.064
χ²/dof: 71.80 / 45
Prob: 0.0001
p_0: 2.99 ± 2.22
p_1: -0.297 ± 0.742
A: 1066.2 ± 19.9
μ: 3.120 ± 0.001
σ: 0.03667 ± 0.00045
Int: 4677.6 ± 68.1
S/B: 518.8
Entries
m(μ, μ) [GeV]

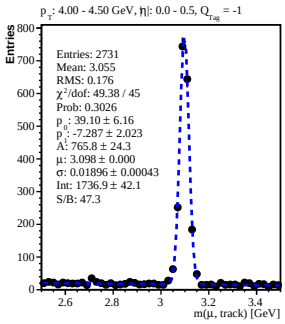
p_T: 4.00 - 4.50 GeV, |η|: 0.0 - 0.5, Q_{Tag} = -1
Entries: 2731
Mean: 3.055
RMS: 0.176
χ²/dof: 49.38 / 45
Prob: 0.3026
p_0: 39.10 ± 6.16
p_1: -7.287 ± 2.023
A: 765.8 ± 24.3
μ: 3.098 ± 0.000
σ: 0.01896 ± 0.00043
Int: 1736.9 ± 42.1
S/B: 47.3
Entries
m(μ, track) [GeV]

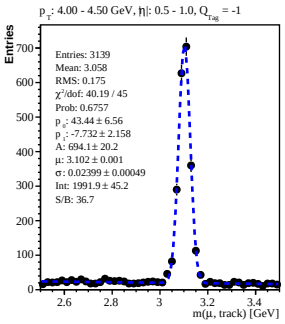
p_T: 4.00 - 4.50 GeV, |η|: 0.5 - 1.0, Q_{Tag} = -1
Entries: 3139
Mean: 3.058
RMS: 0.175
χ²/dof: 40.19 / 45
Prob: 0.6757
p_0: 43.44 ± 6.56
p_1: -7.732 ± 2.158
A: 694.1 ± 20.2
μ: 3.102 ± 0.001
σ: 0.02399 ± 0.00049
Int: 1991.9 ± 45.2
S/B: 36.7
Entries
m(μ, track) [GeV]

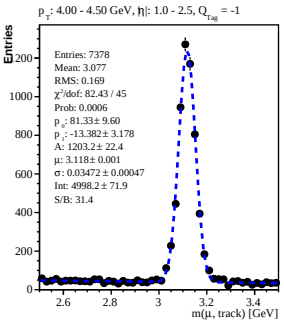
p_T: 4.00 - 4.50 GeV, |η|: 1.0 - 2.5, Q_{Tag} = -1
Entries: 7378
Mean: 3.077
RMS: 0.169
χ²/dof: 82.43 / 45
Prob: 0.0006
p_0: 81.33± 9.60
p_1: -13.382 ± 3.178
A: 1203.2 ± 22.4
μ: 3.118± 0.001
σ: 0.03472 ± 0.00047
Int: 4998.2 ± 71.9
S/B: 31.4
Entries
m(μ, track) [GeV]

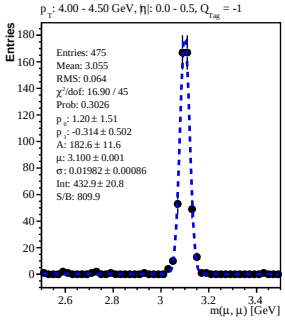
p_T: 4.00 - 4.50 GeV, |η|: 0.0 - 0.5, Q_{Tag} = -1
Entries: 475
Mean: 3.055
RMS: 0.064
χ²/dof: 16.90 / 45
Prob: 0.3026
p_0: 1.20 ± 1.51
p_1: -0.314 ± 0.502
A: 182.6 ± 11.6
μ: 3.100 ± 0.001
σ: 0.01982 ± 0.00086
Int: 432.9 ± 20.8
S/B: 809.9
Entries
m(μ, μ) [GeV]

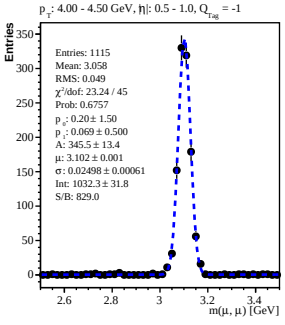
p_T: 4.00 - 4.50 GeV, |η|: 0.5 - 1.0, Q_{Tag} = -1
Entries: 1115
Mean: 3.058
RMS: 0.049
χ²/dof: 23.24 / 45
Prob: 0.6757
p_0: 0.20± 1.50
p_1: 0.069 ± 0.500
A: 345.5 ± 13.4
μ: 3.102 ± 0.001
σ: 0.02498 ± 0.00061
Int: 1032.3 ± 31.8
S/B: 829.0
Entries
m(μ, μ) [GeV]

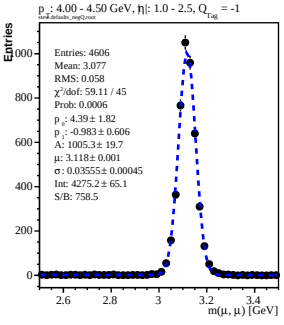
p_T: 4.00 - 4.50 GeV, |η|: 1.0 - 2.5, Q_{Tag} = -1
Entries: 4606
Mean: 3.077
RMS: 0.058
χ²/dof: 59.11 / 45
Prob: 0.0006
p_0: 4.39± 1.82
p_1: -0.983 ± 0.606
A: 1005.3± 19.7
μ: 3.118± 0.001
σ: 0.03555± 0.00045
Int: 4275.2 ± 65.1
S/B: 758.5
Entries
m(μ, μ) [GeV]

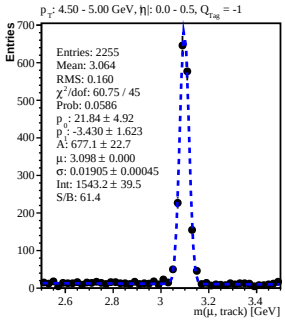
p_T: 4.50 - 5.00 GeV, |η|: 0.0 - 0.5, Q_{Tag} = -1
Entries: 2255
Mean: 3.064
RMS: 0.160
χ²/dof: 60.75 / 45
Prob: 0.0586
p_0: 21.84 ± 4.92
p_1: -3.430 ± 1.623
A: 677.1 ± 22.7
μ: 3.098 ± 0.000
σ: 0.01905 ± 0.00045
Int: 1543.2 ± 39.5
S/B: 61.4
Entries
m(μ, track) [GeV]

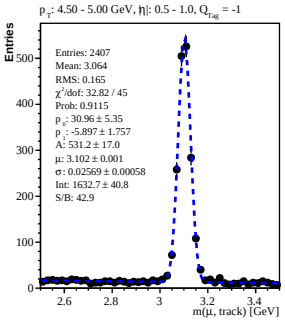
p_T: 4.50 - 5.00 GeV, |η|: 0.5 - 1.0, Q_{Tag} = -1
Entries: 2407
Mean: 3.064
RMS: 0.165
χ²/dof: 32.82 / 45
Prob: 0.9115
p_0: 30.96 ± 5.35
p_1: -5.897 ± 1.757
A: 531.2 ± 17.0
μ: 3.102 ± 0.001
σ: 0.02569 ± 0.00058
Int: 1632.7 ± 40.8
S/B: 42.9
Entries
m(μ, track) [GeV]

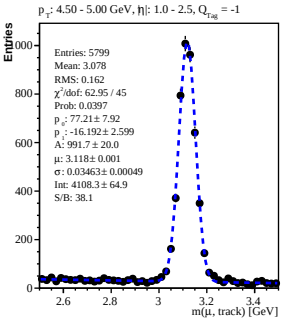
p_T: 4.50 - 5.00 GeV, |η|: 1.0 - 2.5, Q_{Tag} = -1
Entries: 5799
Mean: 3.078
RMS: 0.162
χ²/dof: 62.95 / 45
Prob: 0.0397
p_0: 77.21± 7.92
p_1: -16.192± 2.599
A: 991.7 ± 20.0
μ: 3.118± 0.001
σ: 0.03463± 0.00049
Int: 4108.3 ± 64.9
S/B: 38.1
Entries
m(μ, track) [GeV]

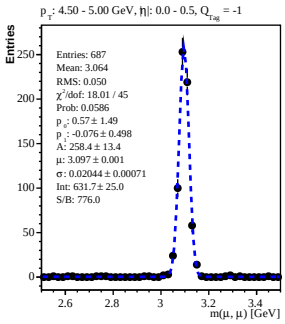
p_T: 4.50 - 5.00 GeV, |η|: 0.0 - 0.5, Q_{Tag} = -1
Entries: 687
Mean: 3.064
RMS: 0.050
χ²/dof: 18.01 / 45
Prob: 0.0586
p_0: 0.57 ± 1.49
p_1: -0.076 ± 0.498
A: 258.4 ± 13.4
μ: 3.097 ± 0.001
σ: 0.02044 ± 0.00071
Int: 631.7 ± 25.0
S/B: 776.0
Entries
m(μ, μ) [GeV]

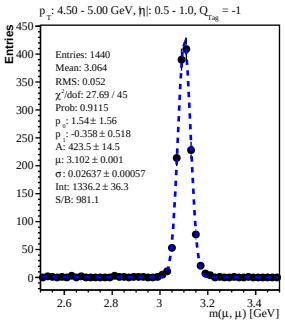
p_T: 4.50 - 5.00 GeV, |η|: 0.5 - 1.0, Q_{Tag} = -1
Entries: 1440
Mean: 3.064
RMS: 0.052
χ²/dof: 27.69 / 45
Prob: 0.9115
p_0: 1.54 ± 1.56
p_1: -0.358 ± 0.518
A: 423.5 ± 14.5
μ: 3.102 ± 0.001
σ: 0.02637 ± 0.00057
Int: 1336.2 ± 36.3
S/B: 981.1
Entries
m(μ, μ) [GeV]

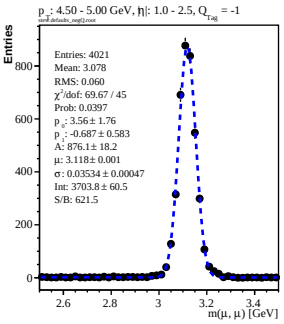
p_T: 4.50 - 5.00 GeV, |η|: 1.0 - 2.5, Q_{Tag} = -1
Entries: 4021
Mean: 3.078
RMS: 0.060
χ²/dof: 69.67 / 45
Prob: 0.0397
p_0: 3.56 ± 1.76
p_1: -0.687 ± 0.583
A: 876.1 ± 18.2
μ: 3.118± 0.001
σ: 0.03534 ± 0.00047
Int: 3703.8 ± 60.5
S/B: 621.5
Entries
m(μ, μ) [GeV]

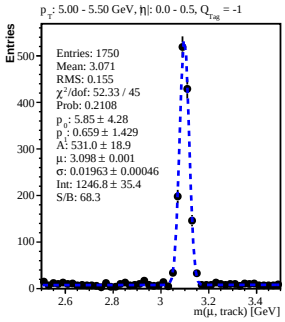
p_T: 5.00 - 5.50 GeV, |η|: 0.0 - 0.5, Q_{Tag} = -1
Entries: 1750
Mean: 3.071
RMS: 0.155
χ²/dof: 52.33 / 45
Prob: 0.2108
p_0: 5.85 ± 4.28
p_1: 0.659 ± 1.429
A: 531.0 ± 18.9
μ: 3.098 ± 0.001
σ: 0.01963 ± 0.00046
Int: 1246.8 ± 35.4
S/B: 68.3
Entries
m(μ, track) [GeV]

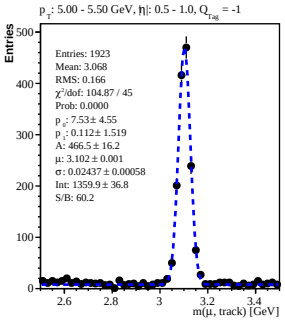
p_T: 5.00 - 5.50 GeV, |η|: 0.5 - 1.0, Q_{Tag} = -1
Entries: 1923
Mean: 3.068
RMS: 0.166
χ²/dof: 104.87 / 45
Prob: 0.0000
p_0: 7.53± 4.55
p_1: 0.112± 1.519
A: 466.5 ± 16.2
μ: 3.102 ± 0.001
σ: 0.02437 ± 0.00058
Int: 1359.9 ± 36.8
S/B: 60.2
Entries
m(μ, track) [GeV]

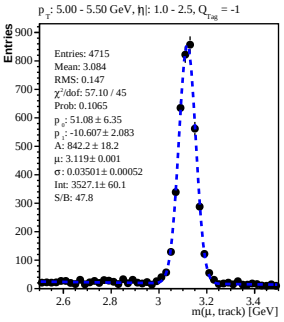
p_T: 5.00 - 5.50 GeV, |η|: 1.0 - 2.5, Q_{Tag} = -1
Entries: 4715
Mean: 3.084
RMS: 0.147
χ²/dof: 57.10 / 45
Prob: 0.1065
p_0: 51.08 ± 6.35
p_1: -10.607 ± 2.083
A: 842.2 ± 18.2
μ: 3.119± 0.001
σ: 0.03501± 0.00052
Int: 3527.1± 60.1
S/B: 47.8
Entries
m(μ, track) [GeV]

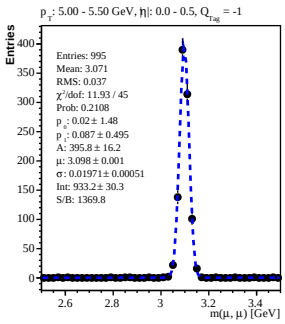
p_T: 5.00 - 5.50 GeV, |η|: 0.0 - 0.5, Q_{Tag} = -1
Entries: 995
Mean: 3.071
RMS: 0.037
χ²/dof: 11.93 / 45
Prob: 0.2108
p_0: 0.02 ± 1.48
p_1: 0.087 ± 0.495
A: 395.8 ± 16.2
μ: 3.098 ± 0.001
σ: 0.01971± 0.00051
Int: 933.2± 30.3
S/B: 1369.8
Entries
m(μ, μ) [GeV]

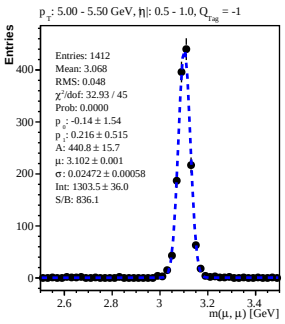
p_T: 5.00 - 5.50 GeV, |η|: 0.5 - 1.0, Q_{Tag} = -1
Entries: 1412
Mean: 3.068
RMS: 0.048
χ²/dof: 32.93 / 45
Prob: 0.0000
p_0: -0.14 ± 1.54
p_1: 0.216 ± 0.515
A: 440.8 ± 15.7
μ: 3.102 ± 0.001
σ: 0.02472 ± 0.00058
Int: 1303.5 ± 36.0
S/B: 836.1
Entries
m(μ, μ) [GeV]

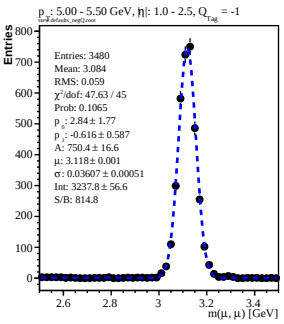
p_T: 5.00 - 5.50 GeV, |η|: 1.0 - 2.5, Q_{Tag} = -1
Entries: 3480
Mean: 3.084
RMS: 0.059
χ²/dof: 47.63 / 45
Prob: 0.1065
p_0: 2.84 ± 1.77
p_1: -0.616 ± 0.587
A: 750.4 ± 16.6
μ: 3.118± 0.001
σ: 0.03607 ± 0.00051
Int: 3237.8 ± 56.6
S/B: 814.8
Entries
m(μ, μ) [GeV]

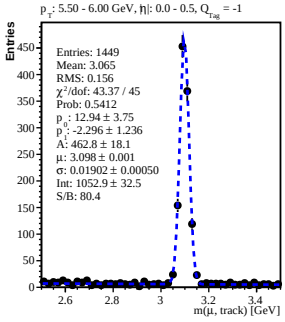
p_T: 5.50 - 6.00 GeV, |η|: 0.0 - 0.5, Q_{Tag} = -1
Entries: 1449
Mean: 3.065
RMS: 0.156
χ²/dof: 43.37 / 45
Prob: 0.5412
p_0: 12.94 ± 3.75
p_1: -2.296 ± 1.236
A: 462.8 ± 18.1
μ: 3.098 ± 0.001
σ: 0.01902 ± 0.00050
Int: 1052.9 ± 32.5
S/B: 80.4
Entries
m(μ, track) [GeV]

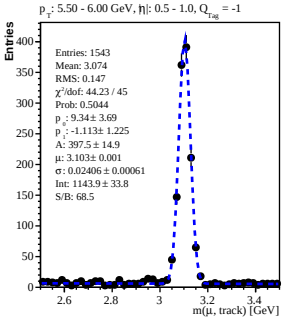
p_T: 5.50 - 6.00 GeV, |η|: 0.5 - 1.0, Q_{Tag} = -1
Entries: 1543
Mean: 3.074
RMS: 0.147
χ²/dof: 44.23 / 45
Prob: 0.5044
p_0: 9.34± 3.69
p_1: -1.113± 1.225
A: 397.5 ± 14.9
μ: 3.103± 0.001
σ: 0.02406 ± 0.00061
Int: 1143.9 ± 33.8
S/B: 68.5
Entries
m(μ, track) [GeV]

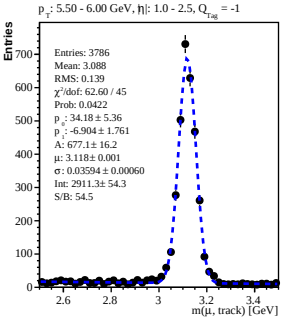
p_T: 5.50 - 6.00 GeV, |η|: 1.0 - 2.5, Q_{Tag} = -1
Entries: 3786
Mean: 3.088
RMS: 0.139
χ²/dof: 62.60 / 45
Prob: 0.0422
p_0: 34.18 ± 5.36
p_1: -6.904 ± 1.761
A: 677.1 ± 16.2
μ: 3.118± 0.001
σ: 0.03594 ± 0.00060
Int: 2911.3± 54.3
S/B: 54.5
Entries
m(μ, track) [GeV]

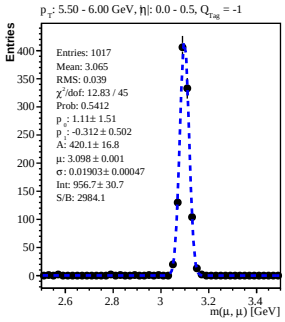
p_T: 5.50 - 6.00 GeV, |η|: 0.0 - 0.5, Q_{Tag} = -1
Entries: 1017
Mean: 3.065
RMS: 0.039
χ²/dof: 12.83 / 45
Prob: 0.5412
p_0: 1.11± 1.51
p_1: -0.312± 0.502
A: 420.1± 16.8
μ: 3.098 ± 0.001
σ: 0.01903± 0.00047
Int: 956.7± 30.7
S/B: 2984.1
Entries
m(μ, μ) [GeV]

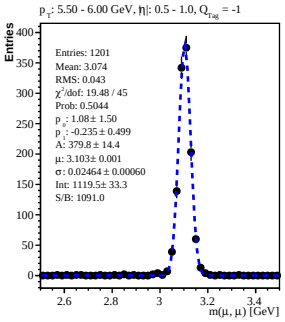
p_T: 5.50 - 6.00 GeV, |η|: 0.5 - 1.0, Q_{Tag} = -1
Entries: 1201
Mean: 3.074
RMS: 0.043
χ²/dof: 19.48 / 45
Prob: 0.5044
p_0: 1.08± 1.50
p_1: -0.235± 0.499
A: 379.8 ± 14.4
μ: 3.103± 0.001
σ: 0.02464 ± 0.00060
Int: 1119.5± 33.3
S/B: 1091.0
Entries
m(μ, μ) [GeV]

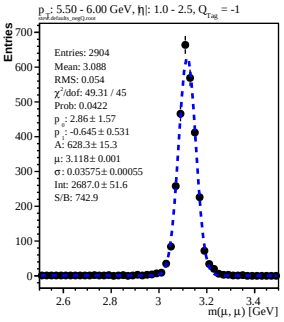
p_T: 5.50 - 6.00 GeV, |η|: 1.0 - 2.5, Q_{Tag} = -1
Entries: 2904
Mean: 3.088
RMS: 0.054
χ²/dof: 49.31 / 45
Prob: 0.0422
p_0: 2.86± 1.57
p_1: -0.645 ± 0.531
A: 628.3± 15.3
μ: 3.118± 0.001
σ: 0.03575± 0.00055
Int: 2687.0 ± 51.6
S/B: 742.9
Entries
m(μ, μ) [GeV]

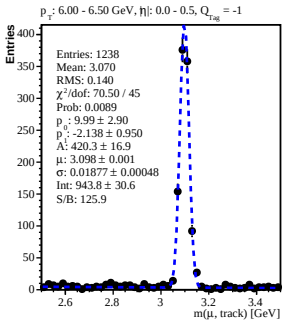
p_T: 6.00 - 6.50 GeV, |η|: 0.0 - 0.5, Q_{Trig} = -1
Entries: 1238
Mean: 3.070
RMS: 0.140
χ²/dof: 70.50 / 45
Prob: 0.0089
p_0: 9.99 ± 2.90
p_1: -2.138 ± 0.950
A: 420.3 ± 16.9
μ: 3.098 ± 0.001
σ: 0.01877 ± 0.00048
Int: 943.8 ± 30.6
S/B: 125.9
Entries
m(μ, track) [GeV]

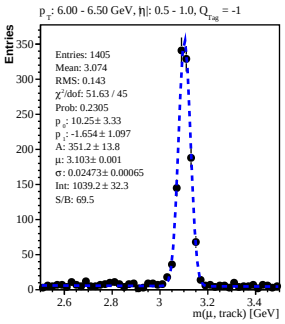
p_T: 6.00 - 6.50 GeV, |η|: 0.5 - 1.0, Q_{Trig} = -1
Entries: 1405
Mean: 3.074
RMS: 0.143
χ²/dof: 51.63 / 45
Prob: 0.2305
p_0: 10.25± 3.33
p_1: -1.654 ± 1.097
A: 351.2 ± 13.8
μ: 3.103± 0.001
σ: 0.02473± 0.00065
Int: 1039.2 ± 32.3
S/B: 69.5
Entries
m(μ, track) [GeV]

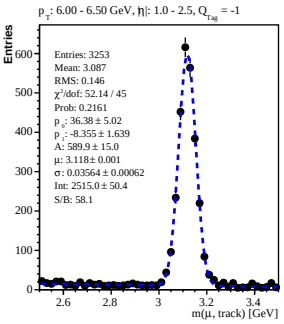
p_T: 6.00 - 6.50 GeV, |η|: 1.0 - 2.5, Q_{Trig} = -1
Entries: 3253
Mean: 3.087
RMS: 0.146
χ²/dof: 52.14 / 45
Prob: 0.2161
p_0: 36.38 ± 5.02
p_1: -8.355 ± 1.639
A: 589.9 ± 15.0
μ: 3.118± 0.001
σ: 0.03564 ± 0.00062
Int: 2515.0 ± 50.4
S/B: 58.1
Entries
m(μ, track) [GeV]

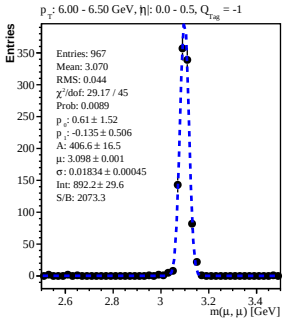
p_T: 6.00 - 6.50 GeV, |η|: 0.0 - 0.5, Q_{Trig} = -1
Entries: 967
Mean: 3.070
RMS: 0.044
χ²/dof: 29.17 / 45
Prob: 0.0089
p_0: 0.61± 1.52
p_1: -0.135 ± 0.506
A: 406.6 ± 16.5
μ: 3.098 ± 0.001
σ: 0.01834 ± 0.00045
Int: 892.2± 29.6
S/B: 2073.3
Entries
m(μ, μ) [GeV]

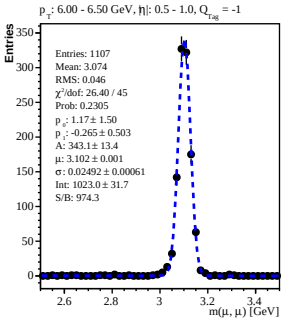
p_T: 6.00 - 6.50 GeV, |η|: 0.5 - 1.0, Q_{Trig} = -1
Entries: 1107
Mean: 3.074
RMS: 0.046
χ²/dof: 26.40 / 45
Prob: 0.2305
p_0: 1.17± 1.50
p_1: -0.265 ± 0.503
A: 343.1± 13.4
μ: 3.102 ± 0.001
σ: 0.02492 ± 0.00061
Int: 1023.0 ± 31.7
S/B: 974.3
Entries
m(μ, μ) [GeV]

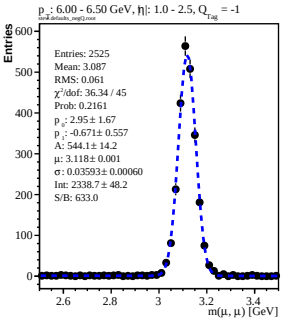
p_T: 6.00 - 6.50 GeV, |η|: 1.0 - 2.5, Q_{Trig} = -1
Entries: 2525
Mean: 3.087
RMS: 0.061
χ²/dof: 36.34 / 45
Prob: 0.2161
p_0: 2.95± 1.67
p_1: -0.671± 0.557
A: 544.1± 14.2
μ: 3.118± 0.001
σ: 0.03593± 0.00060
Int: 2338.7 ± 48.2
S/B: 633.0
Entries
m(μ, μ) [GeV]

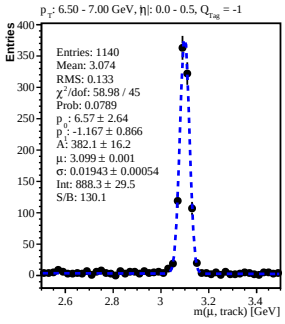
p_T: 6.50 - 7.00 GeV, |η|: 0.0 - 0.5, Q_{Trig} = -1
Entries: 1140
Mean: 3.074
RMS: 0.133
χ²/dof: 58.98 / 45
Prob: 0.0789
p_0: 6.57 ± 2.64
p_1: -1.167 ± 0.866
A: 382.1 ± 16.2
μ: 3.099 ± 0.001
σ: 0.01943 ± 0.00054
Int: 888.3 ± 29.5
S/B: 130.1
Entries
m(μ, track) [GeV]

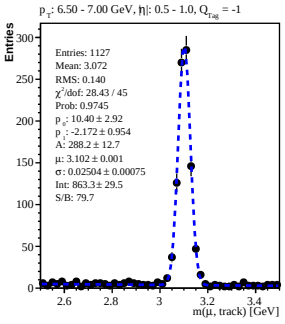
p_T: 6.50 - 7.00 GeV, |η|: 0.5 - 1.0, Q_{Trig} = -1
Entries: 1127
Mean: 3.072
RMS: 0.140
χ²/dof: 28.43 / 45
Prob: 0.9745
p_0: 10.40 ± 2.92
p_1: -2.172 ± 0.954
A: 288.2 ± 12.7
μ: 3.102 ± 0.001
σ: 0.02504 ± 0.00075
Int: 863.3± 29.5
S/B: 79.7
Entries
m(μ, track) [GeV]

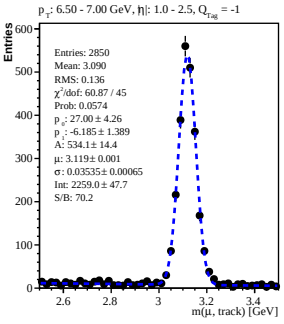
p_T: 6.50 - 7.00 GeV, |η|: 1.0 - 2.5, Q_{Trig} = -1
Entries: 2850
Mean: 3.090
RMS: 0.136
χ²/dof: 60.87 / 45
Prob: 0.0574
p_0: 27.00 ± 4.26
p_1: -6.185 ± 1.389
A: 534.1± 14.4
μ: 3.119± 0.001
σ: 0.03535± 0.00065
Int: 2259.0 ± 47.7
S/B: 70.2
Entries
m(μ, track) [GeV]

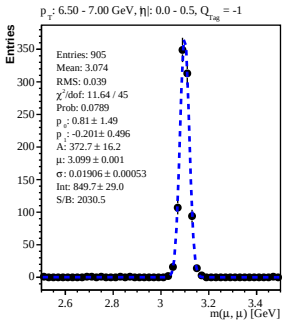
p_T: 6.50 - 7.00 GeV, |η|: 0.0 - 0.5, Q_{Trig} = -1
Entries: 905
Mean: 3.074
RMS: 0.039
χ²/dof: 11.64 / 45
Prob: 0.0789
p_0: 0.81 ± 1.49
p_1: -0.201± 0.496
A: 372.7 ± 16.2
μ: 3.099 ± 0.001
σ: 0.01906 ± 0.00053
Int: 849.7± 29.0
S/B: 2030.5
Entries
m(μ, μ) [GeV]

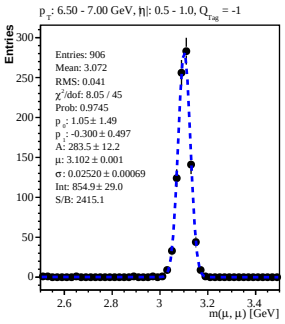
p_T: 6.50 - 7.00 GeV, |η|: 0.5 - 1.0, Q_{Trig} = -1
Entries: 906
Mean: 3.072
RMS: 0.041
χ²/dof: 8.05 / 45
Prob: 0.9745
p_0: 1.05± 1.49
p_1: -0.300 ± 0.497
A: 283.5 ± 12.2
μ: 3.102 ± 0.001
σ: 0.02520 ± 0.00069
Int: 854.9± 29.0
S/B: 2415.1
Entries
m(μ, μ) [GeV]

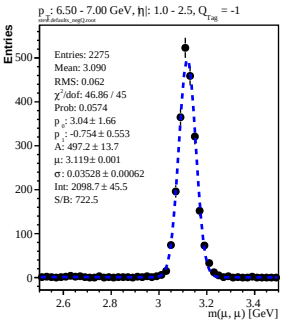
p_T: 6.50 - 7.00 GeV, |η|: 1.0 - 2.5, Q_{Trig} = -1
Entries: 2275
Mean: 3.090
RMS: 0.062
χ²/dof: 46.86 / 45
Prob: 0.0574
p_0: 3.04 ± 1.66
p_1: -0.754 ± 0.553
A: 497.2 ± 13.7
μ: 3.119± 0.001
σ: 0.03528 ± 0.00062
Int: 2098.7 ± 45.5
S/B: 722.5
Entries
m(μ, μ) [GeV]

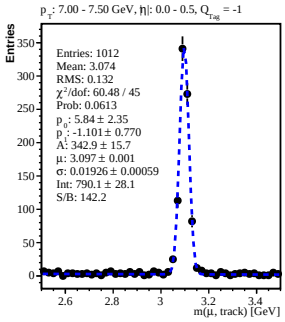
p_T: 7.00 - 7.50 GeV, |η|: 0.0 - 0.5, Q_Tag = -1
Entries: 1012
Mean: 3.074
RMS: 0.132
χ²/dof: 60.48 / 45
Prob: 0.0613
p_0: 5.84 ± 2.35
p_1: -1.101 ± 0.770
A: 342.9 ± 15.7
μ: 3.097 ± 0.001
σ: 0.01926 ± 0.00059
Int: 790.1 ± 28.1
S/B: 142.2
Entries
m(μ, track) [GeV]

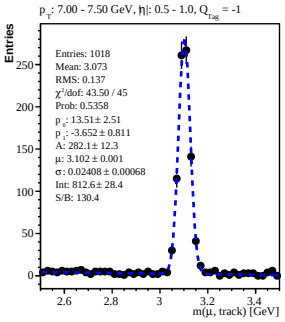
p_T: 7.00 - 7.50 GeV, |η|: 0.5 - 1.0, Q_Tag = -1
Entries: 1018
Mean: 3.073
RMS: 0.137
χ²/dof: 43.50 / 45
Prob: 0.5358
p_0: 13.51 ± 2.51
p_1: -3.652 ± 0.811
A: 282.1 ± 12.3
μ: 3.102 ± 0.001
σ: 0.02408 ± 0.00068
Int: 812.6 ± 28.4
S/B: 130.4
Entries
m(μ, track) [GeV]

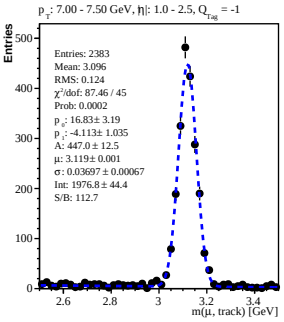
p_T: 7.00 - 7.50 GeV, |η|: 1.0 - 2.5, Q_Tag = -1
Entries: 2383
Mean: 3.096
RMS: 0.124
χ²/dof: 87.46 / 45
Prob: 0.0002
p_0: 16.83 ± 3.19
p_1: -4.113 ± 1.035
A: 447.0 ± 12.5
μ: 3.119 ± 0.001
σ: 0.03697 ± 0.00067
Int: 1976.8 ± 44.4
S/B: 112.7
Entries
m(μ, track) [GeV]

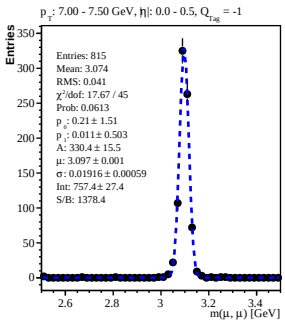
p_T: 7.00 - 7.50 GeV, |η|: 0.0 - 0.5, Q_Tag = -1
Entries: 815
Mean: 3.074
RMS: 0.041
χ²/dof: 17.67 / 45
Prob: 0.0613
p_0: 0.21 ± 1.51
p_1: 0.011 ± 0.503
A: 330.4 ± 15.5
μ: 3.097 ± 0.001
σ: 0.01916 ± 0.00059
Int: 757.4 ± 27.4
S/B: 1378.4
Entries
m(μ, μ) [GeV]

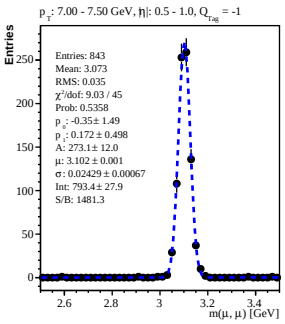
p_T: 7.00 - 7.50 GeV, |η|: 0.5 - 1.0, Q_Tag = -1
Entries: 843
Mean: 3.073
RMS: 0.035
χ²/dof: 9.03 / 45
Prob: 0.5358
p_0: -0.35 ± 1.49
p_1: 0.172 ± 0.498
A: 273.1 ± 12.0
μ: 3.102 ± 0.001
σ: 0.02429 ± 0.00067
Int: 793.4 ± 27.9
S/B: 1481.3
Entries
m(μ, μ) [GeV]

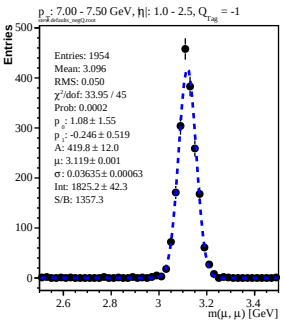
p_T: 7.00 - 7.50 GeV, |η|: 1.0 - 2.5, Q_Tag = -1
Entries: 1954
Mean: 3.096
RMS: 0.050
χ²/dof: 33.95 / 45
Prob: 0.0002
p_0: 1.08 ± 1.55
p_1: -0.246 ± 0.519
A: 419.8 ± 12.0
μ: 3.119 ± 0.001
σ: 0.03635 ± 0.00063
Int: 1825.2 ± 42.3
S/B: 1357.3
Entries
m(μ, μ) [GeV]

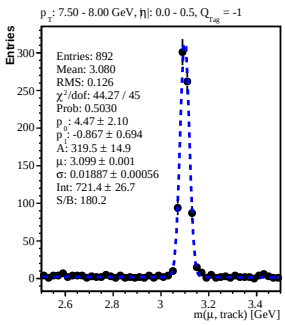
p_T: 7.50 - 8.00 GeV, |η|: 0.0 - 0.5, Q_Tag = -1
Entries: 892
Mean: 3.080
RMS: 0.126
χ²/dof: 44.27 / 45
Prob: 0.5030
p_0: 4.47 ± 2.10
p_1: -0.867 ± 0.694
A: 319.5 ± 14.9
μ: 3.099 ± 0.001
σ: 0.01887 ± 0.00056
Int: 721.4 ± 26.7
S/B: 180.2
Entries
m(μ, track) [GeV]

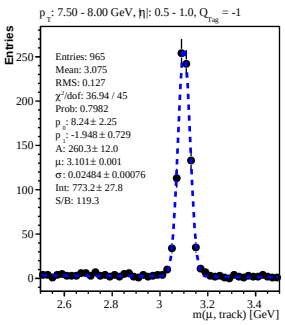
p_T: 7.50 - 8.00 GeV, |η|: 0.5 - 1.0, Q_Tag = -1
Entries: 965
Mean: 3.075
RMS: 0.127
χ²/dof: 36.94 / 45
Prob: 0.7982
p_0: 8.24 ± 2.25
p_1: -1.948 ± 0.729
A: 260.3 ± 12.0
μ: 3.101 ± 0.001
σ: 0.02484 ± 0.00076
Int: 773.2 ± 27.8
S/B: 119.3
Entries
m(μ, track) [GeV]

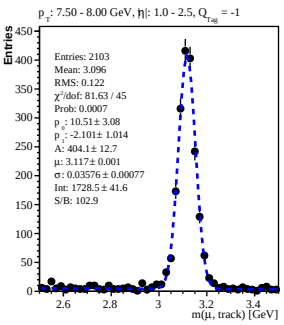
p_T: 7.50 - 8.00 GeV, |η|: 1.0 - 2.5, Q_Tag = -1
Entries: 2103
Mean: 3.096
RMS: 0.122
χ²/dof: 81.63 / 45
Prob: 0.0007
p_0: 10.51 ± 3.08
p_1: -2.101 ± 1.014
A: 404.1 ± 12.7
μ: 3.117 ± 0.001
σ: 0.03576 ± 0.00077
Int: 1728.5 ± 41.6
S/B: 102.9
Entries
m(μ, track) [GeV]

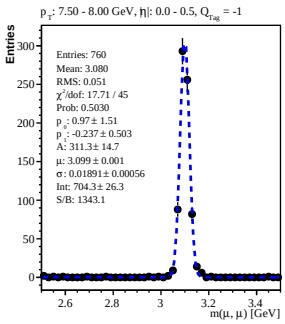
p_T: 7.50 - 8.00 GeV, |η|: 0.0 - 0.5, Q_Tag = -1
Entries: 760
Mean: 3.080
RMS: 0.051
χ²/dof: 17.71 / 45
Prob: 0.5030
p_0: 0.97 ± 1.51
p_1: -0.237 ± 0.503
A: 311.3 ± 14.7
μ: 3.099 ± 0.001
σ: 0.01891 ± 0.00056
Int: 704.3 ± 26.3
S/B: 1343.1
Entries
m(μ, μ) [GeV]

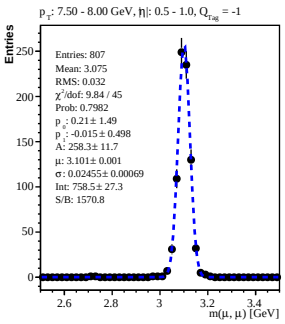
p_T: 7.50 - 8.00 GeV, |η|: 0.5 - 1.0, Q_Tag = -1
Entries: 807
Mean: 3.075
RMS: 0.032
χ²/dof: 9.84 / 45
Prob: 0.7982
p_0: 0.21 ± 1.49
p_1: -0.015 ± 0.498
A: 258.3 ± 11.7
μ: 3.101 ± 0.001
σ: 0.02455 ± 0.00069
Int: 758.5 ± 27.3
S/B: 1570.8
Entries
m(μ, μ) [GeV]

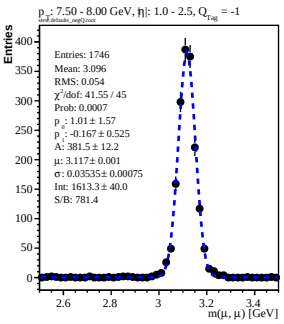
p_T: 7.50 - 8.00 GeV, |η|: 1.0 - 2.5, Q_Tag = -1
Entries: 1746
Mean: 3.096
RMS: 0.054
χ²/dof: 41.55 / 45
Prob: 0.0007
p_0: 1.01 ± 1.57
p_1: -0.167 ± 0.525
A: 381.5 ± 12.2
μ: 3.117 ± 0.001
σ: 0.03535 ± 0.00075
Int: 1613.3 ± 40.0
S/B: 781.4
Entries
m(μ, μ) [GeV]

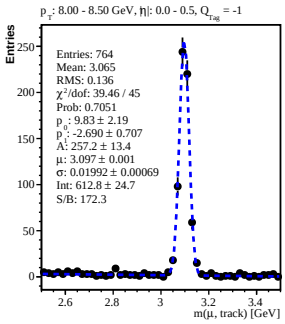
p_T: 8.00 - 8.50 GeV, |η|: 0.0 - 0.5, Q_{Trig} = -1
Entries: 764
Mean: 3.065
RMS: 0.136
χ²/dof: 39.46 / 45
Prob: 0.7051
p_0: 9.83 ± 2.19
p_1: -2.690 ± 0.707
A: 257.2 ± 13.4
μ: 3.097 ± 0.001
σ: 0.01992 ± 0.00069
Int: 612.8 ± 24.7
S/B: 172.3
Entries
m(μ, track) [GeV]

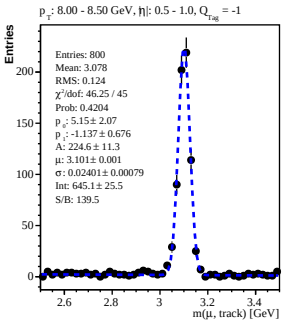
p_T: 8.00 - 8.50 GeV, |η|: 0.5 - 1.0, Q_{Trig} = -1
Entries: 800
Mean: 3.078
RMS: 0.124
χ²/dof: 46.25 / 45
Prob: 0.4204
p_0: 5.15 ± 2.07
p_1: -1.137 ± 0.676
A: 224.6 ± 11.3
μ: 3.101 ± 0.001
σ: 0.02401 ± 0.00079
Int: 645.1 ± 25.5
S/B: 139.5
Entries
m(μ, track) [GeV]

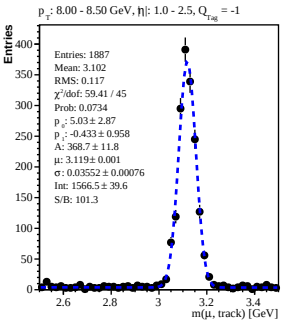
p_T: 8.00 - 8.50 GeV, |η|: 1.0 - 2.5, Q_{Trig} = -1
Entries: 1887
Mean: 3.102
RMS: 0.117
χ²/dof: 59.41 / 45
Prob: 0.0734
p_0: 5.03 ± 2.87
p_1: -0.433 ± 0.958
A: 368.7 ± 11.8
μ: 3.119 ± 0.001
σ: 0.03552 ± 0.00076
Int: 1566.5 ± 39.6
S/B: 101.3
Entries
m(μ, track) [GeV]

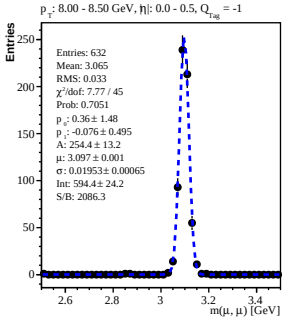
p_T: 8.00 - 8.50 GeV, |η|: 0.0 - 0.5, Q_{Trig} = -1
Entries: 632
Mean: 3.065
RMS: 0.033
χ²/dof: 7.77 / 45
Prob: 0.7051
p_0: 0.36 ± 1.48
p_1: -0.076 ± 0.495
A: 254.4 ± 13.2
μ: 3.097 ± 0.001
σ: 0.01953 ± 0.00065
Int: 594.4 ± 24.2
S/B: 2086.3
Entries
m(μ, μ) [GeV]

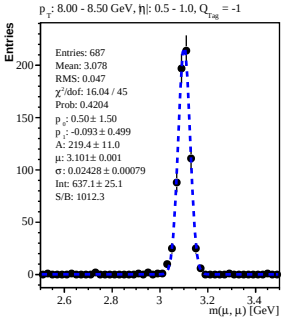
p_T: 8.00 - 8.50 GeV, |η|: 0.5 - 1.0, Q_{Trig} = -1
Entries: 687
Mean: 3.078
RMS: 0.047
χ²/dof: 16.04 / 45
Prob: 0.4204
p_0: 0.50 ± 1.50
p_1: -0.093 ± 0.499
A: 219.4 ± 11.0
μ: 3.101 ± 0.001
σ: 0.02428 ± 0.00079
Int: 637.1 ± 25.1
S/B: 1012.3
Entries
m(μ, μ) [GeV]

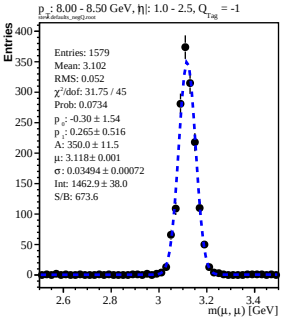
p_T: 8.00 - 8.50 GeV, |η|: 1.0 - 2.5, Q_{Trig} = -1
Entries: 1579
Mean: 3.102
RMS: 0.052
χ²/dof: 31.75 / 45
Prob: 0.0734
p_0: -0.30 ± 1.54
p_1: 0.265 ± 0.516
A: 350.0 ± 11.5
μ: 3.118 ± 0.001
σ: 0.03494 ± 0.00072
Int: 1462.9 ± 38.0
S/B: 673.6
Entries
m(μ, μ) [GeV]

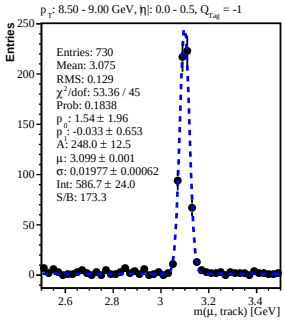
p_T: 8.50 - 9.00 GeV, |η|: 0.0 - 0.5, Q_{Trig} = -1
Entries: 730
Mean: 3.075
RMS: 0.129
χ²/dof: 53.36 / 45
Prob: 0.1838
p_0: 1.54 ± 1.96
p_1: -0.033 ± 0.653
A: 248.0 ± 12.5
μ: 3.099 ± 0.001
σ: 0.01977 ± 0.00062
Int: 586.7 ± 24.0
S/B: 173.3
Entries
m(μ, track) [GeV]

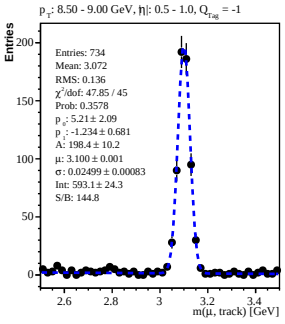
p_T: 8.50 - 9.00 GeV, |η|: 0.5 - 1.0, Q_{Trig} = -1
Entries: 734
Mean: 3.072
RMS: 0.136
χ²/dof: 47.85 / 45
Prob: 0.3578
p_0: 5.21 ± 2.09
p_1: -1.234 ± 0.681
A: 198.4 ± 10.2
μ: 3.100 ± 0.001
σ: 0.02499 ± 0.00083
Int: 593.1 ± 24.3
S/B: 144.8
Entries
m(μ, track) [GeV]

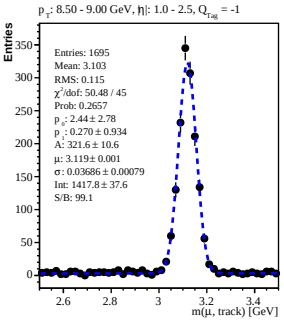
p_T: 8.50 - 9.00 GeV, |η|: 1.0 - 2.5, Q_{Trig} = -1
Entries: 1695
Mean: 3.103
RMS: 0.115
χ²/dof: 50.48 / 45
Prob: 0.2657
p_0: 2.44 ± 2.78
p_1: 0.270 ± 0.934
A: 321.6 ± 10.6
μ: 3.119 ± 0.001
σ: 0.03686 ± 0.00079
Int: 1417.8 ± 37.6
S/B: 99.1
Entries
m(μ, track) [GeV]

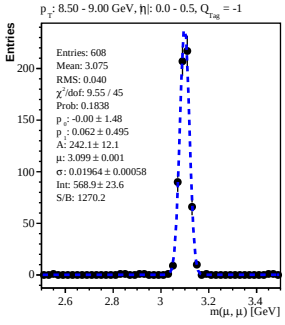
p_T: 8.50 - 9.00 GeV, |η|: 0.0 - 0.5, Q_{Trig} = -1
Entries: 608
Mean: 3.075
RMS: 0.040
χ²/dof: 9.55 / 45
Prob: 0.1838
p_0: -0.00 ± 1.48
p_1: 0.062 ± 0.495
A: 242.1 ± 12.1
μ: 3.099 ± 0.001
σ: 0.01964 ± 0.00058
Int: 568.9 ± 23.6
S/B: 1270.2
Entries
m(μ, μ) [GeV]

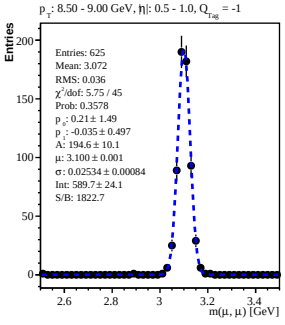
p_T: 8.50 - 9.00 GeV, |η|: 0.5 - 1.0, Q_{Trig} = -1
Entries: 625
Mean: 3.072
RMS: 0.036
χ²/dof: 5.75 / 45
Prob: 0.3578
p_0: 0.21 ± 1.49
p_1: -0.035 ± 0.497
A: 194.6 ± 10.1
μ: 3.100 ± 0.001
σ: 0.02534 ± 0.00084
Int: 589.7 ± 24.1
S/B: 1822.7
Entries
m(μ, μ) [GeV]

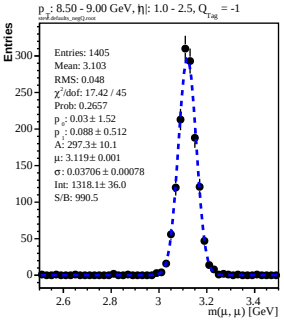
p_T: 8.50 - 9.00 GeV, |η|: 1.0 - 2.5, Q_{Trig} = -1
Entries: 1405
Mean: 3.103
RMS: 0.048
χ²/dof: 17.42 / 45
Prob: 0.2657
p_0: 0.03 ± 1.52
p_1: 0.088 ± 0.512
A: 297.3 ± 10.1
μ: 3.119 ± 0.001
σ: 0.03706 ± 0.00078
Int: 1318.1 ± 36.0
S/B: 990.5
Entries
m(μ, μ) [GeV]

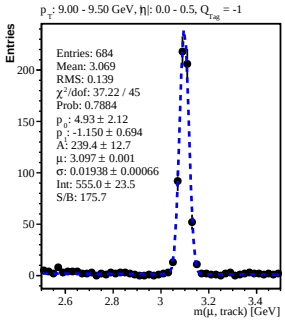
p_T: 9.00 - 9.50 GeV, |η|: 0.0 - 0.5, Q_{Tag} = -1
Entries: 684
Mean: 3.069
RMS: 0.139
χ²/dof: 37.22 / 45
Prob: 0.7884
p0: 4.93 ± 2.12
p1: -1.150 ± 0.694
A: 239.4 ± 12.7
μ: 3.097 ± 0.001
σ: 0.01938 ± 0.00066
Int: 555.0 ± 23.5
S/B: 175.7
Entries
m(μ, track) [GeV]

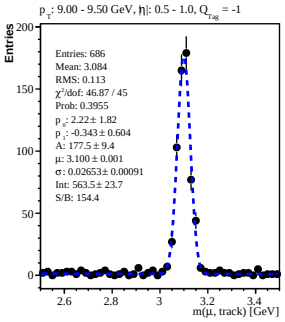
p_T: 9.00 - 9.50 GeV, |η|: 0.5 - 1.0, Q_{Tag} = -1
Entries: 686
Mean: 3.084
RMS: 0.113
χ²/dof: 46.87 / 45
Prob: 0.3955
p0: 2.22 ± 1.82
p1: -0.343 ± 0.604
A: 177.5 ± 9.4
μ: 3.100 ± 0.001
σ: 0.02653 ± 0.00091
Int: 563.5 ± 23.7
S/B: 154.4
Entries
m(μ, track) [GeV]

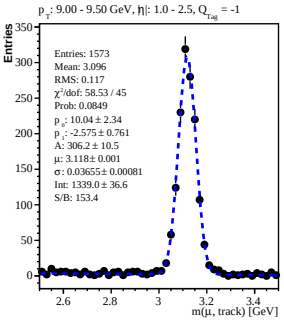
p_T: 9.00 - 9.50 GeV, |η|: 1.0 - 2.5, Q_{Tag} = -1
Entries: 1573
Mean: 3.096
RMS: 0.117
χ²/dof: 58.53 / 45
Prob: 0.0849
p0: 10.04 ± 2.34
p1: -2.575 ± 0.761
A: 306.2 ± 10.5
μ: 3.118 ± 0.001
σ: 0.03655 ± 0.00081
Int: 1339.0 ± 36.6
S/B: 153.4
Entries
m(μ, track) [GeV]

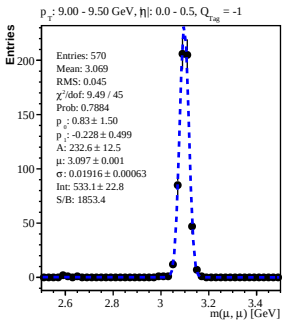
p_T: 9.00 - 9.50 GeV, |η|: 0.0 - 0.5, Q_{Tag} = -1
Entries: 570
Mean: 3.069
RMS: 0.045
χ²/dof: 9.49 / 45
Prob: 0.7884
p0: 0.83 ± 1.50
p1: -0.228 ± 0.499
A: 232.6 ± 12.5
μ: 3.097 ± 0.001
σ: 0.01916 ± 0.00063
Int: 533.1 ± 22.8
S/B: 1853.4
Entries
m(μ, μ) [GeV]

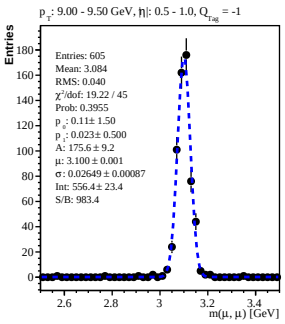
p_T: 9.00 - 9.50 GeV, |η|: 0.5 - 1.0, Q_{Tag} = -1
Entries: 605
Mean: 3.084
RMS: 0.040
χ²/dof: 19.22 / 45
Prob: 0.3955
p0: 0.11 ± 1.50
p1: 0.023 ± 0.500
A: 175.6 ± 9.2
μ: 3.100 ± 0.001
σ: 0.02649 ± 0.00087
Int: 556.4 ± 23.4
S/B: 983.4
Entries
m(μ, μ) [GeV]

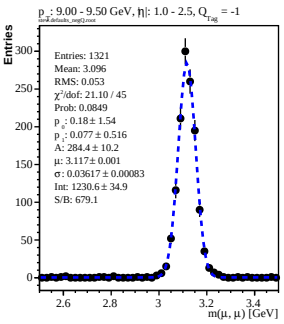
p_T: 9.00 - 9.50 GeV, |η|: 1.0 - 2.5, Q_{Tag} = -1
Entries: 1321
Mean: 3.096
RMS: 0.053
χ²/dof: 21.10 / 45
Prob: 0.0849
p0: 0.18 ± 1.54
p1: 0.077 ± 0.516
A: 284.4 ± 10.2
μ: 3.117 ± 0.001
σ: 0.03617 ± 0.00083
Int: 1230.6 ± 34.9
S/B: 679.1
Entries
m(μ, μ) [GeV]

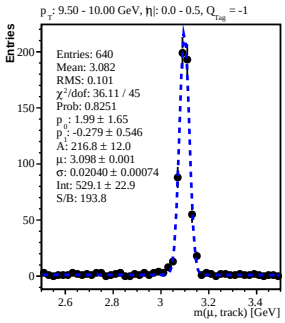
p_T: 9.50 - 10.00 GeV, |η|: 0.0 - 0.5, Q_{Tag} = -1
Entries: 640
Mean: 3.082
RMS: 0.101
χ²/dof: 36.11 / 45
Prob: 0.8251
p0: 1.99 ± 1.65
p1: -0.279 ± 0.546
A: 216.8 ± 12.0
μ: 3.098 ± 0.001
σ: 0.02040 ± 0.00074
Int: 529.1 ± 22.9
S/B: 193.8
Entries
m(μ, track) [GeV]

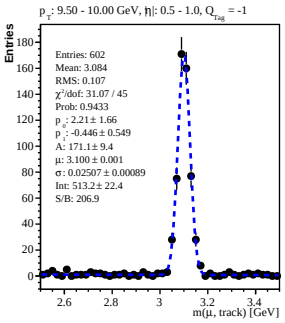
p_T: 9.50 - 10.00 GeV, |η|: 0.5 - 1.0, Q_{Tag} = -1
Entries: 602
Mean: 3.084
RMS: 0.107
χ²/dof: 31.07 / 45
Prob: 0.9433
p0: 2.21 ± 1.66
p1: -0.446 ± 0.549
A: 171.1 ± 9.4
μ: 3.100 ± 0.001
σ: 0.02507 ± 0.00089
Int: 513.2 ± 22.4
S/B: 206.9
Entries
m(μ, track) [GeV]

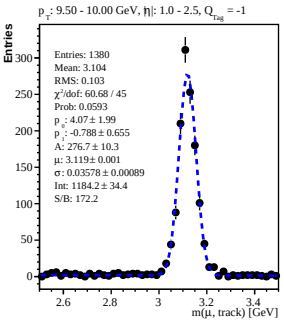
p_T: 9.50 - 10.00 GeV, |η|: 1.0 - 2.5, Q_{Tag} = -1
Entries: 1380
Mean: 3.104
RMS: 0.103
χ²/dof: 60.68 / 45
Prob: 0.0593
p0: 4.07 ± 1.99
p1: -0.788 ± 0.655
A: 276.7 ± 10.3
μ: 3.119 ± 0.001
σ: 0.03578 ± 0.00089
Int: 1184.2 ± 34.4
S/B: 172.2
Entries
m(μ, track) [GeV]

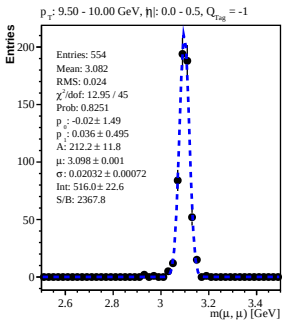
p_T: 9.50 - 10.00 GeV, |η|: 0.0 - 0.5, Q_{Tag} = -1
Entries: 554
Mean: 3.082
RMS: 0.024
χ²/dof: 12.95 / 45
Prob: 0.8251
p0: -0.02 ± 1.49
p1: 0.036 ± 0.495
A: 212.2 ± 11.8
μ: 3.098 ± 0.001
σ: 0.02032 ± 0.00072
Int: 516.0 ± 22.6
S/B: 2367.8
Entries
m(μ, μ) [GeV]

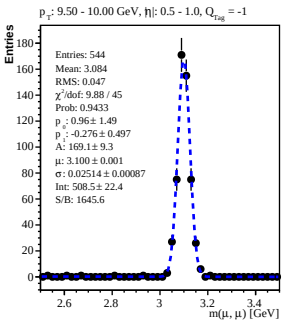
p_T: 9.50 - 10.00 GeV, |η|: 0.5 - 1.0, Q_{Tag} = -1
Entries: 544
Mean: 3.084
RMS: 0.047
χ²/dof: 9.88 / 45
Prob: 0.9433
p0: 0.96 ± 1.49
p1: -0.276 ± 0.497
A: 169.1 ± 9.3
μ: 3.100 ± 0.001
σ: 0.02514 ± 0.00087
Int: 508.5 ± 22.4
S/B: 1645.6
Entries
m(μ, μ) [GeV]

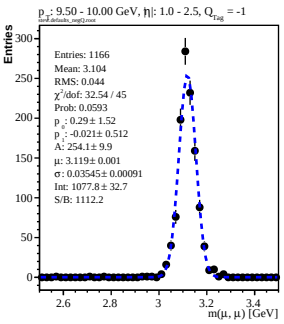
p_T: 9.50 - 10.00 GeV, |η|: 1.0 - 2.5, Q_{Tag} = -1
Entries: 1166
Mean: 3.104
RMS: 0.044
χ²/dof: 32.54 / 45
Prob: 0.0593
p0: 0.29 ± 1.52
p1: -0.021 ± 0.512
A: 254.1 ± 9.9
μ: 3.119 ± 0.001
σ: 0.03545 ± 0.00091
Int: 1077.8 ± 32.7
S/B: 1112.2
Entries
m(μ, μ) [GeV]

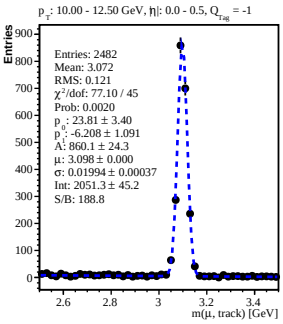
p_T: 10.00 - 12.50 GeV, |η|: 0.0 - 0.5, Q_{Tag} = -1
Entries: 2482
Mean: 3.072
RMS: 0.121
χ²/dof: 77.10 / 45
Prob: 0.0020
p_0: 23.81 ± 3.40
p_1: -6.208 ± 1.091
A: 860.1 ± 24.3
μ: 3.098 ± 0.000
σ: 0.01994 ± 0.00037
Int: 2051.3 ± 45.2
S/B: 188.8
Entries
m(μ, track) [GeV]

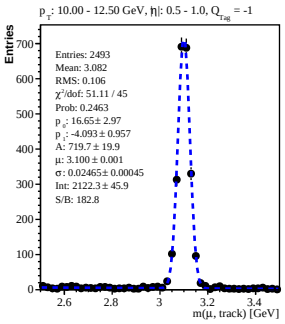
p_T: 10.00 - 12.50 GeV, |η|: 0.5 - 1.0, Q_{Tag} = -1
Entries: 2493
Mean: 3.082
RMS: 0.106
χ²/dof: 51.11 / 45
Prob: 0.2463
p_0: 16.65± 2.97
p_1: -4.093 ± 0.957
A: 719.7 ± 19.9
μ: 3.100 ± 0.001
σ: 0.02465± 0.00045
Int: 2122.3 ± 45.9
S/B: 182.8
Entries
m(μ, track) [GeV]

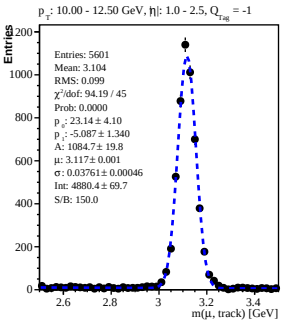
p_T: 10.00 - 12.50 GeV, |η|: 1.0 - 2.5, Q_{Tag} = -1
Entries: 5601
Mean: 3.104
RMS: 0.099
χ²/dof: 94.19 / 45
Prob: 0.0000
p_0: 23.14 ± 4.10
p_1: -5.087 ± 1.340
A: 1084.7 ± 19.8
μ: 3.117± 0.001
σ: 0.03761± 0.00046
Int: 4880.4 ± 69.7
S/B: 150.0
Entries
m(μ, track) [GeV]

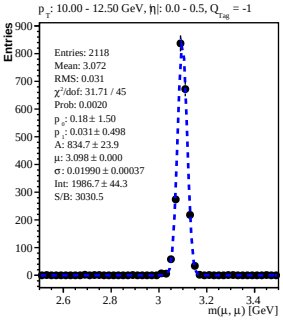
p_T: 10.00 - 12.50 GeV, |η|: 0.0 - 0.5, Q_{Tag} = -1
Entries: 2118
Mean: 3.072
RMS: 0.031
χ²/dof: 31.71 / 45
Prob: 0.0020
p_0: 0.18 ± 1.50
p_1: 0.031± 0.498
A: 834.7 ± 23.9
μ: 3.098 ± 0.000
σ: 0.01990 ± 0.00037
Int: 1986.7 ± 44.3
S/B: 3030.5
Entries
m(μ, μ) [GeV]

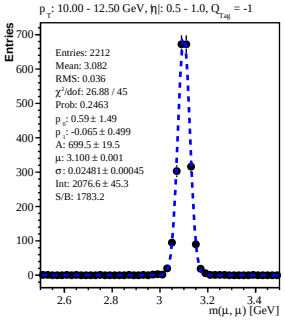
p_T: 10.00 - 12.50 GeV, |η|: 0.5 - 1.0, Q_{Tag} = -1
Entries: 2212
Mean: 3.082
RMS: 0.036
χ²/dof: 26.88 / 45
Prob: 0.2463
p_0: 0.59± 1.49
p_1: -0.065 ± 0.499
A: 699.5 ± 19.5
μ: 3.100 ± 0.001
σ: 0.02481± 0.00045
Int: 2076.6 ± 45.3
S/B: 1783.2
Entries
m(μ, μ) [GeV]

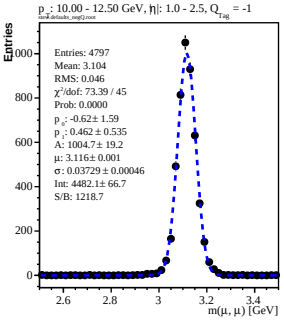
p_T: 10.00 - 12.50 GeV, |η|: 1.0 - 2.5, Q_{Tag} = -1
Entries: 4797
Mean: 3.104
RMS: 0.046
χ²/dof: 73.39 / 45
Prob: 0.0000
p_0: -0.62± 1.59
p_1: 0.462 ± 0.535
A: 1004.7± 19.2
μ: 3.116± 0.001
σ: 0.03729 ± 0.00046
Int: 4482.1± 66.7
S/B: 1218.7
Entries
m(μ, μ) [GeV]

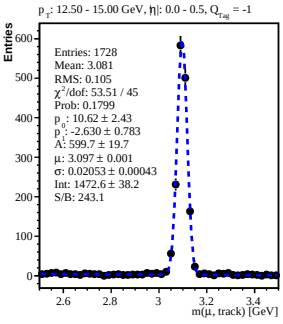
p_T: 12.50 - 15.00 GeV, |η|: 0.0 - 0.5, Q_{Tag} = -1
Entries: 1728
Mean: 3.081
RMS: 0.105
χ²/dof: 53.51 / 45
Prob: 0.1799
p_0: 10.62 ± 2.43
p_1: -2.630 ± 0.783
A: 599.7 ± 19.7
μ: 3.097 ± 0.001
σ: 0.02053 ± 0.00043
Int: 1472.6 ± 38.2
S/B: 243.1
Entries
m(μ, track) [GeV]

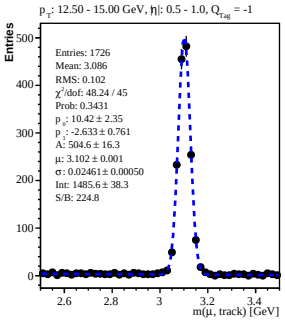
p_T: 12.50 - 15.00 GeV, |η|: 0.5 - 1.0, Q_{Tag} = -1
Entries: 1726
Mean: 3.086
RMS: 0.102
χ²/dof: 48.24 / 45
Prob: 0.3431
p_0: 10.42 ± 2.35
p_1: -2.633 ± 0.761
A: 504.6 ± 16.3
μ: 3.102 ± 0.001
σ: 0.02461± 0.00050
Int: 1485.6 ± 38.3
S/B: 224.8
Entries
m(μ, track) [GeV]

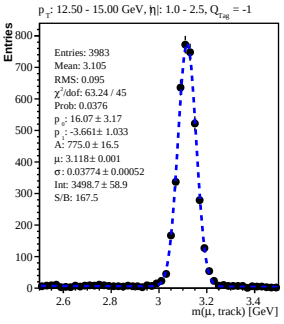
p_T: 12.50 - 15.00 GeV, |η|: 1.0 - 2.5, Q_{Tag} = -1
Entries: 3983
Mean: 3.105
RMS: 0.095
χ²/dof: 63.24 / 45
Prob: 0.0376
p_0: 16.07 ± 3.17
p_1: -3.661± 1.033
A: 775.0 ± 16.5
μ: 3.118± 0.001
σ: 0.03774 ± 0.00052
Int: 3498.7 ± 58.9
S/B: 167.5
Entries
m(μ, track) [GeV]

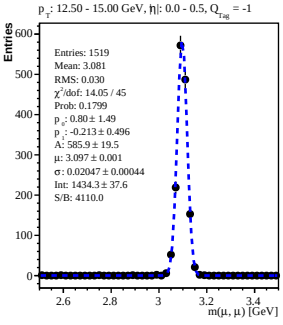
p_T: 12.50 - 15.00 GeV, |η|: 0.0 - 0.5, Q_{Tag} = -1
Entries: 1519
Mean: 3.081
RMS: 0.030
χ²/dof: 14.05 / 45
Prob: 0.1799
p_0: 0.80 ± 1.49
p_1: -0.213 ± 0.496
A: 585.9 ± 19.5
μ: 3.097 ± 0.001
σ: 0.02047 ± 0.00044
Int: 1434.3 ± 37.6
S/B: 4110.0
Entries
m(μ, μ) [GeV]

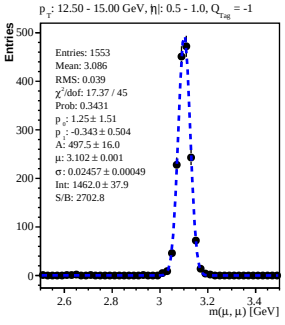
p_T: 12.50 - 15.00 GeV, |η|: 0.5 - 1.0, Q_{Tag} = -1
Entries: 1553
Mean: 3.086
RMS: 0.039
χ²/dof: 17.37 / 45
Prob: 0.3431
p_0: 1.25± 1.51
p_1: -0.343 ± 0.504
A: 497.5 ± 16.0
μ: 3.102 ± 0.001
σ: 0.02457 ± 0.00049
Int: 1462.0 ± 37.9
S/B: 2702.8
Entries
m(μ, μ) [GeV]

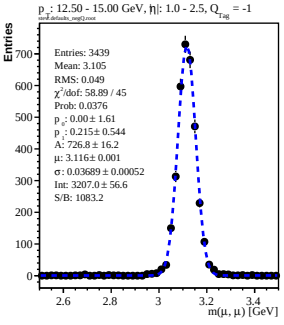
p_T: 12.50 - 15.00 GeV, |η|: 1.0 - 2.5, Q_{Tag} = -1
Entries: 3439
Mean: 3.105
RMS: 0.049
χ²/dof: 58.89 / 45
Prob: 0.0376
p_0: 0.00 ± 1.61
p_1: 0.215± 0.544
A: 726.8 ± 16.2
μ: 3.116± 0.001
σ: 0.03689 ± 0.00052
Int: 3207.0 ± 56.6
S/B: 1083.2
Entries
m(μ, μ) [GeV]

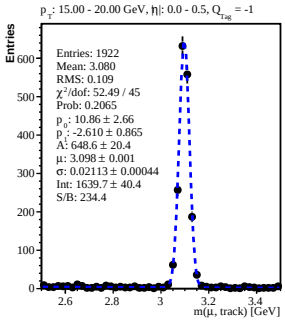
p_T: 15.00 - 20.00 GeV, |η|: 0.0 - 0.5, Q_Tag = -1
Entries: 1922
Mean: 3.080
RMS: 0.109
χ²/dof: 52.49 / 45
Prob: 0.2065
p_0: 10.86 ± 2.66
p_1: -2.610 ± 0.865
A: 648.6 ± 20.4
μ: 3.098 ± 0.001
σ: 0.02113 ± 0.00044
Int: 1639.7 ± 40.4
S/B: 234.4
Entries
m(μ, track) [GeV]

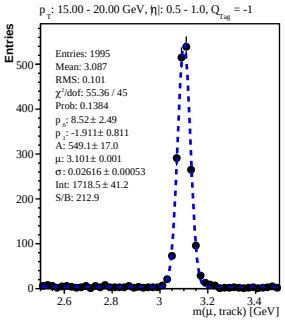
p_T: 15.00 - 20.00 GeV, |η|: 0.5 - 1.0, Q_Tag = -1
Entries: 1995
Mean: 3.087
RMS: 0.101
χ²/dof: 55.36 / 45
Prob: 0.1384
p_0: 8.52± 2.49
p_1: -1.911± 0.811
A: 549.1± 17.0
μ: 3.101± 0.001
σ: 0.02616 ± 0.00053
Int: 1718.5 ± 41.2
S/B: 212.9
Entries
m(μ, track) [GeV]

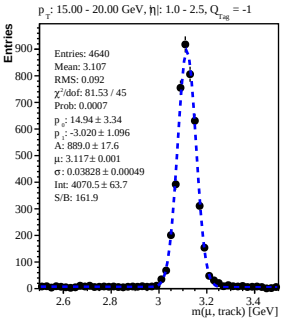
p_T: 15.00 - 20.00 GeV, |η|: 1.0 - 2.5, Q_Tag = -1
Entries: 4640
Mean: 3.107
RMS: 0.092
χ²/dof: 81.53 / 45
Prob: 0.0007
p_0: 14.94 ± 3.34
p_1: -3.020 ± 1.096
A: 889.0 ± 17.6
μ: 3.117± 0.001
σ: 0.03828 ± 0.00049
Int: 4070.5 ± 63.7
S/B: 161.9
Entries
m(μ, track) [GeV]

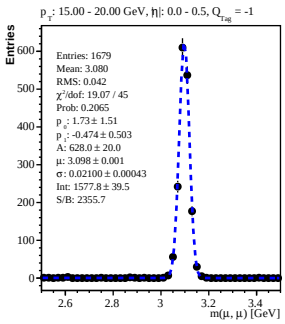
p_T: 15.00 - 20.00 GeV, |η|: 0.0 - 0.5, Q_Tag = -1
Entries: 1679
Mean: 3.080
RMS: 0.042
χ²/dof: 19.07 / 45
Prob: 0.2065
p_0: 1.73± 1.51
p_1: -0.474± 0.503
A: 628.0 ± 20.0
μ: 3.098 ± 0.001
σ: 0.02100 ± 0.00043
Int: 1577.8 ± 39.5
S/B: 2355.7
Entries
m(μ, μ) [GeV]

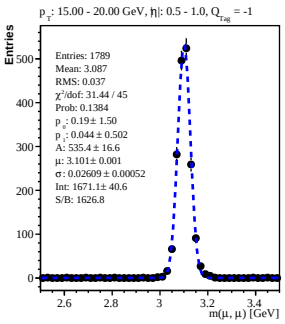
p_T: 15.00 - 20.00 GeV, |η|: 0.5 - 1.0, Q_Tag = -1
Entries: 1789
Mean: 3.087
RMS: 0.037
χ²/dof: 31.44 / 45
Prob: 0.1384
p_0: 0.19± 1.50
p_1: 0.044 ± 0.502
A: 535.4 ± 16.6
μ: 3.101± 0.001
σ: 0.02609 ± 0.00052
Int: 1671.1± 40.6
S/B: 1626.8
Entries
m(μ, μ) [GeV]

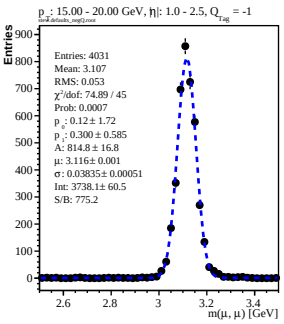
p_T: 15.00 - 20.00 GeV, |η|: 1.0 - 2.5, Q_Tag = -1
Entries: 4031
Mean: 3.107
RMS: 0.053
χ²/dof: 74.89 / 45
Prob: 0.0007
p_0: 0.12± 1.72
p_1: 0.300 ± 0.585
A: 814.8 ± 16.8
μ: 3.116± 0.001
σ: 0.03835± 0.00051
Int: 3738.1± 60.5
S/B: 775.2
Entries
m(μ, μ) [GeV]

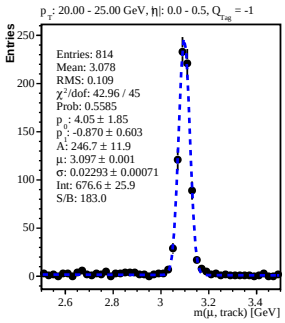
p_T: 20.00 - 25.00 GeV, |η|: 0.0 - 0.5, Q_Tag = -1
Entries: 814
Mean: 3.078
RMS: 0.109
χ²/dof: 42.96 / 45
Prob: 0.5585
p_0: 4.05 ± 1.85
p_1: -0.870 ± 0.603
A: 246.7 ± 11.9
μ: 3.097 ± 0.001
σ: 0.02293 ± 0.00071
Int: 676.6 ± 25.9
S/B: 183.0
Entries
m(μ, track) [GeV]

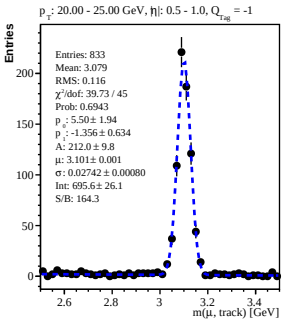
p_T: 20.00 - 25.00 GeV, |η|: 0.5 - 1.0, Q_Tag = -1
Entries: 833
Mean: 3.079
RMS: 0.116
χ²/dof: 39.73 / 45
Prob: 0.6943
p_0: 5.50± 1.94
p_1: -1.356 ± 0.634
A: 212.0 ± 9.8
μ: 3.101± 0.001
σ: 0.02742 ± 0.00080
Int: 695.6± 26.1
S/B: 164.3
Entries
m(μ, track) [GeV]

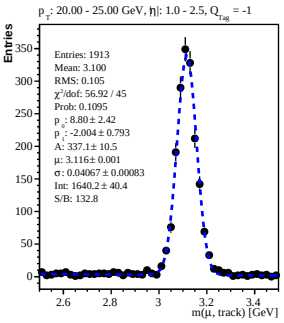
p_T: 20.00 - 25.00 GeV, |η|: 1.0 - 2.5, Q_Tag = -1
Entries: 1913
Mean: 3.100
RMS: 0.105
χ²/dof: 56.92 / 45
Prob: 0.1095
p_0: 8.80± 2.42
p_1: -2.004 ± 0.793
A: 337.1± 10.5
μ: 3.116± 0.001
σ: 0.04067 ± 0.00083
Int: 1640.2 ± 40.4
S/B: 132.8
Entries
m(μ, track) [GeV]

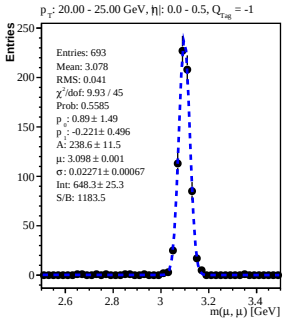
p_T: 20.00 - 25.00 GeV, |η|: 0.0 - 0.5, Q_Tag = -1
Entries: 693
Mean: 3.078
RMS: 0.041
χ²/dof: 9.93 / 45
Prob: 0.5585
p_0: 0.89 ± 1.49
p_1: -0.221± 0.496
A: 238.6 ± 11.5
μ: 3.098 ± 0.001
σ: 0.02271± 0.00067
Int: 648.3± 25.3
S/B: 1183.5
Entries
m(μ, μ) [GeV]

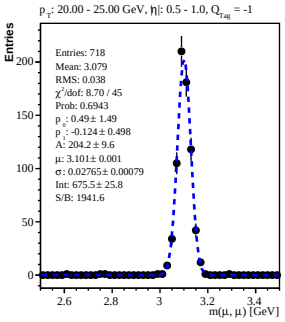
p_T: 20.00 - 25.00 GeV, |η|: 0.5 - 1.0, Q_Tag = -1
Entries: 718
Mean: 3.079
RMS: 0.038
χ²/dof: 8.70 / 45
Prob: 0.6943
p_0: 0.49± 1.49
p_1: -0.124 ± 0.498
A: 204.2 ± 9.6
μ: 3.101± 0.001
σ: 0.02765± 0.00079
Int: 675.5± 25.8
S/B: 1941.6
Entries
m(μ, μ) [GeV]

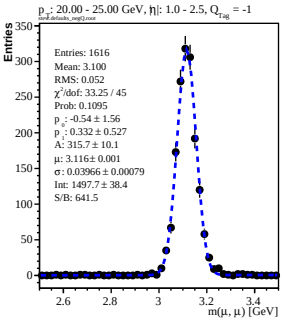
p_T: 20.00 - 25.00 GeV, |η|: 1.0 - 2.5, Q_Tag = -1
Entries: 1616
Mean: 3.100
RMS: 0.052
χ²/dof: 33.25 / 45
Prob: 0.1095
p_0: -0.54 ± 1.56
p_1: 0.332 ± 0.527
A: 315.7 ± 10.1
μ: 3.116± 0.001
σ: 0.03966 ± 0.00079
Int: 1497.7 ± 38.4
S/B: 641.5
Entries
m(μ, μ) [GeV]

Appendix C: Tracker Muon Mass Histogram Fits

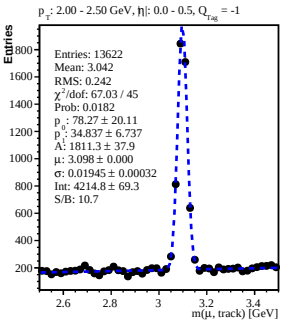

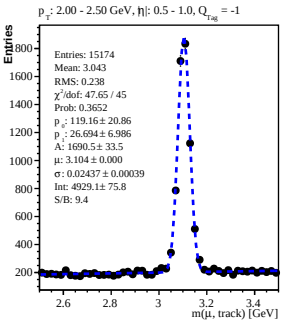

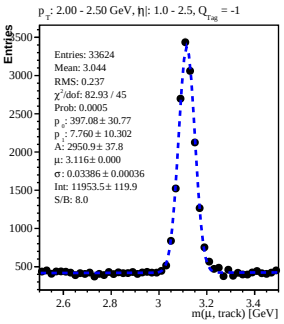

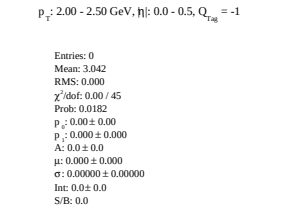

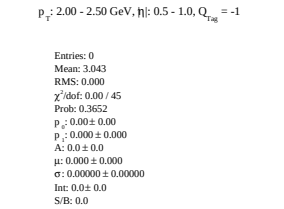

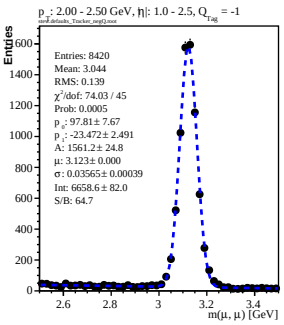

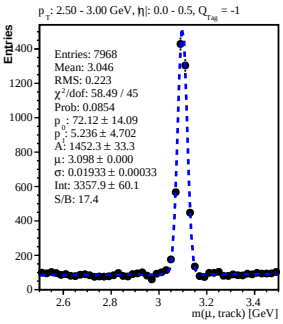

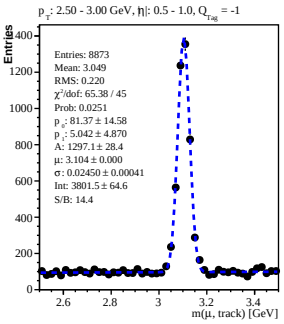

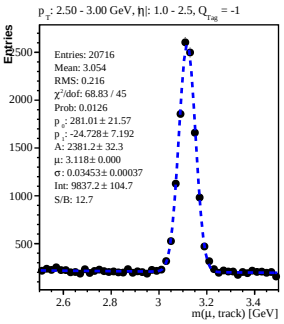

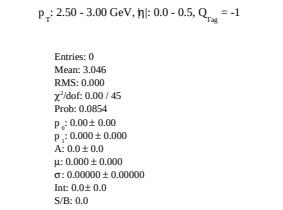

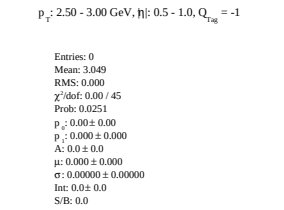

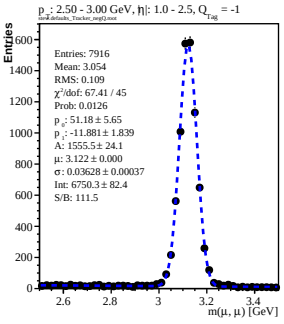

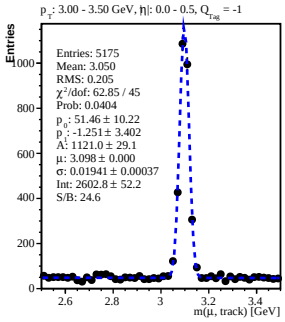
p_T: 3.00 - 3.50 GeV, |η|: 0.0 - 0.5, Q_Tag = -1
Entries: 5175
Mean: 3.050
RMS: 0.205
χ²/dof: 62.85 / 45
Prob: 0.0404
p0: 51.46 ± 10.22
p1: -1.251 ± 3.402
A: 1121.0 ± 29.1
μ: 3.098 ± 0.000
σ: 0.01941 ± 0.00037
Int: 2602.8 ± 52.2
S/B: 24.6
Entries
m(μ, track) [GeV]

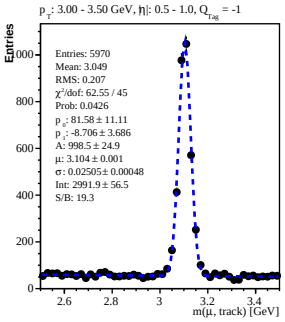
p_T: 3.00 - 3.50 GeV, |η|: 0.5 - 1.0, Q_Tag = -1
Entries: 5970
Mean: 3.049
RMS: 0.207
χ²/dof: 62.55 / 45
Prob: 0.0426
p0: 81.58 ± 11.11
p1: -8.706 ± 3.686
A: 998.5 ± 24.9
μ: 3.104 ± 0.001
σ: 0.02505 ± 0.00048
Int: 2991.9 ± 56.5
S/B: 19.3
Entries
m(μ, track) [GeV]

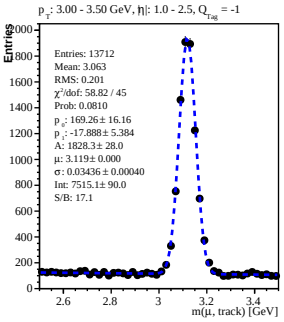
p_T: 3.00 - 3.50 GeV, |η|: 1.0 - 2.5, Q_Tag = -1
Entries: 13712
Mean: 3.063
RMS: 0.201
χ²/dof: 58.82 / 45
Prob: 0.0810
p0: 169.26 ± 16.16
p1: -17.888 ± 5.384
A: 1828.3 ± 28.0
μ: 3.119 ± 0.000
σ: 0.03436 ± 0.00040
Int: 7515.1 ± 90.0
S/B: 17.1
Entries
m(μ, track) [GeV]

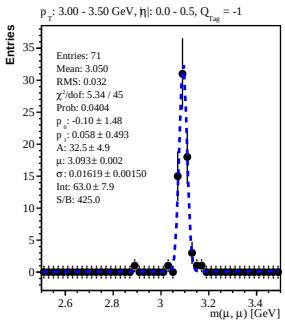
p_T: 3.00 - 3.50 GeV, |η|: 0.0 - 0.5, Q_Tag = -1
Entries: 71
Mean: 3.050
RMS: 0.032
χ²/dof: 5.34 / 45
Prob: 0.0404
p0: -0.10 ± 1.48
p1: 0.058 ± 0.493
A: 32.5 ± 4.9
μ: 3.093 ± 0.002
σ: 0.01619 ± 0.00150
Int: 63.0 ± 7.9
S/B: 425.0
Entries
m(μ, μ) [GeV]

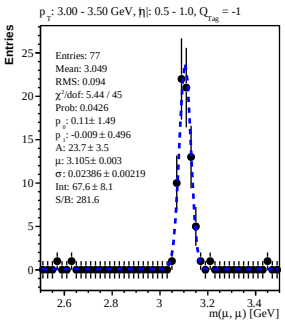
p_T: 3.00 - 3.50 GeV, |η|: 0.5 - 1.0, Q_Tag = -1
Entries: 77
Mean: 3.049
RMS: 0.094
χ²/dof: 5.44 / 45
Prob: 0.0426
p0: 0.11 ± 1.49
p1: -0.009 ± 0.496
A: 23.7 ± 3.5
μ: 3.105 ± 0.003
σ: 0.02386 ± 0.00219
Int: 67.6 ± 8.1
S/B: 281.6
Entries
m(μ, μ) [GeV]

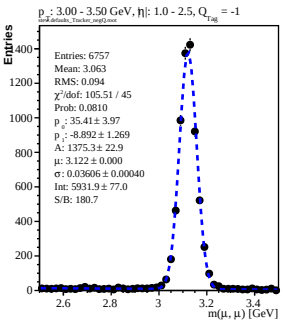
p_T: 3.00 - 3.50 GeV, |η|: 1.0 - 2.5, Q_Tag = -1
Entries: 6757
Mean: 3.063
RMS: 0.094
χ²/dof: 105.51 / 45
Prob: 0.0810
p0: 35.41 ± 3.97
p1: -8.892 ± 1.269
A: 1375.3 ± 22.9
μ: 3.122 ± 0.000
σ: 0.03606 ± 0.00040
Int: 5931.9 ± 77.0
S/B: 180.7
Entries
m(μ, μ) [GeV]

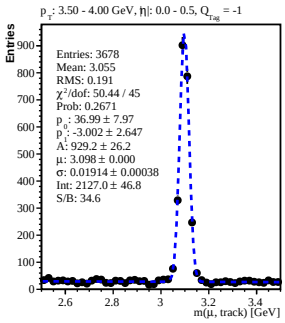
p_T: 3.50 - 4.00 GeV, |η|: 0.0 - 0.5, Q_Tag = -1
Entries: 3678
Mean: 3.055
RMS: 0.191
χ²/dof: 50.44 / 45
Prob: 0.2671
p0: 36.99 ± 7.97
p1: -3.002 ± 2.647
A: 929.2 ± 26.2
μ: 3.098 ± 0.000
σ: 0.01914 ± 0.00038
Int: 2127.0 ± 46.8
S/B: 34.6
Entries
m(μ, track) [GeV]

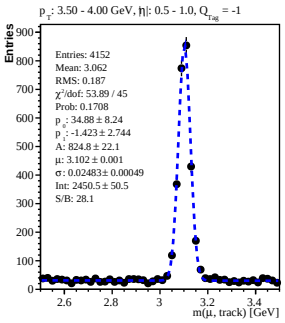
p_T: 3.50 - 4.00 GeV, |η|: 0.5 - 1.0, Q_Tag = -1
Entries: 4152
Mean: 3.062
RMS: 0.187
χ²/dof: 53.89 / 45
Prob: 0.1708
p0: 34.88 ± 8.24
p1: -1.423 ± 2.744
A: 824.8 ± 22.1
μ: 3.102 ± 0.001
σ: 0.02483 ± 0.00049
Int: 2450.5 ± 50.5
S/B: 28.1
Entries
m(μ, track) [GeV]

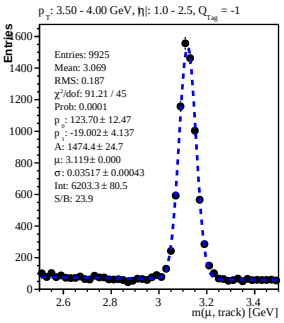
p_T: 3.50 - 4.00 GeV, |η|: 1.0 - 2.5, Q_Tag = -1
Entries: 9925
Mean: 3.069
RMS: 0.187
χ²/dof: 91.21 / 45
Prob: 0.0001
p0: 123.70 ± 12.47
p1: -19.002 ± 4.137
A: 1474.4 ± 24.7
μ: 3.119 ± 0.000
σ: 0.03517 ± 0.00043
Int: 6203.3 ± 80.5
S/B: 23.9
Entries
m(μ, track) [GeV]

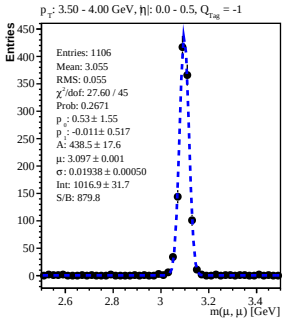
p_T: 3.50 - 4.00 GeV, |η|: 0.0 - 0.5, Q_Tag = -1
Entries: 1106
Mean: 3.055
RMS: 0.055
χ²/dof: 27.60 / 45
Prob: 0.2671
p0: 0.53 ± 1.55
p1: -0.011 ± 0.517
A: 438.5 ± 17.6
μ: 3.097 ± 0.001
σ: 0.01938 ± 0.00050
Int: 1016.9 ± 31.7
S/B: 879.8
Entries
m(μ, μ) [GeV]

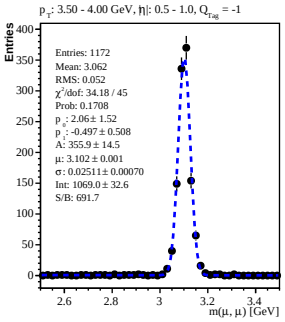
p_T: 3.50 - 4.00 GeV, |η|: 0.5 - 1.0, Q_Tag = -1
Entries: 1172
Mean: 3.062
RMS: 0.052
χ²/dof: 34.18 / 45
Prob: 0.1708
p0: 2.06 ± 1.52
p1: -0.497 ± 0.508
A: 355.9 ± 14.5
μ: 3.102 ± 0.001
σ: 0.02511 ± 0.00070
Int: 1069.0 ± 32.6
S/B: 691.7
Entries
m(μ, μ) [GeV]

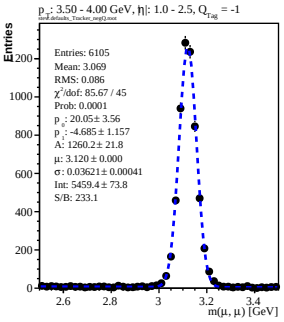
p_T: 3.50 - 4.00 GeV, |η|: 1.0 - 2.5, Q_Tag = -1
Entries: 6105
Mean: 3.069
RMS: 0.086
χ²/dof: 85.67 / 45
Prob: 0.0001
p0: 20.05 ± 3.56
p1: -4.685 ± 1.157
A: 1260.2 ± 21.8
μ: 3.120 ± 0.000
σ: 0.03621 ± 0.00041
Int: 5459.4 ± 73.8
S/B: 233.1
Entries
m(μ, μ) [GeV]

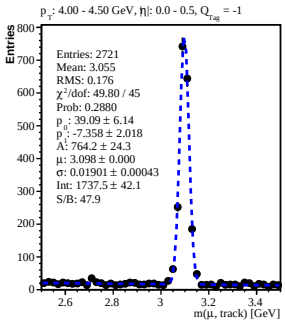
p_T: 4.00 - 4.50 GeV, η|: 0.0 - 0.5, Q_{Tag} = -1
Entries: 2721
Mean: 3.055
RMS: 0.176
χ²/dof: 49.80 / 45
Prob: 0.2880
p_0: -39.09 ± 6.14
p_1: -7.358 ± 2.018
A: 764.2 ± 24.3
μ: 3.098 ± 0.000
σ: 0.01901 ± 0.00043
Int: 1737.5 ± 42.1
S/B: 47.9
Entries
m(μ, track) [GeV]

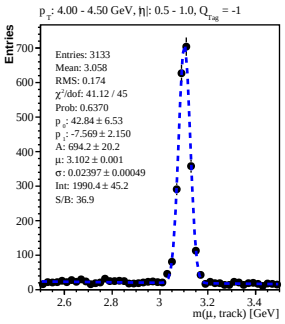
p_T: 4.00 - 4.50 GeV, η|: 0.5 - 1.0, Q_{Tag} = -1
Entries: 3133
Mean: 3.058
RMS: 0.174
χ²/dof: 41.12 / 45
Prob: 0.6370
p_0: 42.84 ± 6.53
p_1: -7.569 ± 2.150
A: 694.2 ± 20.2
μ: 3.102 ± 0.001
σ: 0.02397 ± 0.00049
Int: 1990.4 ± 45.2
S/B: 36.9
Entries
m(μ, track) [GeV]

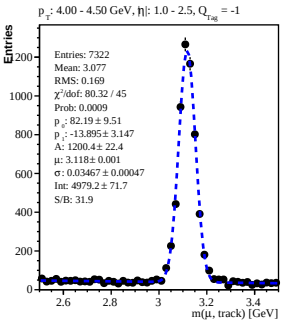
p_T: 4.00 - 4.50 GeV, η|: 1.0 - 2.5, Q_{Tag} = -1
Entries: 7322
Mean: 3.077
RMS: 0.169
χ²/dof: 80.32 / 45
Prob: 0.0009
p_0: 82.19 ± 9.51
p_1: -13.895 ± 3.147
A: 1200.4 ± 22.4
μ: 3.118 ± 0.001
σ: 0.03467 ± 0.00047
Int: 4979.2 ± 71.7
S/B: 31.9
Entries
m(μ, track) [GeV]

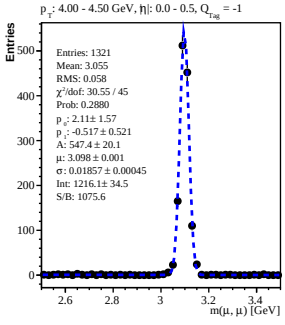
p_T: 4.00 - 4.50 GeV, η|: 0.0 - 0.5, Q_{Tag} = -1
Entries: 1321
Mean: 3.055
RMS: 0.058
χ²/dof: 30.55 / 45
Prob: 0.2880
p_0: 2.11± 1.57
p_1: -0.517 ± 0.521
A: 547.4 ± 20.1
μ: 3.098 ± 0.001
σ: 0.01857 ± 0.00045
Int: 1216.1± 34.5
S/B: 1075.6
Entries
m(μ, μ) [GeV]

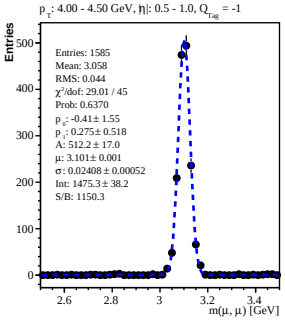
p_T: 4.00 - 4.50 GeV, η|: 0.5 - 1.0, Q_{Tag} = -1
Entries: 1585
Mean: 3.058
RMS: 0.044
χ²/dof: 29.01 / 45
Prob: 0.6370
p_0: -0.41± 1.55
p_1: 0.275± 0.518
A: 512.2 ± 17.0
μ: 3.101± 0.001
σ: 0.02408 ± 0.00052
Int: 1475.3 ± 38.2
S/B: 1150.3
Entries
m(μ, μ) [GeV]

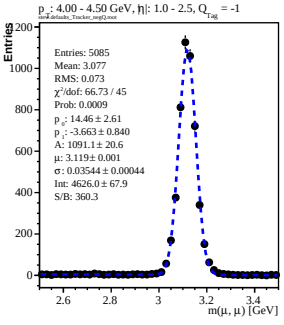
p_T: 4.00 - 4.50 GeV, η|: 1.0 - 2.5, Q_{Tag} = -1
Entries: 5085
Mean: 3.077
RMS: 0.073
χ²/dof: 66.73 / 45
Prob: 0.0009
p_0: 14.46 ± 2.61
p_1: -3.663 ± 0.840
A: 1091.1 ± 20.6
μ: 3.119± 0.001
σ: 0.03544 ± 0.00044
Int: 4626.0 ± 67.9
S/B: 360.3
Entries
m(μ, μ) [GeV]

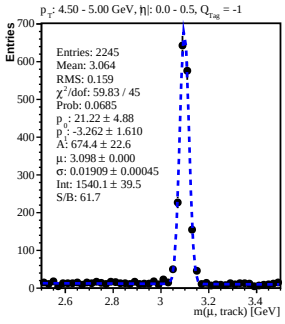
p_T: 4.50 - 5.00 GeV, η|: 0.0 - 0.5, Q_{Tag} = -1
Entries: 2245
Mean: 3.064
RMS: 0.159
χ²/dof: 59.83 / 45
Prob: 0.0685
p_0: 21.22 ± 4.88
p_1: -3.262 ± 1.610
A: 674.4 ± 22.6
μ: 3.098 ± 0.000
σ: 0.01909 ± 0.00045
Int: 1540.1 ± 39.5
S/B: 61.7
Entries
m(μ, track) [GeV]

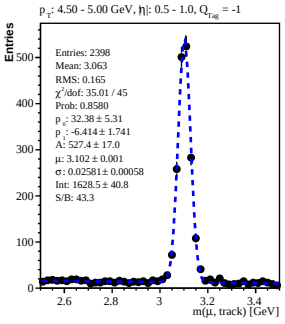
p_T: 4.50 - 5.00 GeV, η|: 0.5 - 1.0, Q_{Tag} = -1
Entries: 2398
Mean: 3.063
RMS: 0.165
χ²/dof: 35.01 / 45
Prob: 0.8580
p_0: 32.38 ± 5.31
p_1: -6.414 ± 1.741
A: 527.4 ± 17.0
μ: 3.102 ± 0.001
σ: 0.02581 ± 0.00058
Int: 1628.5 ± 40.8
S/B: 43.3
Entries
m(μ, track) [GeV]

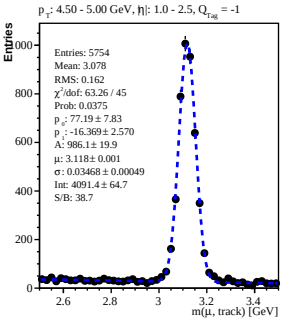
p_T: 4.50 - 5.00 GeV, η|: 1.0 - 2.5, Q_{Tag} = -1
Entries: 5754
Mean: 3.078
RMS: 0.162
χ²/dof: 63.26 / 45
Prob: 0.0375
p_0: 77.19 ± 7.83
p_1: -16.369± 2.570
A: 986.1± 19.9
μ: 3.118± 0.001
σ: 0.03468 ± 0.00049
Int: 4091.4 ± 64.7
S/B: 38.7
Entries
m(μ, track) [GeV]

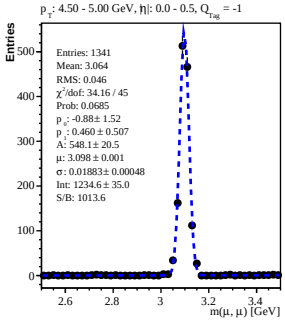
p_T: 4.50 - 5.00 GeV, η|: 0.0 - 0.5, Q_{Tag} = -1
Entries: 1341
Mean: 3.064
RMS: 0.046
χ²/dof: 34.16 / 45
Prob: 0.8685
p_0: -8.88± 1.52
p_1: 0.460 ± 0.507
A: 548.1± 20.5
μ: 3.098 ± 0.001
σ: 0.01883± 0.00048
Int: 1234.6 ± 35.0
S/B: 1013.6
Entries
m(μ, μ) [GeV]

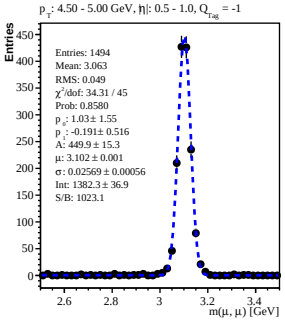
p_T: 4.50 - 5.00 GeV, η|: 0.5 - 1.0, Q_{Tag} = -1
Entries: 1494
Mean: 3.063
RMS: 0.049
χ²/dof: 34.31 / 45
Prob: 0.8580
p_0: 1.03± 1.55
p_1: -0.191± 0.516
A: 449.9 ± 15.3
μ: 3.102 ± 0.001
σ: 0.02569 ± 0.00056
Int: 1382.3 ± 36.9
S/B: 1023.1
Entries
m(μ, μ) [GeV]

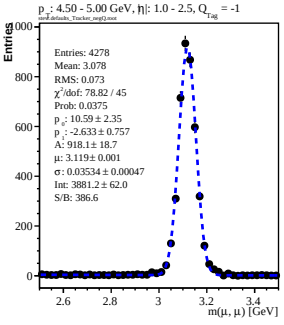
p_T: 4.50 - 5.00 GeV, η|: 1.0 - 2.5, Q_{Tag} = -1
Entries: 4278
Mean: 3.078
RMS: 0.073
χ²/dof: 78.82 / 45
Prob: 0.0375
p_0: 10.59 ± 2.35
p_1: -2.633 ± 0.757
A: 918.1 ± 18.7
μ: 3.119± 0.001
σ: 0.03534 ± 0.00047
Int: 3881.2 ± 62.0
S/B: 386.6
Entries
m(μ, μ) [GeV]

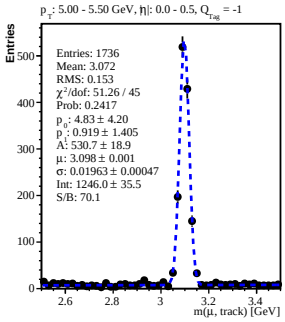
p_T: 5.00 - 5.50 GeV, |η|: 0.0 - 0.5, Q_{Tag} = -1
Entries: 1736
Mean: 3.072
RMS: 0.153
χ²/dof: 51.26 / 45
Prob: 0.2417
p0: 4.83 ± 4.20
p1: 0.919 ± 1.405
A: 530.7 ± 18.9
μ: 3.098 ± 0.001
σ: 0.01963 ± 0.00047
Int: 1246.0 ± 35.5
S/B: 70.1
Entries
m(μ, track) [GeV]

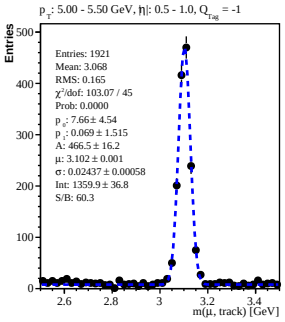
p_T: 5.00 - 5.50 GeV, |η|: 0.5 - 1.0, Q_{Tag} = -1
Entries: 1921
Mean: 3.068
RMS: 0.165
χ²/dof: 103.07 / 45
Prob: 0.0000
p0: 7.66± 4.54
p1: 0.069 ± 1.515
A: 466.5 ± 16.2
μ: 3.102 ± 0.001
σ: 0.02437 ± 0.00058
Int: 1359.9 ± 36.8
S/B: 60.3
Entries
m(μ, track) [GeV]

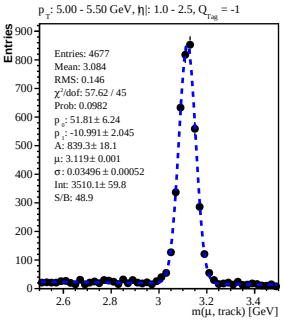
p_T: 5.00 - 5.50 GeV, |η|: 1.0 - 2.5, Q_{Tag} = -1
Entries: 4677
Mean: 3.084
RMS: 0.146
χ²/dof: 57.62 / 45
Prob: 0.0982
p0: 51.81± 6.24
p1: -10.991± 2.045
A: 839.3± 18.1
μ: 3.119± 0.001
σ: 0.03496 ± 0.00052
Int: 3510.1± 59.8
S/B: 48.9
Entries
m(μ, track) [GeV]

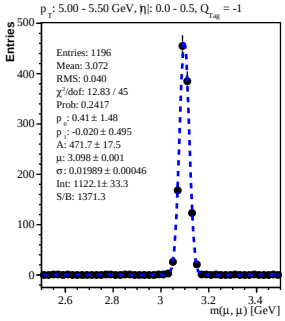
p_T: 5.00 - 5.50 GeV, |η|: 0.0 - 0.5, Q_{Tag} = -1
Entries: 1196
Mean: 3.072
RMS: 0.040
χ²/dof: 12.83 / 45
Prob: 0.2417
p0: 0.41 ± 1.48
p1: -0.020 ± 0.495
A: 471.7 ± 17.5
μ: 3.098 ± 0.001
σ: 0.01989 ± 0.00046
Int: 1122.1± 33.3
S/B: 1371.3
Entries
m(μ, μ) [GeV]

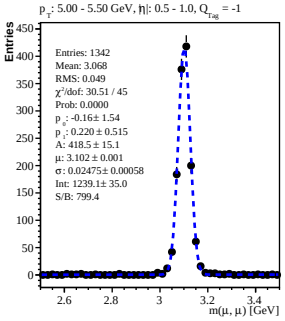
p_T: 5.00 - 5.50 GeV, |η|: 0.5 - 1.0, Q_{Tag} = -1
Entries: 1342
Mean: 3.068
RMS: 0.049
χ²/dof: 30.51 / 45
Prob: 0.0000
p0: -0.16± 1.54
p1: 0.220 ± 0.515
A: 418.5 ± 15.1
μ: 3.102 ± 0.001
σ: 0.02475± 0.00058
Int: 1239.1± 35.0
S/B: 799.4
Entries
m(μ, μ) [GeV]

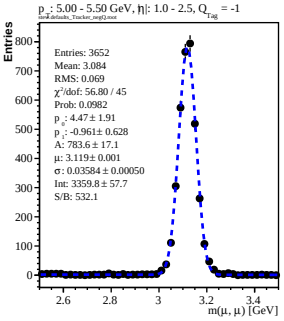
p_T: 5.00 - 5.50 GeV, |η|: 1.0 - 2.5, Q_{Tag} = -1
Entries: 3652
Mean: 3.084
RMS: 0.069
χ²/dof: 56.80 / 45
Prob: 0.0982
p0: 4.47 ± 1.91
p1: -0.961± 0.628
A: 783.6 ± 17.1
μ: 3.119± 0.001
σ: 0.03584 ± 0.00050
Int: 3359.8 ± 57.7
S/B: 532.1
Entries
m(μ, μ) [GeV]

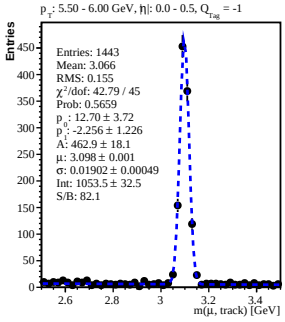
p_T: 5.50 - 6.00 GeV, |η|: 0.0 - 0.5, Q_{Tag} = -1
Entries: 1443
Mean: 3.066
RMS: 0.155
χ²/dof: 42.79 / 45
Prob: 0.5659
p0: 12.70 ± 3.72
p1: -2.256 ± 1.226
A: 462.9 ± 18.1
μ: 3.098 ± 0.001
σ: 0.01902 ± 0.00049
Int: 1053.5 ± 32.5
S/B: 82.1
Entries
m(μ, track) [GeV]

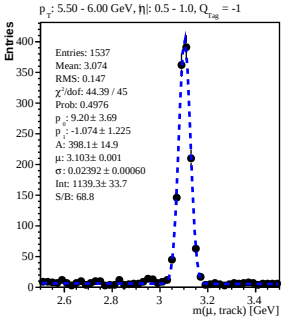
p_T: 5.50 - 6.00 GeV, |η|: 0.5 - 1.0, Q_{Tag} = -1
Entries: 1537
Mean: 3.074
RMS: 0.147
χ²/dof: 44.39 / 45
Prob: 0.4976
p0: 9.20± 3.69
p1: -1.074 ± 1.225
A: 398.1± 14.9
μ: 3.103± 0.001
σ: 0.02392 ± 0.00060
Int: 1139.3± 33.7
S/B: 68.8
Entries
m(μ, track) [GeV]

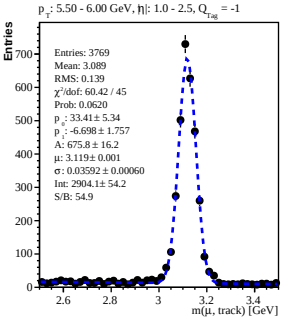
p_T: 5.50 - 6.00 GeV, |η|: 1.0 - 2.5, Q_{Tag} = -1
Entries: 3769
Mean: 3.089
RMS: 0.139
χ²/dof: 60.42 / 45
Prob: 0.0620
p0: 33.41± 5.34
p1: -6.698 ± 1.757
A: 675.8 ± 16.2
μ: 3.119± 0.001
σ: 0.03592 ± 0.00060
Int: 2904.1± 54.2
S/B: 54.9
Entries
m(μ, track) [GeV]

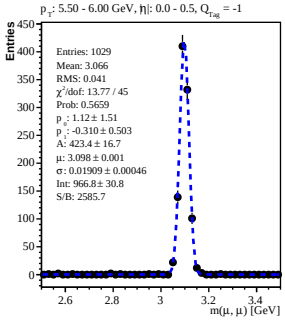
p_T: 5.50 - 6.00 GeV, |η|: 0.0 - 0.5, Q_{Tag} = -1
Entries: 1029
Mean: 3.066
RMS: 0.041
χ²/dof: 13.77 / 45
Prob: 0.5659
p0: 1.12± 1.51
p1: -0.310 ± 0.503
A: 423.4 ± 16.7
μ: 3.098 ± 0.001
σ: 0.01909 ± 0.00046
Int: 966.8± 30.8
S/B: 2585.7
Entries
m(μ, μ) [GeV]

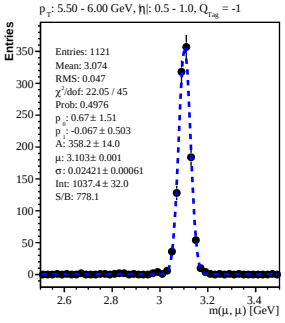
p_T: 5.50 - 6.00 GeV, |η|: 0.5 - 1.0, Q_{Tag} = -1
Entries: 1121
Mean: 3.074
RMS: 0.047
χ²/dof: 22.05 / 45
Prob: 0.4976
p0: 0.67± 1.51
p1: -0.067 ± 0.503
A: 358.2 ± 14.0
μ: 3.103± 0.001
σ: 0.02421± 0.00061
Int: 1037.4 ± 32.0
S/B: 778.1
Entries
m(μ, μ) [GeV]

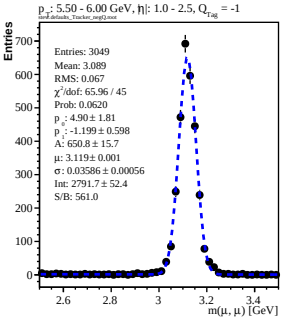
p_T: 5.50 - 6.00 GeV, |η|: 1.0 - 2.5, Q_{Tag} = -1
Entries: 3049
Mean: 3.089
RMS: 0.067
χ²/dof: 65.96 / 45
Prob: 0.0620
p0: 4.90± 1.81
p1: -1.199 ± 0.598
A: 650.8 ± 15.7
μ: 3.119± 0.001
σ: 0.03586 ± 0.00056
Int: 2791.7 ± 52.4
S/B: 561.0
Entries
m(μ, μ) [GeV]

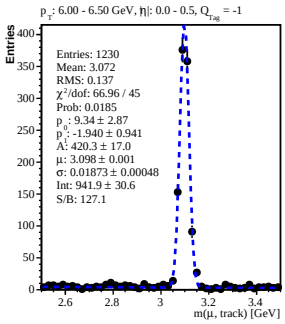
p_T: 6.00 - 6.50 GeV, |η|: 0.0 - 0.5, Q_{Tag} = -1
Entries: 1230
Mean: 3.072
RMS: 0.137
χ²/dof: 66.96 / 45
Prob: 0.0185
p0: 9.34 ± 2.87
p1: -1.940 ± 0.941
A: 420.3 ± 17.0
μ: 3.098 ± 0.001
σ: 0.01873 ± 0.00048
Int: 941.9 ± 30.6
S/B: 127.1
Entries
m(μ, track) [GeV]

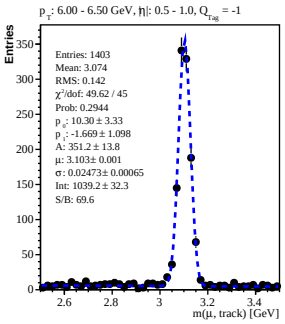
p_T: 6.00 - 6.50 GeV, |η|: 0.5 - 1.0, Q_{Tag} = -1
Entries: 1403
Mean: 3.074
RMS: 0.142
χ²/dof: 49.62 / 45
Prob: 0.2944
p0: 10.30 ± 3.33
p1: -1.669 ± 1.098
A: 351.2 ± 13.8
μ: 3.103± 0.001
σ: 0.02473± 0.00065
Int: 1039.2 ± 32.3
S/B: 69.6
Entries
m(μ, track) [GeV]

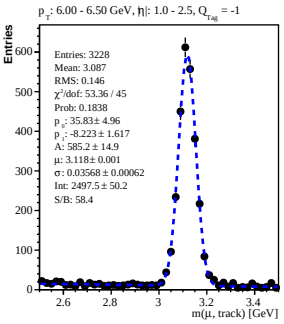
p_T: 6.00 - 6.50 GeV, |η|: 1.0 - 2.5, Q_{Tag} = -1
Entries: 3228
Mean: 3.087
RMS: 0.146
χ²/dof: 53.36 / 45
Prob: 0.1838
p0: 35.83± 4.96
p1: -8.223 ± 1.617
A: 585.2 ± 14.9
μ: 3.118± 0.001
σ: 0.03568 ± 0.00062
Int: 2497.5 ± 50.2
S/B: 58.4
Entries
m(μ, track) [GeV]

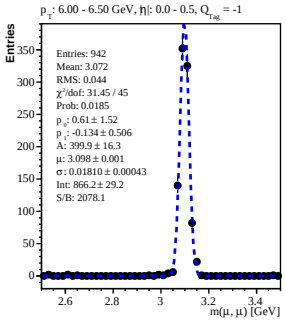
p_T: 6.00 - 6.50 GeV, |η|: 0.0 - 0.5, Q_{Tag} = -1
Entries: 942
Mean: 3.072
RMS: 0.044
χ²/dof: 31.45 / 45
Prob: 0.0185
p0: 0.61 ± 1.52
p1: -0.134 ± 0.506
A: 399.9 ± 16.3
μ: 3.098 ± 0.001
σ: 0.01810 ± 0.00043
Int: 866.2± 29.2
S/B: 2078.1
Entries
m(μ, μ) [GeV]

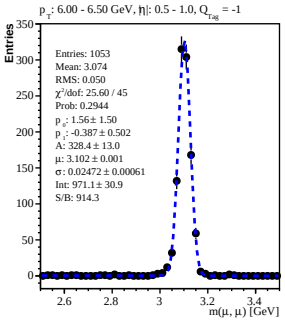
p_T: 6.00 - 6.50 GeV, |η|: 0.5 - 1.0, Q_{Tag} = -1
Entries: 1053
Mean: 3.074
RMS: 0.050
χ²/dof: 25.60 / 45
Prob: 0.2944
p0: 1.56± 1.50
p1: -0.387 ± 0.502
A: 328.4 ± 13.0
μ: 3.102 ± 0.001
σ: 0.02472 ± 0.00061
Int: 971.1 ± 30.9
S/B: 914.3
Entries
m(μ, μ) [GeV]

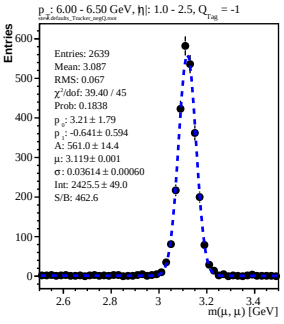
p_T: 6.00 - 6.50 GeV, |η|: 1.0 - 2.5, Q_{Tag} = -1
Entries: 2639
Mean: 3.087
RMS: 0.067
χ²/dof: 39.40 / 45
Prob: 0.1838
p0: 3.21 ± 1.79
p1: -0.641± 0.594
A: 561.0 ± 14.4
μ: 3.119± 0.001
σ: 0.03614 ± 0.00060
Int: 2425.5 ± 49.0
S/B: 462.6
Entries
m(μ, μ) [GeV]

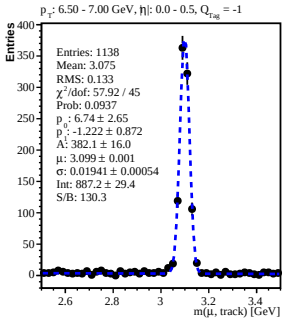
p_T: 6.50 - 7.00 GeV, |η|: 0.0 - 0.5, Q_{Tag} = -1
Entries: 1138
Mean: 3.075
RMS: 0.133
χ²/dof: 57.92 / 45
Prob: 0.0937
p0: 6.74 ± 2.65
p1: -1.222 ± 0.872
A: 382.1 ± 16.0
μ: 3.099 ± 0.001
σ: 0.01941 ± 0.00054
Int: 887.2 ± 29.4
S/B: 130.3
Entries
m(μ, track) [GeV]

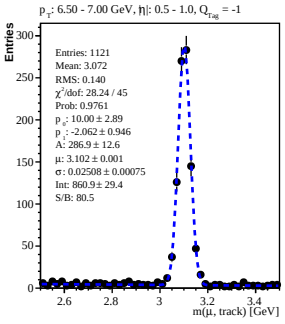
p_T: 6.50 - 7.00 GeV, |η|: 0.5 - 1.0, Q_{Tag} = -1
Entries: 1121
Mean: 3.072
RMS: 0.140
χ²/dof: 28.24 / 45
Prob: 0.9761
p0: 10.00 ± 2.89
p1: -2.062 ± 0.946
A: 286.9 ± 12.6
μ: 3.102 ± 0.001
σ: 0.02508 ± 0.00075
Int: 860.9± 29.4
S/B: 80.5
Entries
m(μ, track) [GeV]

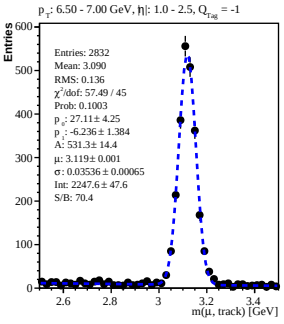
p_T: 6.50 - 7.00 GeV, |η|: 1.0 - 2.5, Q_{Tag} = -1
Entries: 2832
Mean: 3.090
RMS: 0.136
χ²/dof: 57.49 / 45
Prob: 0.1003
p0: 27.11± 4.25
p1: -6.236 ± 1.384
A: 531.3± 14.4
μ: 3.119± 0.001
σ: 0.03536 ± 0.00065
Int: 2247.6 ± 47.6
S/B: 70.4
Entries
m(μ, track) [GeV]

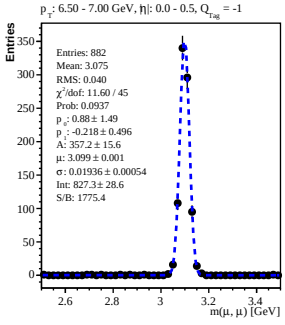
p_T: 6.50 - 7.00 GeV, |η|: 0.0 - 0.5, Q_{Tag} = -1
Entries: 882
Mean: 3.075
RMS: 0.040
χ²/dof: 11.60 / 45
Prob: 0.0937
p0: 0.88 ± 1.49
p1: -0.218 ± 0.496
A: 357.2 ± 15.6
μ: 3.099 ± 0.001
σ: 0.01936 ± 0.00054
Int: 827.3± 28.6
S/B: 1775.4
Entries
m(μ, μ) [GeV]

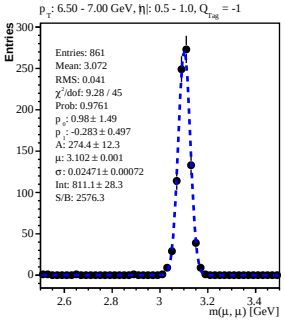
p_T: 6.50 - 7.00 GeV, |η|: 0.5 - 1.0, Q_{Tag} = -1
Entries: 861
Mean: 3.072
RMS: 0.041
χ²/dof: 9.28 / 45
Prob: 0.9761
p0: 0.98± 1.49
p1: -0.283 ± 0.497
A: 274.4 ± 12.3
μ: 3.102 ± 0.001
σ: 0.02471± 0.00072
Int: 811.1 ± 28.3
S/B: 2576.3
Entries
m(μ, μ) [GeV]

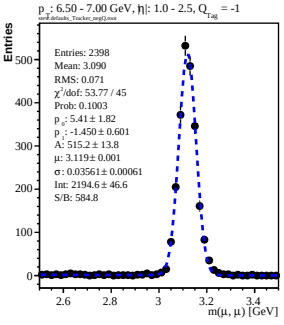
p_T: 6.50 - 7.00 GeV, |η|: 1.0 - 2.5, Q_{Tag} = -1
Entries: 2398
Mean: 3.090
RMS: 0.071
χ²/dof: 53.77 / 45
Prob: 0.1003
p0: 5.41± 1.82
p1: -1.450 ± 0.601
A: 515.2 ± 13.8
μ: 3.119± 0.001
σ: 0.03561± 0.00061
Int: 2194.6 ± 46.6
S/B: 584.8
Entries
m(μ, μ) [GeV]

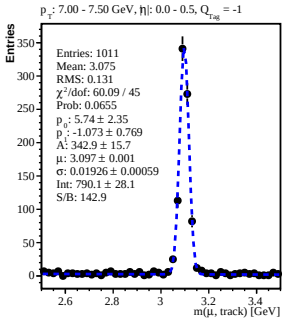
p_T: 7.00 - 7.50 GeV, |η|: 0.0 - 0.5, Q_Tag = -1
Entries: 1011
Mean: 3.075
RMS: 0.131
χ²/dof: 60.09 / 45
Prob: 0.0655
p_0: 5.74 ± 2.35
p_1: -1.073 ± 0.769
A: 342.9 ± 15.7
μ: 3.097 ± 0.001
σ: 0.01926 ± 0.00059
Int: 790.1 ± 28.1
S/B: 142.9
Entries
m(μ, track) [GeV]

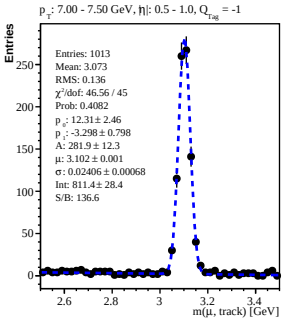
p_T: 7.00 - 7.50 GeV, |η|: 0.5 - 1.0, Q_Tag = -1
Entries: 1013
Mean: 3.073
RMS: 0.136
χ²/dof: 46.56 / 45
Prob: 0.4082
p_0: 12.31 ± 2.46
p_1: -3.298 ± 0.798
A: 281.9 ± 12.3
μ: 3.102 ± 0.001
σ: 0.02406 ± 0.00068
Int: 811.4 ± 28.4
S/B: 136.6
Entries
m(μ, track) [GeV]

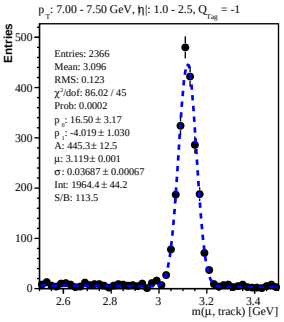
p_T: 7.00 - 7.50 GeV, |η|: 1.0 - 2.5, Q_Tag = -1
Entries: 2366
Mean: 3.096
RMS: 0.123
χ²/dof: 86.02 / 45
Prob: 0.0002
p_0: 16.50 ± 3.17
p_1: -4.019 ± 1.030
A: 445.3 ± 12.5
μ: 3.119 ± 0.001
σ: 0.03687 ± 0.00067
Int: 1964.4 ± 44.2
S/B: 113.5
Entries
m(μ, track) [GeV]

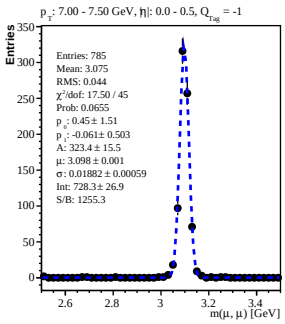
p_T: 7.00 - 7.50 GeV, |η|: 0.0 - 0.5, Q_Tag = -1
Entries: 785
Mean: 3.075
RMS: 0.044
χ²/dof: 17.50 / 45
Prob: 0.0655
p_0: 0.45 ± 1.51
p_1: -0.061 ± 0.503
A: 323.4 ± 15.5
μ: 3.098 ± 0.001
σ: 0.01882 ± 0.00059
Int: 728.3 ± 26.9
S/B: 1255.3
Entries
m(μ, μ) [GeV]

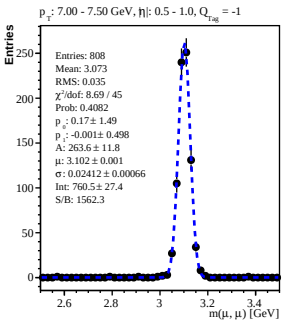
p_T: 7.00 - 7.50 GeV, |η|: 0.5 - 1.0, Q_Tag = -1
Entries: 808
Mean: 3.073
RMS: 0.035
χ²/dof: 8.69 / 45
Prob: 0.4082
p_0: 0.17 ± 1.49
p_1: -0.001 ± 0.498
A: 263.6 ± 11.8
μ: 3.102 ± 0.001
σ: 0.02412 ± 0.00066
Int: 760.5 ± 27.4
S/B: 1562.3
Entries
m(μ, μ) [GeV]

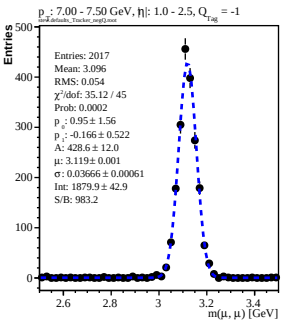
p_T: 7.00 - 7.50 GeV, |η|: 1.0 - 2.5, Q_Tag = -1
Entries: 2017
Mean: 3.096
RMS: 0.054
χ²/dof: 35.12 / 45
Prob: 0.0002
p_0: 0.95 ± 1.56
p_1: -0.166 ± 0.522
A: 428.6 ± 12.0
μ: 3.119 ± 0.001
σ: 0.03666 ± 0.00061
Int: 1879.9 ± 42.9
S/B: 983.2
Entries
m(μ, μ) [GeV]

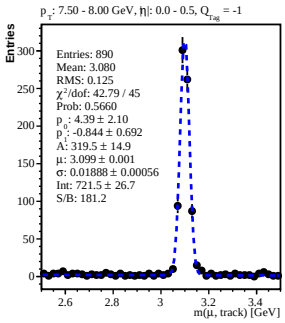
p_T: 7.50 - 8.00 GeV, |η|: 0.0 - 0.5, Q_Tag = -1
Entries: 890
Mean: 3.080
RMS: 0.125
χ²/dof: 42.79 / 45
Prob: 0.5660
p_0: 4.39 ± 2.10
p_1: -0.844 ± 0.692
A: 319.5 ± 14.9
μ: 3.099 ± 0.001
σ: 0.01888 ± 0.00056
Int: 721.5 ± 26.7
S/B: 181.2
Entries
m(μ, track) [GeV]

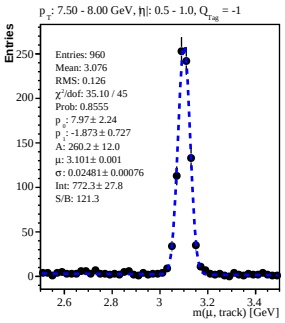
p_T: 7.50 - 8.00 GeV, |η|: 0.5 - 1.0, Q_Tag = -1
Entries: 960
Mean: 3.076
RMS: 0.126
χ²/dof: 35.10 / 45
Prob: 0.8555
p_0: 7.97 ± 2.24
p_1: -1.873 ± 0.727
A: 260.2 ± 12.0
μ: 3.101 ± 0.001
σ: 0.02481 ± 0.00076
Int: 772.3 ± 27.8
S/B: 121.3
Entries
m(μ, track) [GeV]

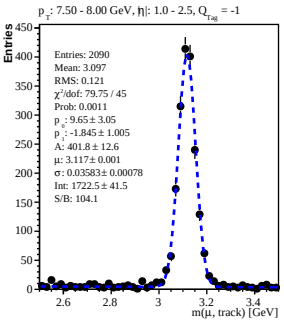
p_T: 7.50 - 8.00 GeV, |η|: 1.0 - 2.5, Q_Tag = -1
Entries: 2090
Mean: 3.097
RMS: 0.121
χ²/dof: 79.75 / 45
Prob: 0.0011
p_0: 9.65 ± 3.05
p_1: -1.845 ± 1.005
A: 401.8 ± 12.6
μ: 3.117 ± 0.001
σ: 0.03583 ± 0.00078
Int: 1722.5 ± 41.5
S/B: 104.1
Entries
m(μ, track) [GeV]

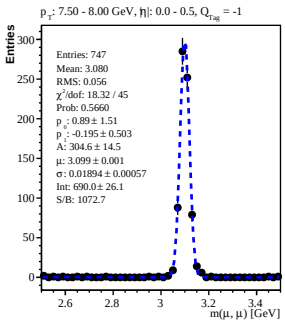
p_T: 7.50 - 8.00 GeV, |η|: 0.0 - 0.5, Q_Tag = -1
Entries: 747
Mean: 3.080
RMS: 0.056
χ²/dof: 18.32 / 45
Prob: 0.5660
p_0: 0.89 ± 1.51
p_1: -0.195 ± 0.503
A: 304.6 ± 14.5
μ: 3.099 ± 0.001
σ: 0.01894 ± 0.00057
Int: 690.0 ± 26.1
S/B: 1072.7
Entries
m(μ, μ) [GeV]

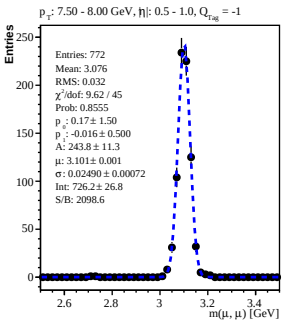
p_T: 7.50 - 8.00 GeV, |η|: 0.5 - 1.0, Q_Tag = -1
Entries: 772
Mean: 3.076
RMS: 0.032
χ²/dof: 9.62 / 45
Prob: 0.8555
p_0: 0.17 ± 1.50
p_1: -0.016 ± 0.500
A: 243.8 ± 11.3
μ: 3.101 ± 0.001
σ: 0.02490 ± 0.00072
Int: 726.2 ± 26.8
S/B: 2098.6
Entries
m(μ, μ) [GeV]

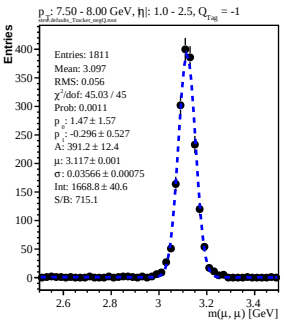
p_T: 7.50 - 8.00 GeV, |η|: 1.0 - 2.5, Q_Tag = -1
Entries: 1811
Mean: 3.097
RMS: 0.056
χ²/dof: 45.03 / 45
Prob: 0.0011
p_0: 1.47 ± 1.57
p_1: -0.296 ± 0.527
A: 391.2 ± 12.4
μ: 3.117 ± 0.001
σ: 0.03566 ± 0.00075
Int: 1668.8 ± 40.6
S/B: 715.1
Entries
m(μ, μ) [GeV]

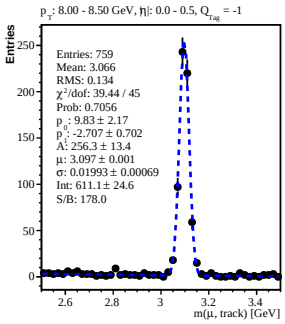
p_T: 8.00 - 8.50 GeV, |η|: 0.0 - 0.5, Q_{Tag} = -1
Entries: 759
Mean: 3.066
RMS: 0.134
χ²/dof: 39.44 / 45
Prob: 0.7056
p_0: 9.83 ± 2.17
p_1: -2.707 ± 0.702
A: 256.3 ± 13.4
μ: 3.097 ± 0.001
σ: 0.01993 ± 0.00069
Int: 611.1 ± 24.6
S/B: 178.0
Entries
m(μ, track) [GeV]

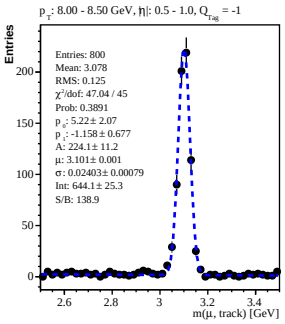
p_T: 8.00 - 8.50 GeV, |η|: 0.5 - 1.0, Q_{Tag} = -1
Entries: 800
Mean: 3.078
RMS: 0.125
χ²/dof: 47.04 / 45
Prob: 0.3891
p_0: 5.22 ± 2.07
p_1: -1.158 ± 0.677
A: 224.1 ± 11.2
μ: 3.101 ± 0.001
σ: 0.02403 ± 0.00079
Int: 644.1 ± 25.3
S/B: 138.9
Entries
m(μ, track) [GeV]

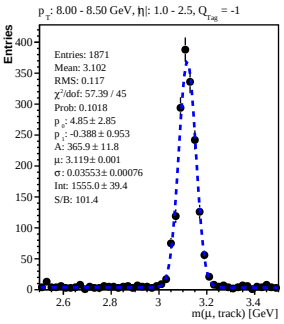
p_T: 8.00 - 8.50 GeV, |η|: 1.0 - 2.5, Q_{Tag} = -1
Entries: 1871
Mean: 3.102
RMS: 0.117
χ²/dof: 57.39 / 45
Prob: 0.1018
p_0: 4.85 ± 2.85
p_1: -0.388 ± 0.953
A: 365.9 ± 11.8
μ: 3.119 ± 0.001
σ: 0.03553 ± 0.00076
Int: 1555.0 ± 39.4
S/B: 101.4
Entries
m(μ, track) [GeV]

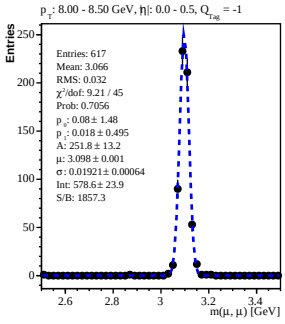
p_T: 8.00 - 8.50 GeV, |η|: 0.0 - 0.5, Q_{Tag} = -1
Entries: 617
Mean: 3.066
RMS: 0.032
χ²/dof: 9.21 / 45
Prob: 0.7056
p_0: 0.08 ± 1.48
p_1: 0.018 ± 0.495
A: 251.8 ± 13.2
μ: 3.098 ± 0.001
σ: 0.01921 ± 0.00064
Int: 578.6 ± 23.9
S/B: 1857.3
Entries
m(μ, μ) [GeV]

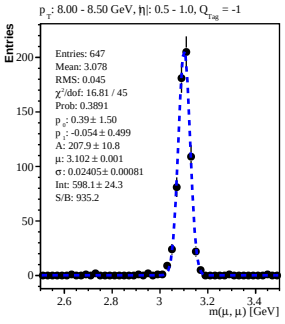
p_T: 8.00 - 8.50 GeV, |η|: 0.5 - 1.0, Q_{Tag} = -1
Entries: 647
Mean: 3.078
RMS: 0.045
χ²/dof: 16.81 / 45
Prob: 0.3891
p_0: 0.39 ± 1.50
p_1: -0.054 ± 0.499
A: 207.9 ± 10.8
μ: 3.102 ± 0.001
σ: 0.02405 ± 0.00081
Int: 598.1 ± 24.3
S/B: 935.2
Entries
m(μ, μ) [GeV]

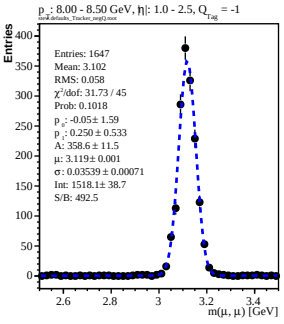
p_T: 8.00 - 8.50 GeV, |η|: 1.0 - 2.5, Q_{Tag} = -1
Entries: 1647
Mean: 3.102
RMS: 0.058
χ²/dof: 31.73 / 45
Prob: 0.1018
p_0: -0.05 ± 1.59
p_1: 0.250 ± 0.533
A: 358.6 ± 11.5
μ: 3.119 ± 0.001
σ: 0.03539 ± 0.00071
Int: 1518.1 ± 38.7
S/B: 492.5
Entries
m(μ, μ) [GeV]

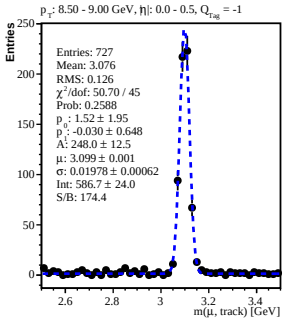
p_T: 8.50 - 9.00 GeV, |η|: 0.0 - 0.5, Q_{Tag} = -1
Entries: 727
Mean: 3.076
RMS: 0.126
χ²/dof: 50.70 / 45
Prob: 0.2588
p_0: 1.52 ± 1.95
p_1: -0.030 ± 0.648
A: 248.0 ± 12.5
μ: 3.099 ± 0.001
σ: 0.01978 ± 0.00062
Int: 586.7 ± 24.0
S/B: 174.4
Entries
m(μ, track) [GeV]

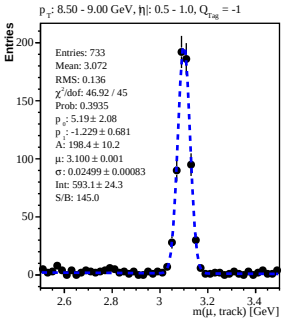
p_T: 8.50 - 9.00 GeV, |η|: 0.5 - 1.0, Q_{Tag} = -1
Entries: 733
Mean: 3.072
RMS: 0.136
χ²/dof: 46.92 / 45
Prob: 0.3935
p_0: 5.19 ± 2.08
p_1: -1.229 ± 0.681
A: 198.4 ± 10.2
μ: 3.100 ± 0.001
σ: 0.02499 ± 0.00083
Int: 593.1 ± 24.3
S/B: 145.0
Entries
m(μ, track) [GeV]

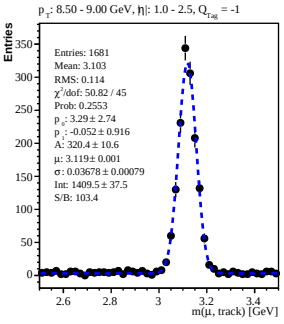
p_T: 8.50 - 9.00 GeV, |η|: 1.0 - 2.5, Q_{Tag} = -1
Entries: 1681
Mean: 3.103
RMS: 0.114
χ²/dof: 50.82 / 45
Prob: 0.2553
p_0: 3.29 ± 2.74
p_1: -0.052 ± 0.916
A: 320.4 ± 10.6
μ: 3.119 ± 0.001
σ: 0.03678 ± 0.00079
Int: 1409.5 ± 37.5
S/B: 103.4
Entries
m(μ, track) [GeV]

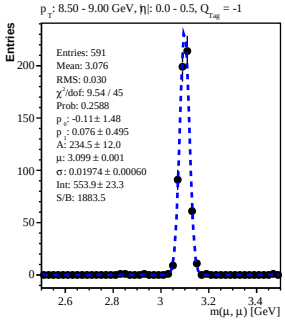
p_T: 8.50 - 9.00 GeV, |η|: 0.0 - 0.5, Q_{Tag} = -1
Entries: 591
Mean: 3.076
RMS: 0.030
χ²/dof: 9.54 / 45
Prob: 0.2588
p_0: -0.11 ± 1.48
p_1: 0.076 ± 0.495
A: 234.5 ± 12.0
μ: 3.099 ± 0.001
σ: 0.01974 ± 0.00060
Int: 553.9 ± 23.3
S/B: 1883.5
Entries
m(μ, μ) [GeV]

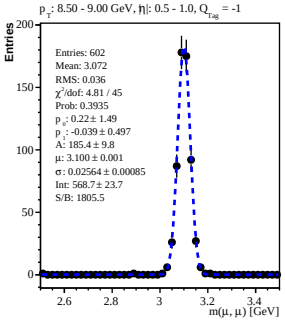
p_T: 8.50 - 9.00 GeV, |η|: 0.5 - 1.0, Q_{Tag} = -1
Entries: 602
Mean: 3.072
RMS: 0.036
χ²/dof: 4.81 / 45
Prob: 0.3935
p_0: 0.22 ± 1.49
p_1: -0.039 ± 0.497
A: 185.4 ± 9.8
μ: 3.100 ± 0.001
σ: 0.02564 ± 0.00085
Int: 568.7 ± 23.7
S/B: 1805.5
Entries
m(μ, μ) [GeV]

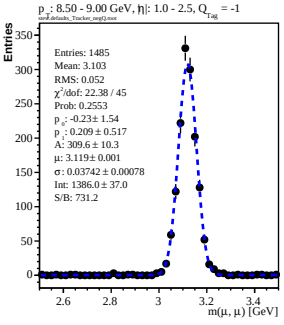
p_T: 8.50 - 9.00 GeV, |η|: 1.0 - 2.5, Q_{Tag} = -1
Entries: 1485
Mean: 3.103
RMS: 0.052
χ²/dof: 22.38 / 45
Prob: 0.2553
p_0: -0.23 ± 1.54
p_1: 0.209 ± 0.517
A: 309.6 ± 10.3
μ: 3.119 ± 0.001
σ: 0.03742 ± 0.00078
Int: 1386.0 ± 37.0
S/B: 731.2
Entries
m(μ, μ) [GeV]

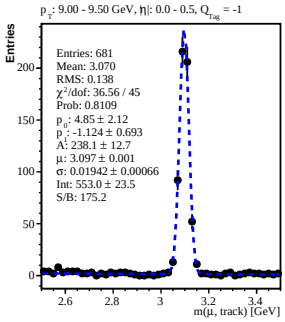
p_T: 9.00 - 9.50 GeV, |η|: 0.0 - 0.5, Q_{Tag} = -1
Entries: 681
Mean: 3.070
RMS: 0.138
χ²/dof: 36.56 / 45
Prob: 0.8109
p_0: 4.85 ± 2.12
p_1: -1.124 ± 0.693
A: 238.1 ± 12.7
μ: 3.097 ± 0.001
σ: 0.01942 ± 0.00066
Int: 553.0 ± 23.5
S/B: 175.2
Entries
m(μ, track) [GeV]

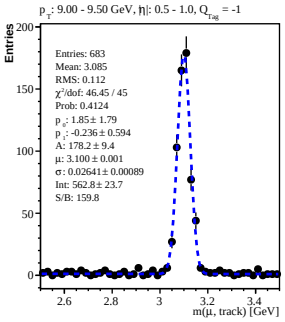
p_T: 9.00 - 9.50 GeV, |η|: 0.5 - 1.0, Q_{Tag} = -1
Entries: 683
Mean: 3.085
RMS: 0.112
χ²/dof: 46.45 / 45
Prob: 0.4124
p_0: 1.85± 1.79
p_1: -0.236 ± 0.594
A: 178.2 ± 9.4
μ: 3.100 ± 0.001
σ: 0.02641± 0.00089
Int: 562.8± 23.7
S/B: 159.8
Entries
m(μ, track) [GeV]

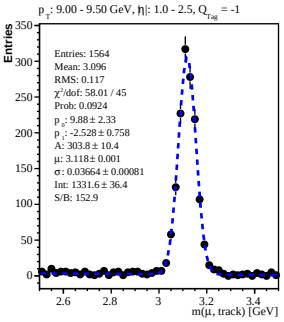
p_T: 9.00 - 9.50 GeV, |η|: 1.0 - 2.5, Q_{Tag} = -1
Entries: 1564
Mean: 3.096
RMS: 0.117
χ²/dof: 58.01 / 45
Prob: 0.0924
p_0: 9.88± 2.33
p_1: -2.528 ± 0.758
A: 303.8 ± 10.4
μ: 3.118± 0.001
σ: 0.03664 ± 0.00081
Int: 1331.6 ± 36.4
S/B: 152.9
Entries
m(μ, track) [GeV]

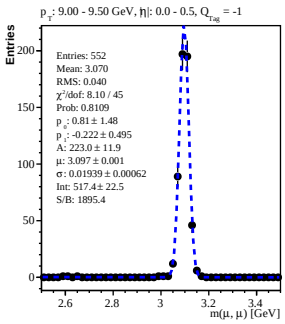
p_T: 9.00 - 9.50 GeV, |η|: 0.0 - 0.5, Q_{Tag} = -1
Entries: 552
Mean: 3.070
RMS: 0.040
χ²/dof: 8.10 / 45
Prob: 0.8109
p_0: 0.81 ± 1.48
p_1: -0.222 ± 0.495
A: 223.0 ± 11.9
μ: 3.097 ± 0.001
σ: 0.01939 ± 0.00062
Int: 517.4± 22.5
S/B: 1895.4
Entries
m(μ, μ) [GeV]

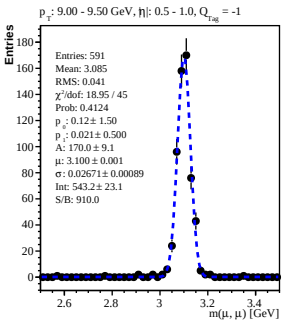
p_T: 9.00 - 9.50 GeV, |η|: 0.5 - 1.0, Q_{Tag} = -1
Entries: 591
Mean: 3.085
RMS: 0.041
χ²/dof: 18.95 / 45
Prob: 0.4124
p_0: 0.12± 1.50
p_1: 0.021± 0.500
A: 170.0 ± 9.1
μ: 3.100 ± 0.001
σ: 0.02671± 0.00089
Int: 543.2± 23.1
S/B: 910.0
Entries
m(μ, μ) [GeV]

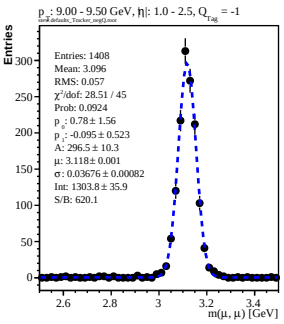
p_T: 9.00 - 9.50 GeV, |η|: 1.0 - 2.5, Q_{Tag} = -1
Entries: 1408
Mean: 3.096
RMS: 0.057
χ²/dof: 28.51 / 45
Prob: 0.0924
p_0: 0.78± 1.56
p_1: -0.095 ± 0.523
A: 296.5 ± 10.3
μ: 3.118± 0.001
σ: 0.03676 ± 0.00082
Int: 1303.8 ± 35.9
S/B: 620.1
Entries
m(μ, μ) [GeV]

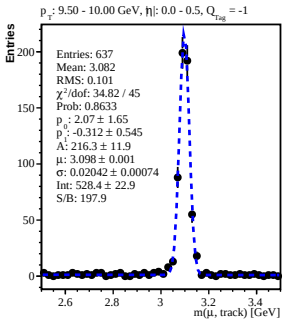
p_T: 9.50 - 10.00 GeV, |η|: 0.0 - 0.5, Q_{Tag} = -1
Entries: 637
Mean: 3.082
RMS: 0.101
χ²/dof: 34.82 / 45
Prob: 0.8633
p_0: 2.07 ± 1.65
p_1: -0.312 ± 0.545
A: 216.3 ± 11.9
μ: 3.098 ± 0.001
σ: 0.02042 ± 0.00074
Int: 528.4 ± 22.9
S/B: 197.9
Entries
m(μ, track) [GeV]

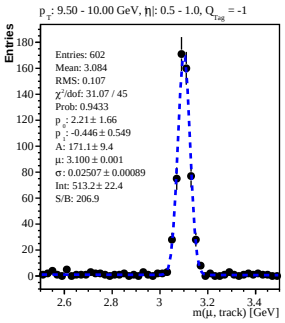
p_T: 9.50 - 10.00 GeV, |η|: 0.5 - 1.0, Q_{Tag} = -1
Entries: 602
Mean: 3.084
RMS: 0.107
χ²/dof: 31.07 / 45
Prob: 0.9433
p_0: 2.21± 1.66
p_1: -0.446 ± 0.549
A: 171.1± 9.4
μ: 3.100 ± 0.001
σ: 0.02507 ± 0.00089
Int: 513.2± 22.4
S/B: 206.9
Entries
m(μ, track) [GeV]

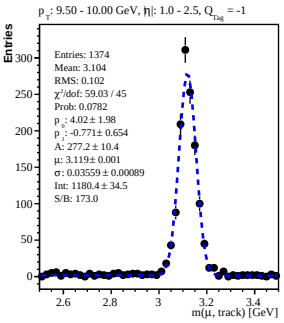
p_T: 9.50 - 10.00 GeV, |η|: 1.0 - 2.5, Q_{Tag} = -1
Entries: 1374
Mean: 3.104
RMS: 0.102
χ²/dof: 59.03 / 45
Prob: 0.0782
p_0: 4.02± 1.98
p_1: -0.771± 0.654
A: 277.2 ± 10.4
μ: 3.119± 0.001
σ: 0.03559 ± 0.00089
Int: 1180.4 ± 34.5
S/B: 173.0
Entries
m(μ, track) [GeV]

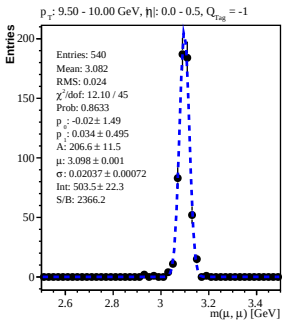
p_T: 9.50 - 10.00 GeV, |η|: 0.0 - 0.5, Q_{Tag} = -1
Entries: 540
Mean: 3.082
RMS: 0.024
χ²/dof: 12.10 / 45
Prob: 0.8633
p_0: -0.02± 1.49
p_1: 0.034 ± 0.495
A: 206.6 ± 11.5
μ: 3.098 ± 0.001
σ: 0.02037 ± 0.00072
Int: 503.5± 22.3
S/B: 2366.2
Entries
m(μ, μ) [GeV]

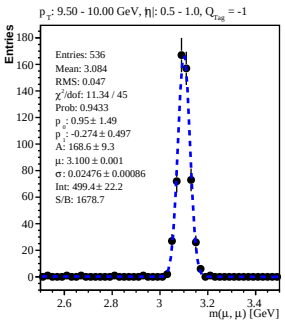
p_T: 9.50 - 10.00 GeV, |η|: 0.5 - 1.0, Q_{Tag} = -1
Entries: 536
Mean: 3.084
RMS: 0.047
χ²/dof: 11.34 / 45
Prob: 0.9433
p_0: 0.95± 1.49
p_1: -0.274 ± 0.497
A: 168.6 ± 9.3
μ: 3.100 ± 0.001
σ: 0.02476 ± 0.00086
Int: 499.4± 22.2
S/B: 1678.7
Entries
m(μ, μ) [GeV]

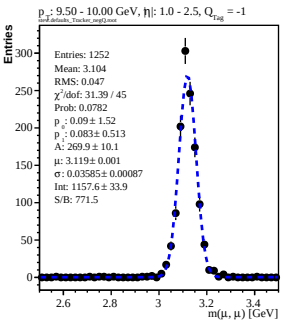
p_T: 9.50 - 10.00 GeV, |η|: 1.0 - 2.5, Q_{Tag} = -1
Entries: 1252
Mean: 3.104
RMS: 0.047
χ²/dof: 31.39 / 45
Prob: 0.0782
p_0: 0.09± 1.52
p_1: 0.083± 0.513
A: 269.9 ± 10.1
μ: 3.119± 0.001
σ: 0.03585± 0.00087
Int: 1157.6± 33.9
S/B: 771.5
Entries
m(μ, μ) [GeV]

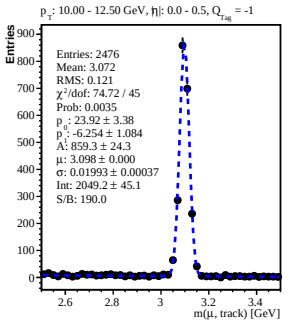
p_T: 10.00 - 12.50 GeV, |η|: 0.0 - 0.5, Q_{Trk} = -1
Entries: 2476
Mean: 3.072
RMS: 0.121
χ²/dof: 74.72 / 45
Prob: 0.0035
p_0: 23.92 ± 3.38
p_1: -6.254 ± 1.084
A: 859.3 ± 24.3
μ: 3.098 ± 0.000
σ: 0.01993 ± 0.00037
Int: 2049.2 ± 45.1
S/B: 190.0
Entries
m(μ, track) [GeV]

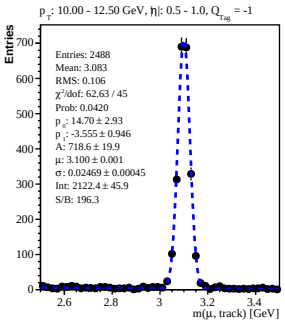
p_T: 10.00 - 12.50 GeV, |η|: 0.5 - 1.0, Q_{Trk} = -1
Entries: 2488
Mean: 3.083
RMS: 0.106
χ²/dof: 62.63 / 45
Prob: 0.0420
p_0: 14.70 ± 2.93
p_1: -3.555 ± 0.946
A: 718.6 ± 19.9
μ: 3.100 ± 0.001
σ: 0.02469 ± 0.00045
Int: 2122.4 ± 45.9
S/B: 196.3
Entries
m(μ, track) [GeV]

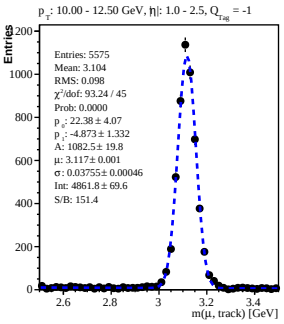
p_T: 10.00 - 12.50 GeV, |η|: 1.0 - 2.5, Q_{Trk} = -1
Entries: 5575
Mean: 3.104
RMS: 0.098
χ²/dof: 93.24 / 45
Prob: 0.0000
p_0: 22.38 ± 4.07
p_1: -4.873 ± 1.332
A: 1082.5 ± 19.8
μ: 3.117 ± 0.001
σ: 0.03755 ± 0.00046
Int: 4861.8 ± 69.6
S/B: 151.4
Entries
m(μ, track) [GeV]

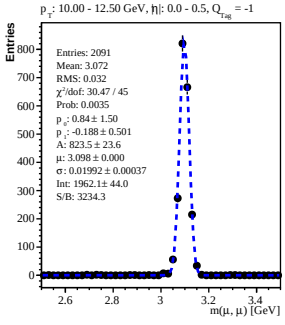
p_T: 10.00 - 12.50 GeV, |η|: 0.0 - 0.5, Q_{Trk} = -1
Entries: 2091
Mean: 3.072
RMS: 0.032
χ²/dof: 30.47 / 45
Prob: 0.0035
p_0: 0.84 ± 1.50
p_1: -0.188 ± 0.501
A: 823.5 ± 23.6
μ: 3.098 ± 0.000
σ: 0.01992 ± 0.00037
Int: 1962.1 ± 44.0
S/B: 3234.3
Entries
m(μ, μ) [GeV]

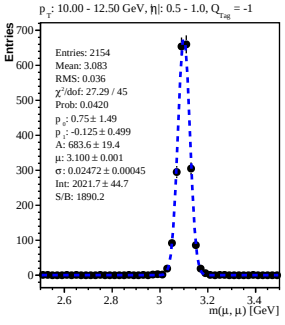
p_T: 10.00 - 12.50 GeV, |η|: 0.5 - 1.0, Q_{Trk} = -1
Entries: 2154
Mean: 3.083
RMS: 0.036
χ²/dof: 27.29 / 45
Prob: 0.0420
p_0: 0.75 ± 1.49
p_1: -0.125 ± 0.499
A: 683.6 ± 19.4
μ: 3.100 ± 0.001
σ: 0.02472 ± 0.00045
Int: 2021.7 ± 44.7
S/B: 1890.2
Entries
m(μ, μ) [GeV]

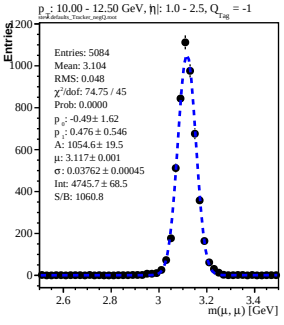
p_T: 10.00 - 12.50 GeV, |η|: 1.0 - 2.5, Q_{Trk} = -1
Entries: 5084
Mean: 3.104
RMS: 0.048
χ²/dof: 74.75 / 45
Prob: 0.0000
p_0: -0.49 ± 1.62
p_1: 0.476 ± 0.546
A: 1054.6 ± 19.5
μ: 3.117 ± 0.001
σ: 0.03762 ± 0.00045
Int: 4745.7 ± 68.5
S/B: 1060.8
Entries
m(μ, μ) [GeV]

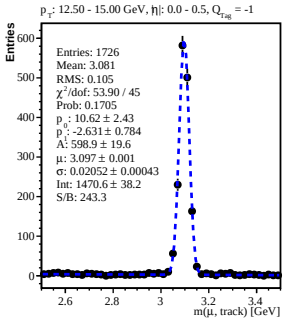
p_T: 12.50 - 15.00 GeV, |η|: 0.0 - 0.5, Q_{Trk} = -1
Entries: 1726
Mean: 3.081
RMS: 0.105
χ²/dof: 53.90 / 45
Prob: 0.1705
p_0: 10.62 ± 2.43
p_1: -2.631 ± 0.784
A: 598.9 ± 19.6
μ: 3.097 ± 0.001
σ: 0.02052 ± 0.00043
Int: 1470.6 ± 38.2
S/B: 243.3
Entries
m(μ, track) [GeV]

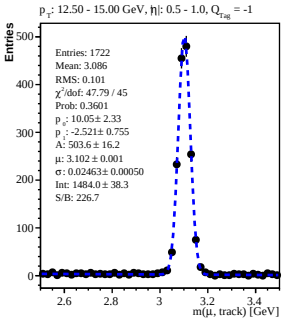
p_T: 12.50 - 15.00 GeV, |η|: 0.5 - 1.0, Q_{Trk} = -1
Entries: 1722
Mean: 3.086
RMS: 0.101
χ²/dof: 47.79 / 45
Prob: 0.3601
p_0: 10.05 ± 2.33
p_1: -2.521 ± 0.755
A: 503.6 ± 16.2
μ: 3.102 ± 0.001
σ: 0.02463 ± 0.00050
Int: 1484.0 ± 38.3
S/B: 226.7
Entries
m(μ, track) [GeV]

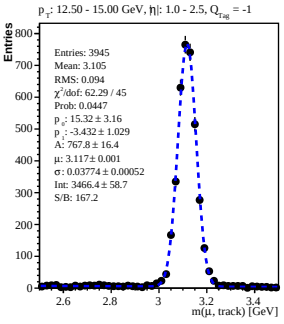
p_T: 12.50 - 15.00 GeV, |η|: 1.0 - 2.5, Q_{Trk} = -1
Entries: 3945
Mean: 3.105
RMS: 0.094
χ²/dof: 62.29 / 45
Prob: 0.0447
p_0: 15.32 ± 3.16
p_1: -3.432 ± 1.029
A: 767.8 ± 16.4
μ: 3.117 ± 0.001
σ: 0.03774 ± 0.00052
Int: 3466.4 ± 58.7
S/B: 167.2
Entries
m(μ, track) [GeV]

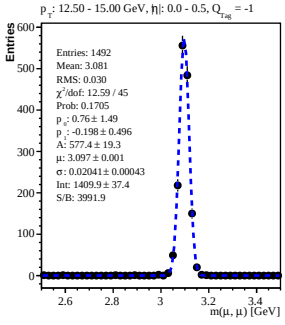
p_T: 12.50 - 15.00 GeV, |η|: 0.0 - 0.5, Q_{Trk} = -1
Entries: 1492
Mean: 3.081
RMS: 0.030
χ²/dof: 12.59 / 45
Prob: 0.1705
p_0: 0.76 ± 1.49
p_1: -0.198 ± 0.496
A: 577.4 ± 19.3
μ: 3.097 ± 0.001
σ: 0.02041 ± 0.00043
Int: 1409.9 ± 37.4
S/B: 3991.9
Entries
m(μ, μ) [GeV]

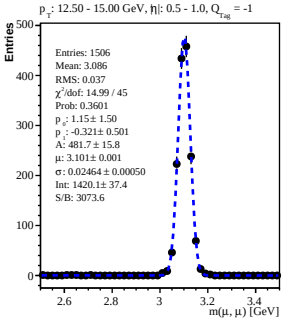
p_T: 12.50 - 15.00 GeV, |η|: 0.5 - 1.0, Q_{Trk} = -1
Entries: 1506
Mean: 3.086
RMS: 0.037
χ²/dof: 14.99 / 45
Prob: 0.3601
p_0: 1.15 ± 1.50
p_1: -0.321 ± 0.501
A: 481.7 ± 15.8
μ: 3.101 ± 0.001
σ: 0.02464 ± 0.00050
Int: 1420.1 ± 37.4
S/B: 3073.6
Entries
m(μ, μ) [GeV]

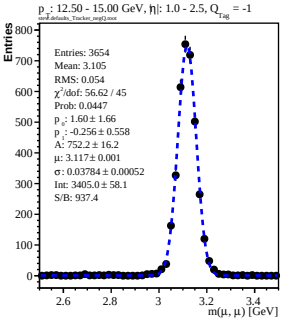
p_T: 12.50 - 15.00 GeV, |η|: 1.0 - 2.5, Q_{Trk} = -1
Entries: 3654
Mean: 3.105
RMS: 0.054
χ²/dof: 56.62 / 45
Prob: 0.0447
p_0: 1.60 ± 1.66
p_1: -0.256 ± 0.558
A: 752.2 ± 16.2
μ: 3.117 ± 0.001
σ: 0.03784 ± 0.00052
Int: 3405.0 ± 58.1
S/B: 937.4
Entries
m(μ, μ) [GeV]

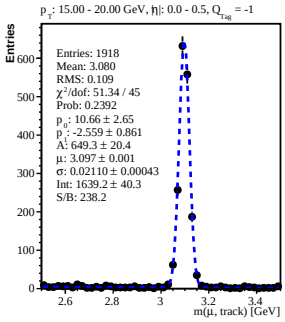
p_T: 15.00 - 20.00 GeV, |η|: 0.0 - 0.5, Q_Tag = -1
Entries: 1918
Mean: 3.080
RMS: 0.109
χ²/dof: 51.34 / 45
Prob: 0.2392
p_0: 10.66 ± 2.65
p_1: -2.559 ± 0.861
A: 649.3 ± 20.4
μ: 3.097 ± 0.001
σ: 0.02110 ± 0.00043
Int: 1639.2 ± 40.3
S/B: 238.2
Entries
m(μ, track) [GeV]

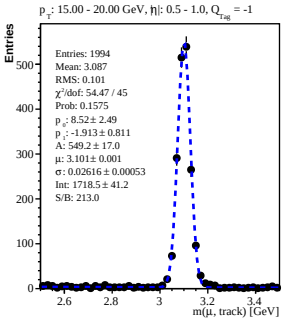
p_T: 15.00 - 20.00 GeV, |η|: 0.5 - 1.0, Q_Tag = -1
Entries: 1994
Mean: 3.087
RMS: 0.101
χ²/dof: 54.47 / 45
Prob: 0.1575
p_0: 8.52 ± 2.49
p_1: -1.913 ± 0.811
A: 549.2 ± 17.0
μ: 3.101 ± 0.001
σ: 0.02616 ± 0.00053
Int: 1718.5 ± 41.2
S/B: 213.0
Entries
m(μ, track) [GeV]

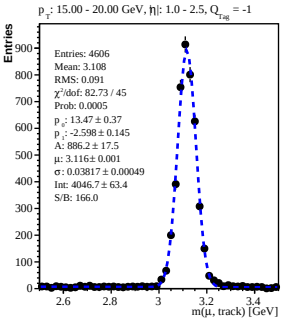
p_T: 15.00 - 20.00 GeV, |η|: 1.0 - 2.5, Q_Tag = -1
Entries: 4606
Mean: 3.108
RMS: 0.091
χ²/dof: 82.73 / 45
Prob: 0.0005
p_0: 13.47 ± 0.37
p_1: -2.598 ± 0.145
A: 886.2 ± 17.5
μ: 3.116 ± 0.001
σ: 0.03817 ± 0.00049
Int: 4046.7 ± 63.4
S/B: 166.0
Entries
m(μ, track) [GeV]

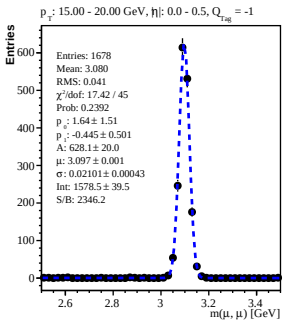
p_T: 15.00 - 20.00 GeV, |η|: 0.0 - 0.5, Q_Tag = -1
Entries: 1678
Mean: 3.080
RMS: 0.041
χ²/dof: 17.42 / 45
Prob: 0.2392
p_0: 1.64 ± 1.51
p_1: -0.445 ± 0.501
A: 628.1 ± 20.0
μ: 3.097 ± 0.001
σ: 0.02101 ± 0.00043
Int: 1578.5 ± 39.5
S/B: 2346.2
Entries
m(μ, μ) [GeV]

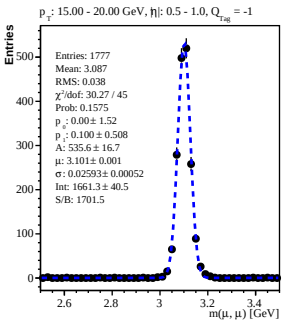
p_T: 15.00 - 20.00 GeV, |η|: 0.5 - 1.0, Q_Tag = -1
Entries: 1777
Mean: 3.087
RMS: 0.038
χ²/dof: 30.27 / 45
Prob: 0.1575
p_0: 0.00 ± 1.52
p_1: 0.100 ± 0.508
A: 535.6 ± 16.7
μ: 3.101 ± 0.001
σ: 0.02593 ± 0.00052
Int: 1661.3 ± 40.5
S/B: 1701.5
Entries
m(μ, μ) [GeV]

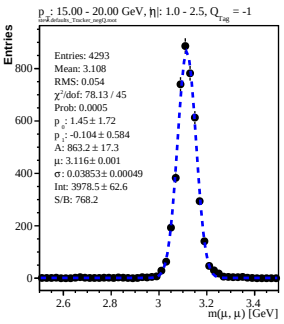
p_T: 15.00 - 20.00 GeV, |η|: 1.0 - 2.5, Q_Tag = -1
Entries: 4293
Mean: 3.108
RMS: 0.054
χ²/dof: 78.13 / 45
Prob: 0.0005
p_0: 1.45 ± 1.72
p_1: -0.104 ± 0.584
A: 863.2 ± 17.3
μ: 3.116 ± 0.001
σ: 0.03853 ± 0.00049
Int: 3978.5 ± 62.6
S/B: 768.2
Entries
m(μ, μ) [GeV]

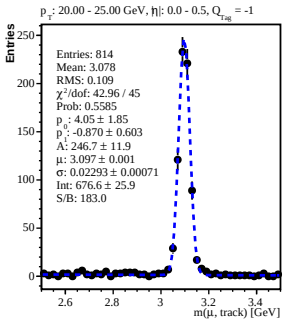
p_T: 20.00 - 25.00 GeV, |η|: 0.0 - 0.5, Q_Tag = -1
Entries: 814
Mean: 3.078
RMS: 0.109
χ²/dof: 42.96 / 45
Prob: 0.5585
p_0: 4.05 ± 1.85
p_1: -0.870 ± 0.603
A: 246.7 ± 11.9
μ: 3.097 ± 0.001
σ: 0.02293 ± 0.00071
Int: 676.6 ± 25.9
S/B: 183.0
Entries
m(μ, track) [GeV]

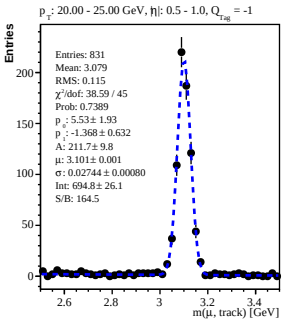
p_T: 20.00 - 25.00 GeV, |η|: 0.5 - 1.0, Q_Tag = -1
Entries: 831
Mean: 3.079
RMS: 0.115
χ²/dof: 38.59 / 45
Prob: 0.7389
p_0: 5.53 ± 1.93
p_1: -1.368 ± 0.632
A: 211.7 ± 9.8
μ: 3.101 ± 0.001
σ: 0.02744 ± 0.00080
Int: 694.8 ± 26.1
S/B: 164.5
Entries
m(μ, track) [GeV]

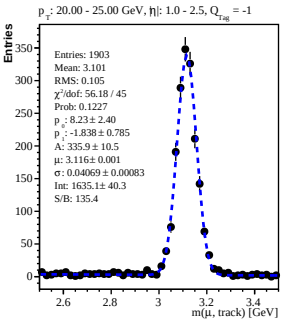
p_T: 20.00 - 25.00 GeV, |η|: 1.0 - 2.5, Q_Tag = -1
Entries: 1903
Mean: 3.101
RMS: 0.105
χ²/dof: 56.18 / 45
Prob: 0.1227
p_0: 8.23 ± 2.40
p_1: -1.838 ± 0.785
A: 335.9 ± 10.5
μ: 3.116 ± 0.001
σ: 0.04069 ± 0.00083
Int: 1635.1 ± 40.3
S/B: 135.4
Entries
m(μ, track) [GeV]

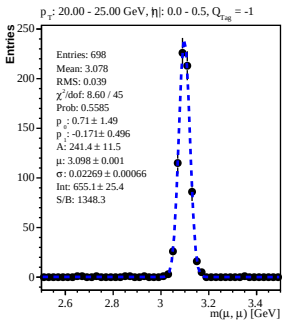
p_T: 20.00 - 25.00 GeV, |η|: 0.0 - 0.5, Q_Tag = -1
Entries: 698
Mean: 3.078
RMS: 0.039
χ²/dof: 8.60 / 45
Prob: 0.5585
p_0: 0.71 ± 1.49
p_1: -0.171 ± 0.496
A: 241.4 ± 11.5
μ: 3.098 ± 0.001
σ: 0.02269 ± 0.00066
Int: 655.1 ± 25.4
S/B: 1348.3
Entries
m(μ, μ) [GeV]

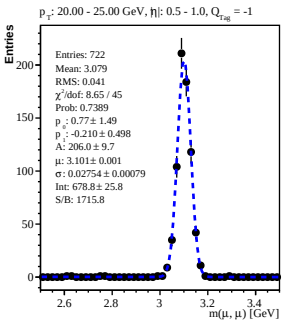
p_T: 20.00 - 25.00 GeV, |η|: 0.5 - 1.0, Q_Tag = -1
Entries: 722
Mean: 3.079
RMS: 0.041
χ²/dof: 8.65 / 45
Prob: 0.7389
p_0: 0.77 ± 1.49
p_1: -0.210 ± 0.498
A: 206.0 ± 9.7
μ: 3.101 ± 0.001
σ: 0.02754 ± 0.00079
Int: 678.8 ± 25.8
S/B: 1715.8
Entries
m(μ, μ) [GeV]

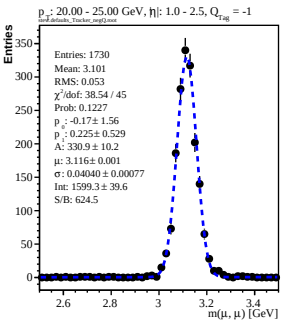
p_T: 20.00 - 25.00 GeV, |η|: 1.0 - 2.5, Q_Tag = -1
Entries: 1730
Mean: 3.101
RMS: 0.053
χ²/dof: 38.54 / 45
Prob: 0.1227
p_0: -0.17 ± 1.56
p_1: 0.225 ± 0.529
A: 330.9 ± 10.2
μ: 3.116 ± 0.001
σ: 0.04040 ± 0.00077
Int: 1599.3 ± 39.6
S/B: 624.5
Entries
m(μ, μ) [GeV]

Acknowledgements

My thanks go to Prof. Dr. Urs Langenegger giving me the opportunity of participating in the CMS experiment during this extraordinary exciting period as well as for his intensive care and relevant suggestions. I would also like to express my gratitude to Christina Eggel for her support, valuable inputs and for providing me with data to analyze. Further, I am grateful for the kind hospitality also experienced by the other group members Sarah Dambach and Peter Trüeb. In addition I am indebted to my Diploma Thesis colleagues Michel De Cian and Benjamin Stieger for helpful and constructive discussions.

Finally, thanks go to my parents which have supported me during my studies at ETH.

Bibliography

[BR+01] R. Brun, F. Rademakers, et al. ROOT web page, `http://root.cern.ch/`, 2001.

[COW98] Glen COWAN. *Statistical data analysis*. Clarendon Press, Oxford, 1998.

[Del06] Della Negra, Michel and Foà, L and Hervé, A and Petrilli, Achille. *CMS physics: Technical Design Report*. Technical Design Report CMS. CERN, Geneva, 2006. There is an error on cover due to a technical problem for some items.

[Lan06] Urs Langenegger. Study of $B_s \to \mu^+\mu^-$ in CMS, 2006.

[Mar01] Marko Milek, Christopher Hearty. Lepton Identification Efficiencies and Systematic Errors. *BABAR Analysis Document 126*, Version 5, February 12, 2001.

[Oli07] Oliver Kortner. Muon Identification at ATLAS and CMS, 2007.

[W.-06] W.-M. Yao et al. Review of Particle Physics. *Journal of Physics G*, 33, 2006.